

UNCLASSIFIED

Copy No.

~~RESTRICTED~~

RM No. L7G31

NACA RM. No. L7G31



RESEARCH MEMORANDUM

21 OCT 1947

LATERAL STABILITY AND CONTROL CHARACTERISTICS OF AN AIRPLANE
MODEL HAVING A 42.8° SWEEPBACK CIRCULAR-ARC WING
WITH ASPECT RATIO 4.00, TAPER RATIO 0.50,
AND SWEEPBACK TAIL SURFACES

By

Kenneth W. Goodson and Paul Comisarow

Langley Memorial Aeronautical Laboratory

Langley Field, Va.

CLASSIFICATION CHANGED
UNCLASSIFIED

CLASSIFICATION CHANGED

CLASSIFIED DOCUMENT

This document contains classified information affecting the National Defense of the United States within the meaning of the Espionage Act, 18 USC, 793 and 794. Its transmission or revelation of its contents in any manner to an unauthorized person is prohibited by law. Information so classified may be exempt from automatic downgrading and declassification. It is the policy of the United States Government to have a legitimate interest in the security and integrity of its information. It is the policy of the United States Government to have a legitimate interest in the security and integrity of its information.

~~CONFIDENTIAL~~

CONFIDENTIAL
NACA 2197 EO 10501

Langley Field, Va. Date 12/14/53
11/1/54

*NACA Res also
1RN-128*

By authority of _____ Date _____
*effective
June 24, 1958*

APR 8-12 58

NATIONAL ADVISORY COMMITTEE FOR AERONAUTICS

WASHINGTON

October 17, 1947

UNCLASSIFIED ~~RESTRICTED~~

NACA LIBRARY
LANGLEY MEMORIAL AERONAUTICAL
LABORATORY
Langley Field, Va.

~~CONFIDENTIAL~~

NATIONAL ADVISORY COMMITTEE FOR AERONAUTICS

RESEARCH MEMORANDUM

LATERAL STABILITY AND CONTROL CHARACTERISTICS OF AN AIRPLANE

MODEL HAVING A 42.8° SWEEPBACK CIRCULAR-ARC WING

WITH ASPECT RATIO 4.00, TAPER RATIO 0.50,

AND SWEEPBACK TAIL SURFACES

By Kenneth W. Goodson and Paul Comisarow

SUMMARY

Tests were made in the Langley 300 MPH 7- by 10-foot tunnel of an airplane model having a 42.8° sweptback wing with an aspect ratio 4.00, taper ratio 0.50, a 42.8° sweptback horizontal tail, and a 40.3° sweptback vertical tail to determine the low-speed lateral stability and control characteristics. A series of changes including lowering the wing, incorporating a smaller-fineness-ratio fuselage, and increasing the vertical-tail size were made to improve the aerodynamic characteristics of the original model configuration.

The effective dihedral for the semihigh circular-arc wing reached a maximum positive value at a lift coefficient corresponding to that of wing-tip stall. The maximum value of $C_{L\dot{\psi}}$ occurred at a higher lift coefficient when split flaps and nose flaps were deflected because of the improved flow over the sharp leading edge of the wing. Incorporation of $5^\circ 51'$ of geometric dihedral and wing fillets into the low wing approximately compensated for the decrease in effective dihedral caused by lowering the wing.

The directional stability for the semihigh wing was very low but was improved when the split and nose flaps were deflected. The model was directionally unstable at lift coefficients above the stall, but lowering the wing, incorporating several degrees of geometric dihedral, and adding wing fillets made the model directionally stable for the flaps-neutral configuration. The low wing improved the directional stability through the lift-coefficient range up to stall for the flaps-neutral configurations.

~~CONFIDENTIAL~~~~CONFIDENTIAL~~

The aileron effectiveness decreased with increase in angle of attack for down aileron deflections but remained nearly constant for up deflections.

INTRODUCTION

The accelerated development of jet-propelled aircraft during World War II resulted in the creation of motors (turbojet, ram jet, and rocket) capable of propelling airplanes at supersonic speeds. Airplanes that are to fly through the transonic into the supersonic range are radical in design and present many low-speed stability problems. It is therefore desirable to make low-speed wind-tunnel tests in order to predict the low-speed stability characteristics of proposed supersonic airplanes.

This report presents the low-speed stability and control characteristics of a specific airplane. The model of the airplane tested had a circular-arc wing with 42.8° sweepback, 4.00 aspect ratio, 0.50 taper ratio, a 42.8° sweptback horizontal tail, and a 40.3° sweptback vertical tail. The original model configuration was tested with a semihigh wing. A series of changes including lowering the wing, incorporating a smaller-fineness-ratio fuselage, and using a larger vertical tail were made to improve the aerodynamic characteristics of the model. The nature of the investigation accounts for the fact that only limited data were obtained for some configurations.

The longitudinal stability and control characteristics of the model are presented in reference 1.

An investigation (reference 2) was made on a similar model with a 45.1° sweptback wing having an aspect ratio of 2.50 and a taper ratio of 0.42. The wing had an NACA 65-110 airfoil section.

COEFFICIENTS AND SYMBOLS

The results of the tests are presented as standard NACA coefficients of forces and moments. Rolling-moment, yawing-moment, and pitching-moment coefficients are referred to the test center of gravity shown in figure 1 (26 percent mean aerodynamic chord). The data are referred to the stability axes, which are a system of axes having their origin at the center of gravity and in which

the Z-axis is in the plane of symmetry and perpendicular to the relative wind, the X-axis is in the plane of symmetry and perpendicular to the Z-axis, and the Y-axis is perpendicular to the plane of symmetry. The positive directions of the stability axes, of angular displacements of the airplane and control surfaces, and of hinge moments are shown in figure 2.

The coefficients and symbols are defined as follows:

C_L lift coefficient $\left(\frac{\text{Lift}}{qS}\right)$

C_X longitudinal-force coefficient $\left(\frac{X}{qS}\right)$

C_Y side-force coefficient $\left(\frac{Y}{qS}\right)$

C_L rolling-moment coefficient $\left(\frac{L}{qSb}\right)$

C_m pitching-moment coefficient $\left(\frac{M}{qSc^2}\right)$

C_n yawing-moment coefficient $\left(\frac{N}{qSb}\right)$

C_h hinge-moment coefficient $\left(\frac{H}{qb'c^2}\right)$

Lift = -Z

Drag = -X (only) at $\psi = 0^\circ$

$\left. \begin{array}{l} X \\ Y \\ Z \end{array} \right\}$ forces along axes, pounds

$\left. \begin{array}{l} L \\ M \\ N \end{array} \right\}$ moments about axes, pound-feet

H hinge moment of control surface, pound-feet

q free-stream dynamic pressure, pounds per square foot $\left(\frac{\rho V^2}{2}\right)$

S wing area (12.70 sq ft on model)

c chord measured perpendicular to wing reference line

c'	wing mean aerodynamic chord (M.A.C.) (1.85 ft on model)
\bar{c}	root-mean-square chord of control surface back of hinge line, feet
b	wing span (7.12 ft on model)
b'	rudder control-surface span measured perpendicular to fuselage center line
V	air velocity, feet per second
ρ	mass density of air, slugs per cubic foot
α	angle of attack of fuselage center line, degrees
ψ	angle of yaw, degrees
i_t	angle of root chord of stabilizer measured with respect to fuselage center line; positive when trailing edge is down
δ_r	rudder deflection measured in plane parallel to fuselage center line, degrees
δ_a	aileron deflection measured in plane perpendicular to wing reference line, degrees (a_R , a_L , right and left, respectively)
δ_{f_s}	split-flap deflection measured in plane perpendicular to wing reference line, degrees
δ_{f_p}	plain flap deflection measured in plane perpendicular to wing reference line, degrees
δ_{f_n}	nose flap (wing leading edge) deflection measured in plane perpendicular to wing reference line, degrees
Γ	geometric dihedral angle, degrees (measured with respect to chord plane and normal to plane of symmetry)
A	aspect ratio $\left(\frac{b^2}{S}\right)$
Λ	angle of sweepback measured to leading edge, degrees

λ taper ratio $\left(\frac{\text{Tip chord}}{\text{Root chord}} \right)$

M_∞ free-stream Mach number

Subscript:

ψ denotes partial derivatives of coefficient with respect to yaw, for example, $C_{L\psi} = \frac{\partial C_L}{\partial \psi}$

DESIGNATION

In a previous paper (reference 2) it was found desirable to designate the swept wing and tail plan forms in an abbreviated manner. This method of designation will also be followed in this paper. The abbreviated designation is as follows:

Sweepback - Aspect ratio - Taper ratio
 Λ A λ

For example, in a wing designation of the form

42.8 - 4.00 - 0.50

the number preceding the first dash (42.8) gives the sweepback Λ in degrees measured with respect to the leading edge, the number following the first dash (4.00) gives the aspect ratio A , and the number following the second dash (0.50) gives the taper ratio λ .

MODEL AND APPARATUS

The large fuselage model tested consisted of a 42.8 - 4.00 - 0.50 wing, a 42.8 - 3.87 - 0.49 horizontal tail, and a 40.3 - 1.26 - 0.31 vertical tail. The wing had a 10-percent-thick circular-arc airfoil measured normal to the wing reference line (fig. 1). The horizontal tail had an NACA 65-008 airfoil section measured perpendicular to the tail reference line. The vertical tail was made of a thin steel plate. The large fuselage (figs. 1(a) and 3) was designed in such a manner as to facilitate testing the wing in a semihigh ($\Gamma = 0^\circ$) and in a low ($\Gamma = 5^\circ 51'$) position as shown

in figure 1(a). The circular-arc, aspect ratio 4, wing was constructed of mahogany and was fitted with 20-percent-chord split flaps and with 15-percent-chord nose flaps (measured perpendicular to the wing reference line). The split flaps and the nose flaps are shown deflected in figure 4. The split-flap deflection angle was measured between the lower contour of the wing and the flap surface, and the nose-flap deflection was measured with respect to the chord lines of the wing and the nose flap. (See section A-A of fig. 1.) A drawing of a slot in the wing leading edge is shown in figure 5. The large fuselage was fitted with a flat-top dorsal as shown in the three-view drawing of figure 1(a). The semihigh wing was tested without wing fillets, whereas the low wing was tested with fillets as shown in the photograph of figure 6.

The large fuselage was replaced by a fuselage (figs. 1, 7, and 8) having smaller length and diameter and a higher fineness ratio (9.46 versus 7.89). The small fuselage had a shorter nose length than that of the large fuselage. The wing was tested in the low position shown in the three-view drawing of figure 1(b). The wing of the small fuselage had a 20-percent-chord plain flap and aileron (measured perpendicular to the wing reference line). The plain flap and the aileron deflection angles were measured between the wing chord line and the respective flap or aileron chord line (fig. 1(b)). The small fuselage had a vertical tail (small) of the same plan form as the large fuselage but used an NACA 27-010 airfoil section instead of the thin steel plate. The model was also tested with a large vertical tail (fig. 1(b)) having a 40.3 - 1.35 - 0.35 plan form. The large vertical tail consisted of an NACA 27-010 airfoil section at the root and an NACA 27-008 airfoil section at the tip. The horizontal tail was the same as for the large fuselage. Several dorsal and ventral fairing configurations, shown in figure 9, were tested with the large and the small vertical tails. The lower vertical tail is shown in figure 9. A drawing showing the wing stall-control vane or fence used on the model is shown in figure 10. The selection of this vane was determined by tests of reference 1. In order to facilitate the installation of the horizontal tail in the raised positions (fig. 11), a $\frac{5}{16}$ -inch-thick steel plate of the same plan form as the large vertical tail was used. The physical characteristics of the model are presented in table I.

The rudder hinge moments were measured with a resistance-type strain gage and a Brown potentiometer.

For some tests a net made of $\frac{3}{16}$ -inch chord, and having a mesh measuring $1\frac{1}{4}$ inches on a side, was installed (fig. 3) upstream of the model to increase the turbulence factor of the tunnel, thus increasing the effective Reynolds number of the tests.

TESTS AND RESULTS

Test Conditions

The tests were made at dynamic pressures of about 40.0 pounds per square foot, corresponding to an airspeed of about 125 miles per hour ($M_0 = 0.16$). The tests were made at a Reynolds number of about 2.15×10^6 based upon the mean aerodynamic chord of 1.85 feet. The turbulence factor for the tunnel is not known but is believed to be approximately 1.0 because of the high tunnel contraction ratio (14:1).

Several tests were made at a turbulence factor of 2.24 with the turbulence net installed in the tunnel upstream of the model. The effective Reynolds number thus obtained was about 4.82×10^6 .

Corrections

Tares were not applied inasmuch as they were considered negligible as determined in tests of reference 2. Jet-boundary corrections were computed as follows (reference 3)

$$\alpha = \alpha_M + 1.42C_{L_M}$$

$$C_X = C_{X_M} - 0.0203C_{L_M}^2$$

$$C_m = C_{m_M} + 0.010C_{L_M} \quad (\text{for tail on})$$

where subscript M denotes measured value.

All force and moment coefficients were corrected for blocking by the method of reference 4.

The data have been corrected for the horizontal buoyancy caused by the longitudinal static-pressure gradient in the tunnel.

Presentation of Results

An outline of the figures presenting the results of tests made on the model is presented below:

	Figure
Semihigh wing with large fuselage ($\Gamma = 0^\circ$), thin vertical tail:	
Lateral-stability derivatives	12
Aerodynamic characteristics in yaw	13
Low wing with large fuselage ($\Gamma = 5.7^\circ$), thin vertical tail:	
Lateral-stability derivatives	14
Aerodynamic characteristics in yaw	15
Effect of Reynolds number	16 and 17
Wing-alone aerodynamic characteristics in yaw ($\Gamma = 3.0^\circ$)	18
Low wing with small fuselage ($\Gamma = 3.0^\circ$), small vertical tail:	
Effect of dorsal and ventral fairings on the aerodynamic characteristics in yaw	19
Lateral-stability derivatives	20
Aerodynamic characteristics in yaw	21
Low wing with small fuselage ($\Gamma = 3.0^\circ$), large vertical tail:	
Effect of dorsal fairings on the aerodynamic characteristics in yaw	22
Lateral-stability derivatives	23
Aerodynamic characteristics in yaw	24
Effect of horizontal-tail location on the aerodynamic characteristics in yaw (thin vertical tail)	25
Effect of stall-control vane in yaw	26
Effect of aileron deflection in yaw, with and without the stall-control vane	27
Effect of rudder deflection in yaw	28

DISCUSSION

Semihigh Wing with Large Fuselage (Small Thin Vertical Tail)

The effective dihedral for the flaps-up condition reached a maximum at a lift coefficient of about 0.25 (fig. 12(a)). The maximum values of $C_{L\psi}$ were delayed when the split flaps and nose flaps were deflected. (See figs. 12(a) and 12(b).) The maximum values of $C_{L\psi}$ occur at about the same lift coefficient as wing-tip stall. (See tuft sketches presented in reference 1.) The tuft studies showed that the stall at the wing tips and along the sharp leading edge was delayed considerably with deflection of the split flaps and nose flaps. A 60-percent-span slot (fig. 5) caused the maximum value of $C_{L\psi}$ to occur at a higher lift coefficient (fig. 12(a)).

The directional stability was very low through the small yaw range (figs. 12 and 13), being almost neutral for the flaps-neutral configuration. The extent of the flat spot can be seen in the yawing-moment curves of figure 13. The flat spot in the yawing-moment curve might be attributed to the flow break away near the root of the vertical tail as mentioned in reference 2 and also to adverse sidewash conditions. The model becomes directionally unstable when the semihigh wing is completely stalled for both the flaps neutral and deflected condition.

The large symbols plotted on the parameter curves are values of slopes measured from tests through the yaw range. The stability parameters were computed from tests made through the angle-of-attack range at $\pm 5^\circ$ of yaw.

Low Wing with Large Fuselage (Small Thin Vertical Tail)

There was very little increase in effective dihedral (figs. 12(a) and 14(a)) for the complete model with flaps neutral when the wing was lowered which indicates that incorporation of $5^\circ 51'$ geometric dihedral in the low wing and the addition of wing fillets just about compensated for the reduction in effective dihedral caused by lowering the wing. Data were not obtained for the tail-on, wing-fillet-off configuration, but data for the tail-off, wing-fillet-off and wing-fillet-on configurations (fig. 14(a))

show that addition of the wing fillets to the low-wing model (tail-off) decreased the effective dihedral. The tail contribution to the effective dihedral was greater for the low wing than for the semihigh wing.

The low-wing model with 5°51' of geometric dihedral and wing fillets altered the flow characteristics sufficiently to produce stable yawing moments at the stall (compare figs. 12(a) and 14(a)) for the flaps-neutral configuration. Lowering the wing also increased the directional stability (flaps neutral) through the range of lift coefficients. The addition of wing fillets to the low-wing configuration did not appreciably affect the tail-off directional stability of the model (fig. 14(a)). The flat spot noted in the yawing-moment curve of the semihigh-wing configuration is present for the low-wing configuration (fig. 15); however, there is considerable improvement over that of the semihigh wing. It can be seen that the model is directionally unstable at angles of yaw greater than 10° (fig. 15).

The effect of Reynolds number (in the range tested) on the lateral-stability derivatives (fig. 16) is negligible for both the flaps-neutral and the flaps-deflected configurations.

Low Wing with Small Fuselage (Small Vertical Tail)

The weathercock stability (fig. 19(a)) was slightly less when the large dorsal and no ventral fairing were used than it was with the flat dorsal and a ventral fairing. The ventral-fairing contribution to the directional stability was negligible, thus indicating that most of the directional-stability change was caused by the dorsal.

Although the data of figures 14(b) and 20 are not directly comparable, it can be seen that the directional stability for the small fuselage model was increased for all configurations tested. The directional instability at the stall was not improved. The lower vertical tail (fig. 9) increased the directional stability ($\Delta C_{n\psi} = -0.00070$) as shown in figure 21.

Although the low-wing, small-fuselage model incorporated less geometric dihedral than did the low-wing, large-fuselage model, there was a small increase in $C_{l\psi}$ at low-lift coefficients.

This increase was probably caused by improved flow conditions obtained through the use of the smaller fuselage. The maximum value of $C_{l_{\psi}}$ occurred at a much lower lift coefficient and was of smaller magnitude than that of the model with the large fuselage. (Compare figs. 14(b) and 20.) This change of maximum $C_{l_{\psi}}$ position was a result of the smaller span nose flaps used on the small fuselage model.

Low Wing with Small Fuselage (Large Vertical Tail)

The results of additional tests made with dorsal and ventral fairings (fig. 9) for the small fuselage model with the large vertical tail (fig. 22) show little difference as compared with the previous dorsal and ventral configurations.

It appears (from figs. 20 and 23(b)) that the use of the large vertical tail increased the flap-down directional stability by approximately -0.0005.

The effect of horizontal-tail position on the lateral characteristics is very small (fig. 25) for both the flaps-neutral and flaps-deflected configurations.

The results of tests made to determine the effect of a stall-control-vane configuration (fig. 10) are shown in figure 26. Comparison of slopes measured from figure 26 with the parameter data of figure 23 shows that the effect of the stall-control vanes on lateral stability was negligible.

The aileron effectiveness (fig. 27) decreases with increase in angle of attack for positive aileron deflections but remains nearly constant for negative deflections. The effect of the stall-control vanes on the aileron characteristics was negligible.

Rudder-control and hinge-moment characteristics are presented in figure 28. The rudder effectiveness $\partial C_n / \partial \delta_r$ at small angles of yaw is about -0.0010 for both the flaps-neutral and the flaps-deflected configurations. It appears for both the flaps-neutral and the flaps-deflected configurations that the rudder ($\delta_r = 30^\circ$) can hold a sideslip angle of about -12° . For small rudder deflections, the variation of the rudder hinge moment with angle of yaw is positive at small angles of yaw but becomes negative at large angles of yaw.

CONCLUDING REMARKS

The lateral stability and control characteristics of a model with a 42.8 - 4.00 - 0.50 wing based upon low-speed wind-tunnel tests are summarized as follows:

1. The effective dihedral for the flaps-up, high-wing ($\Gamma = 0^\circ$) configuration reached a maximum value at a lift coefficient of about 0.25. The maximum value of $C_{L\psi}$ occurred at about the same lift coefficient at which the wing stalled. Nose-flap deflection increased the lift coefficient at which the maximum $C_{L\psi}$ occurred. Incorporation of $5^\circ 51'$ of geometric dihedral and addition of wing fillets to the low-wing configuration just about compensated for the decrease in effective dihedral caused by lowering the wing. The tail contribution to the effective dihedral was greater for the low wing than for the semihigh wing.

2. The directional stability for the semihigh wing was very low through the small yaw range, being almost neutral for the flaps-neutral configuration, but was improved when split flaps were deflected. The model becomes directionally unstable at lift coefficients above stall. Lowering the wing, incorporating $5^\circ 51'$ of geometric dihedral, and adding wing fillets increased the directional stability through the lift-coefficient range (up to stall) for the flaps-neutral configurations. The model also became directionally stable at the stall for the flaps-neutral configuration when the wing was lowered.

3. The aileron effectiveness decreased with increase in angle of attack for down aileron deflections but remained nearly constant for up deflections.

Langley Memorial Aeronautical Laboratory
National Advisory Committee for Aeronautics
Langley Field, Va.

REFERENCES

1. Weil, Joseph, Comisarow, Paul, and Goodson, Kenneth W.:
Longitudinal Stability and Control Characteristics of an Airplane Model Having a 42.8° Sweptback Circular-Arc Wing with Aspect Ratio 4.00, Taper Ratio 0.50, and Sweptback Tail Surfaces. NACA RM No. L7G28, 1947.
2. Schuldenfrei, Marvin, Comisarow, Paul, and Goodson, Kenneth W.:
Stability and Control Characteristics of an Airplane Model Having a 45.1° Swept-Back Wing with Aspect Ratio 2.50 and Taper Ratio 0.42 and 42.8° Swept-Back Horizontal Tail with Aspect Ratio 3.87 and Taper Ratio 0.49. NACA RM No. L7B25, 1947.
3. Gillis, Clarence L., Polhamus, Edward C., and Gray, Joseph L., Jr.:
Charts for Determining Jet-Boundary Corrections for Complete Models in 7- by 10-Foot Closed Rectangular Wind Tunnels. NACA ARR No. L5G31, 1945.
4. Thom, A.: Blockage Corrections in a Closed High-Speed Tunnel. R. & M. No. 2033, British A.R.C., 1943.

TABLE I

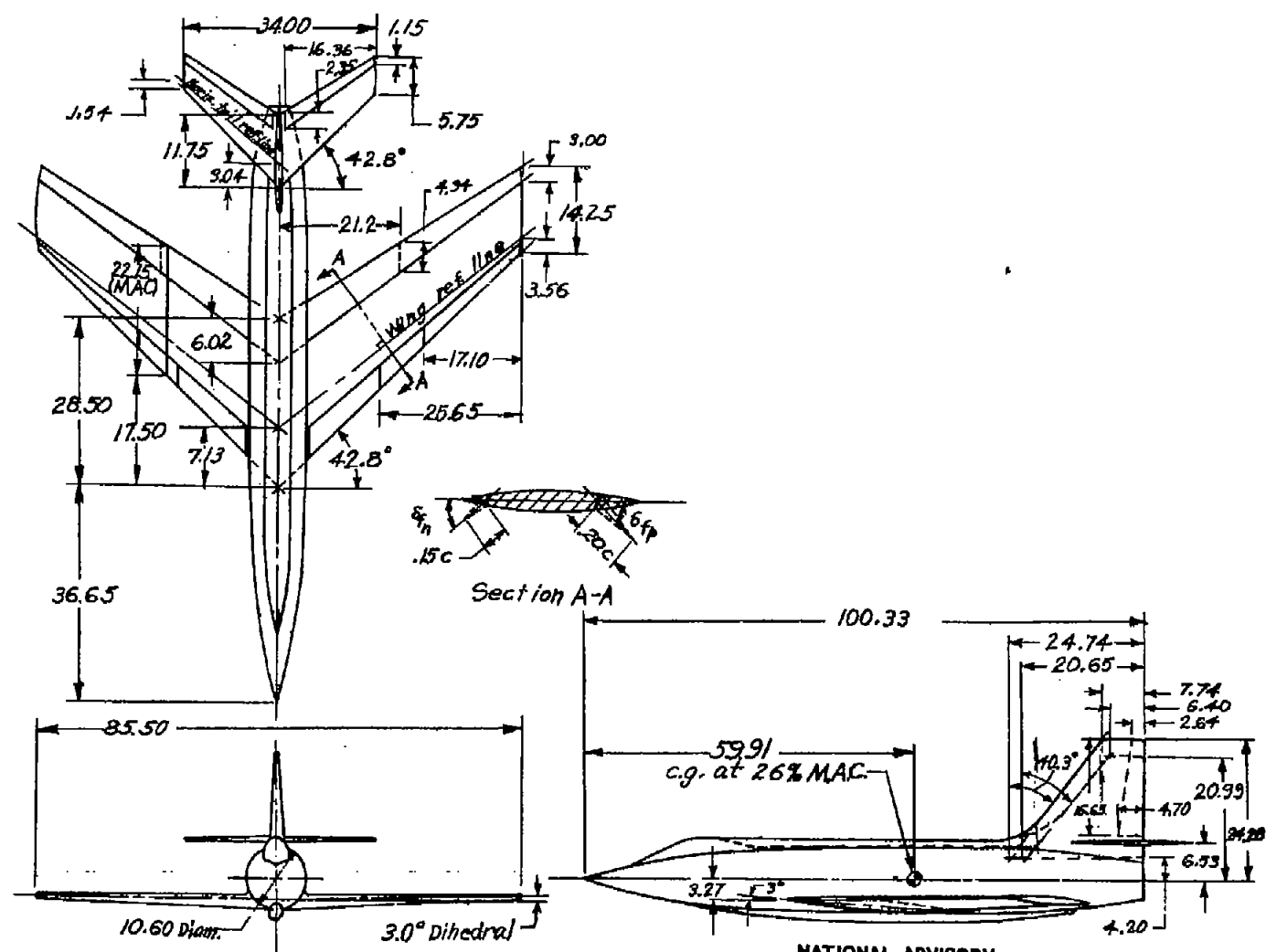
PHYSICAL CHARACTERISTICS OF A MODEL WITH A 42.8 - 4.00 - 0.50 WING

14

	Wing	Horizontal tail	Vertical tail	
			Small	Large
Area, ft ²	12.70	2.06	1.54	2.08
Span, in.	85.50	34.00	16.70	20.08
Sweepback of leading edge, deg	42.8	42.8	40.3	40.3
Aspect ratio	4.00	3.87	1.26	1.35
Taper ratio	0.50	0.49	0.31	0.35
Dihedral, deg				
Semihigh wing, large fuselage	0	0		
Low wing, large fuselage	5°51'	0		
Low wing, small fuselage	3	0		
Angle of incidence of root chord with respect to fuselage center line, deg	3	Varies		
Mean aerodynamic chord, in.	22.15			
Root chord, in.	28.50	11.75	20.80	22.14
Theoretical tip chord, in.	14.25	5.75	6.40	7.74
Root airfoil section	NACA 2S-(50)(05)-(50)(05)	NACA 65-008	NACA 27-010	NACA 27-010
Tip airfoil section	NACA 2S-(50)(05)-(50)(05)	NACA 65-008	NACA 27-010	NACA 27-008

NACA RM No. L7G31

NATIONAL ADVISORY
COMMITTEE FOR AERONAUTICS



(b) Small fuselage.
Figure 1... Concluded.

NATIONAL ADVISORY
COMMITTEE FOR AERONAUTICS

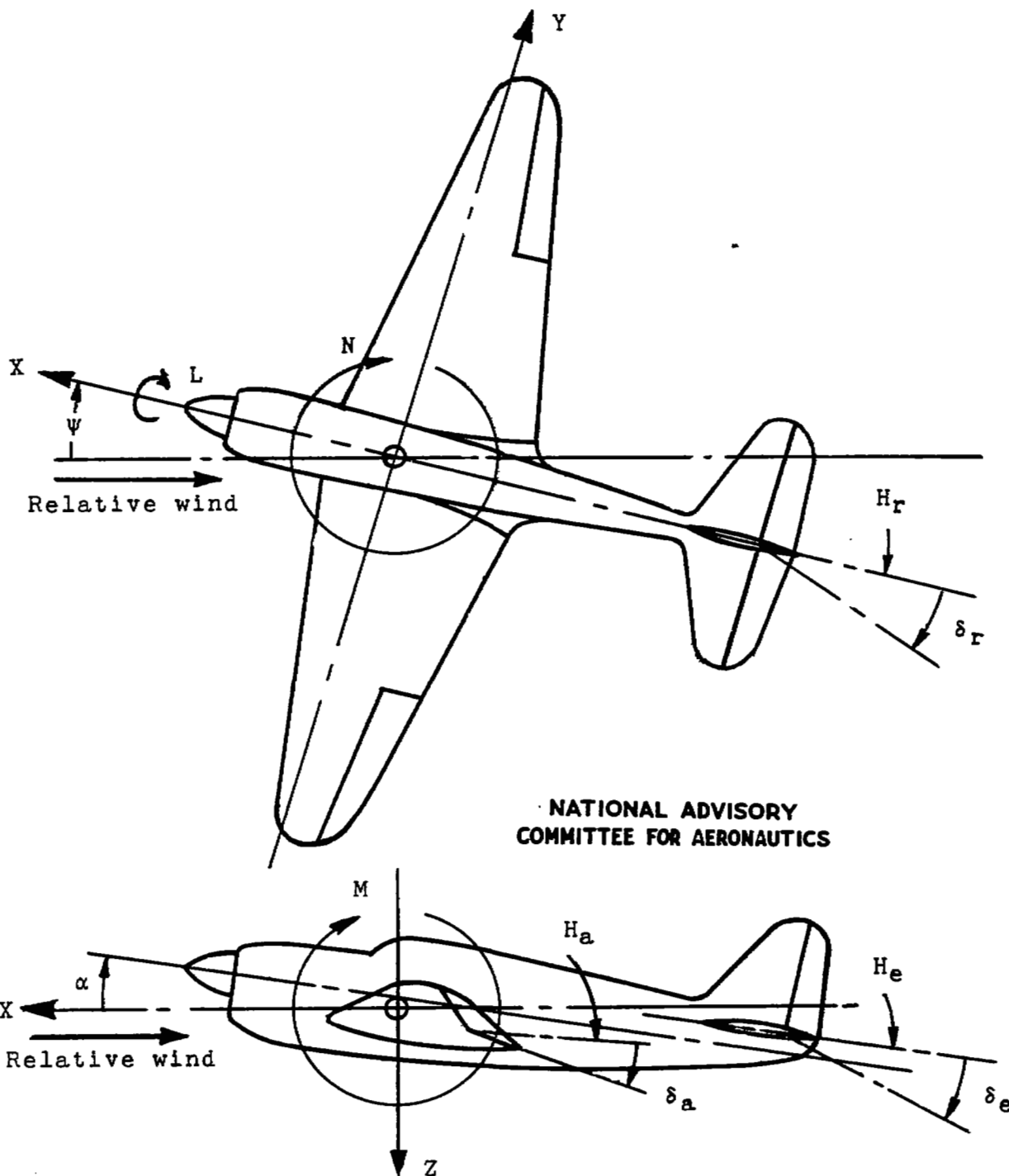
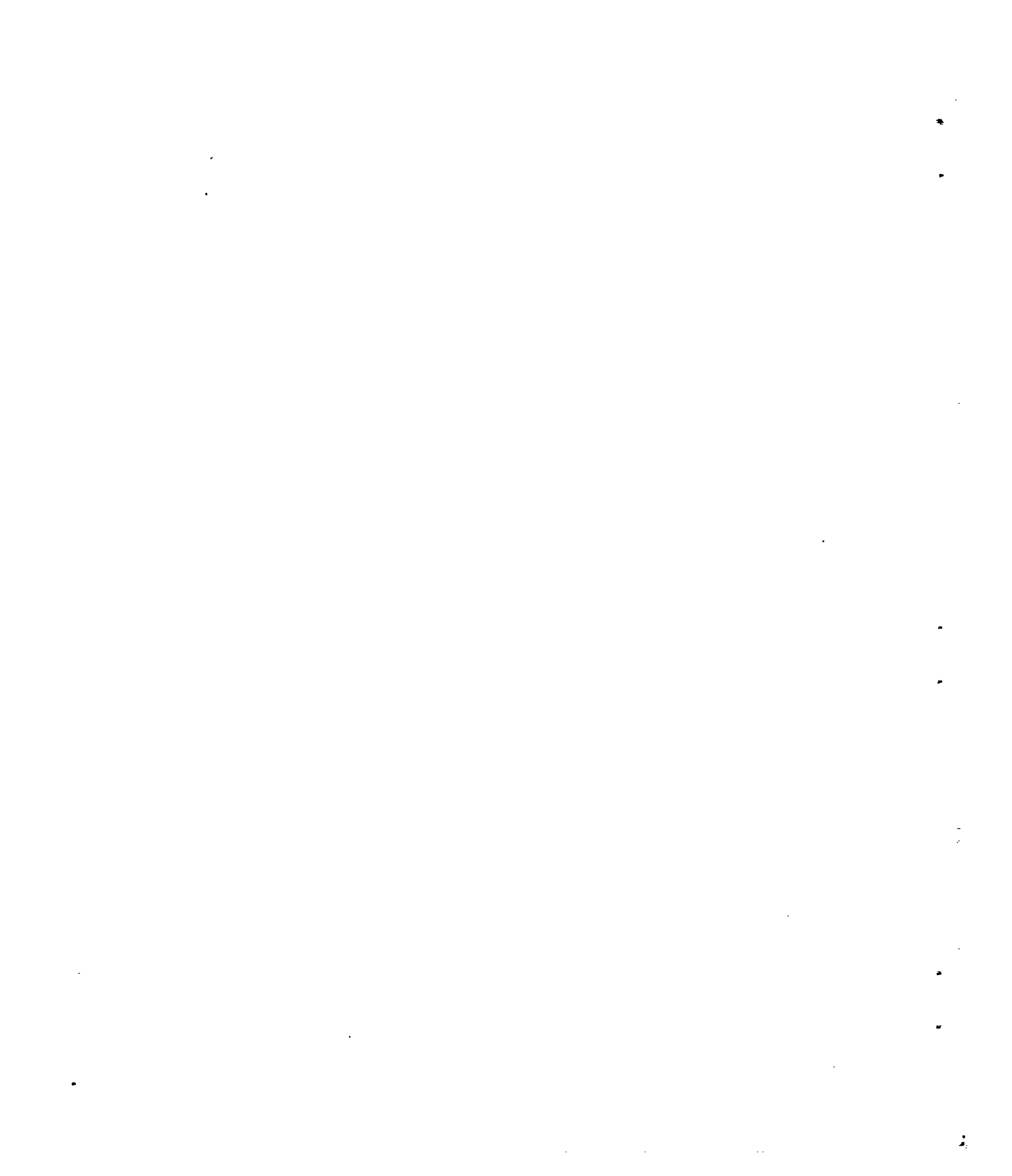


Figure 2.- System of axes and control-surface hinge moments and deflections. Positive values of forces, moments, and angles are indicated by arrows.



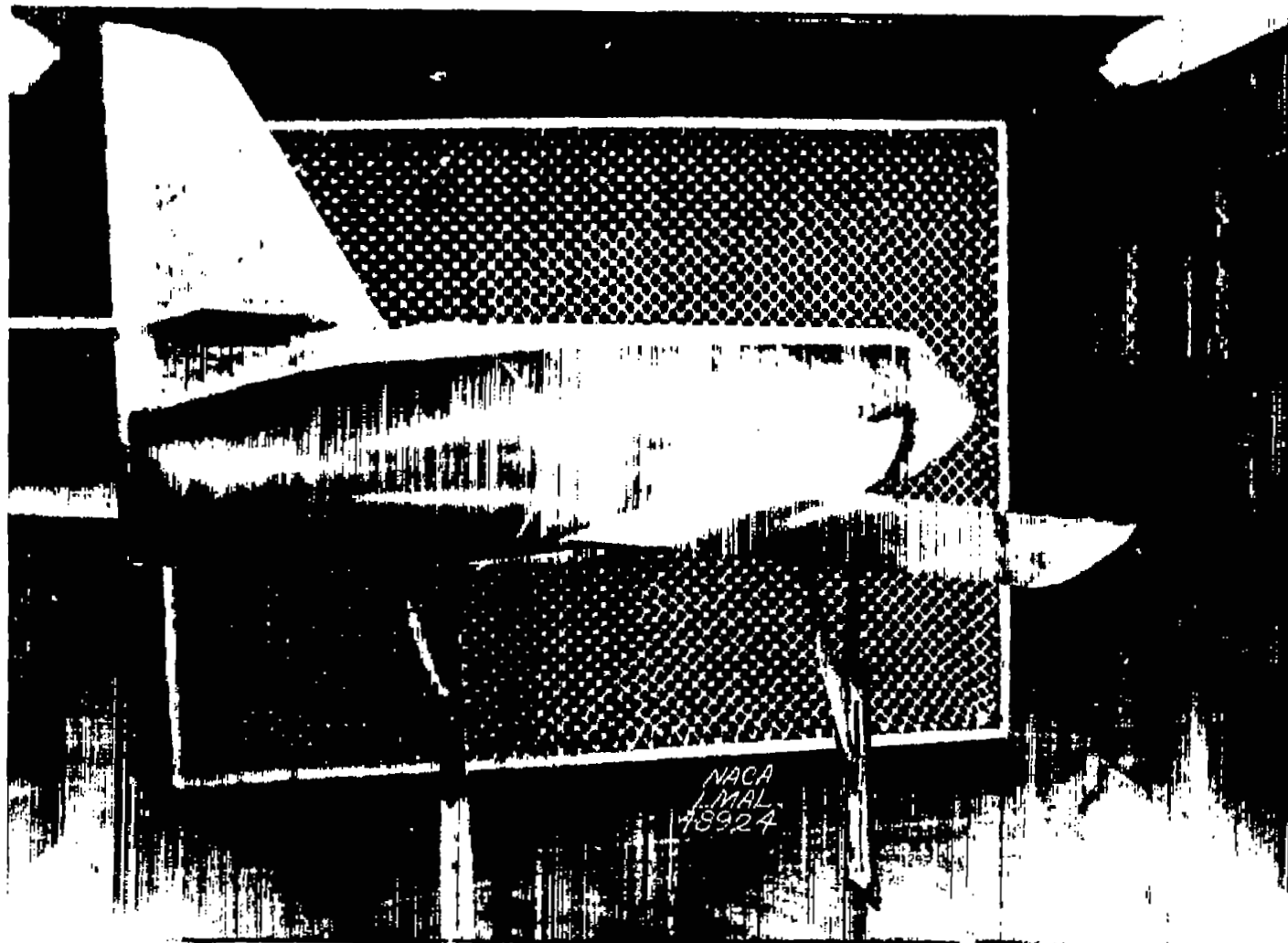
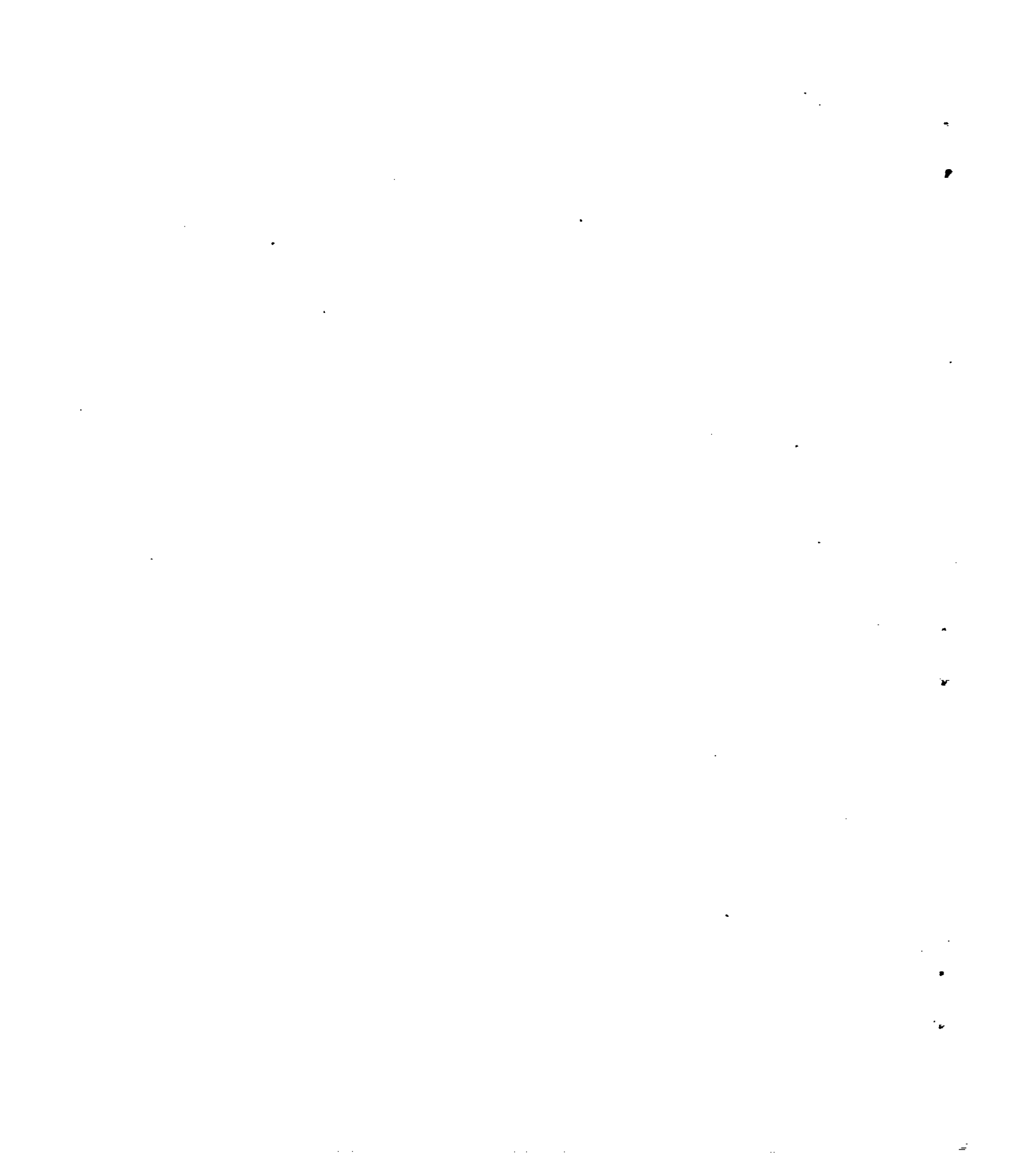


Figure 3.- A three-quarter rear view of the large fuselage model with a 42.8-4.00-0.50 wing mounted in the Langley 300 MPH 7- by 10-foot tunnel. $\delta_{f_s} = 0^{\circ}$; $\delta_{f_n} = 0^{\circ}$; thin steel vertical tail. Turbulence net in tunnel.



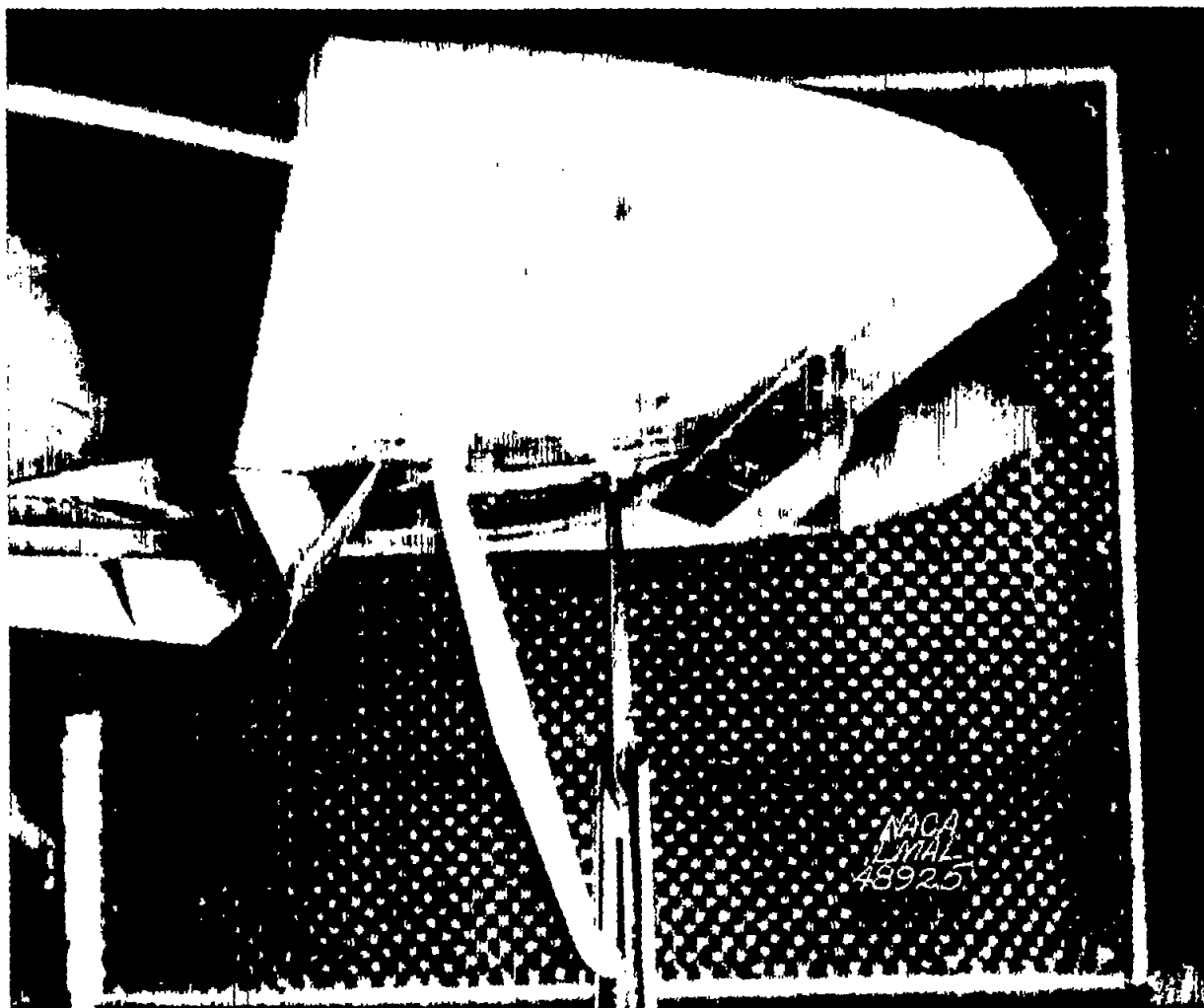
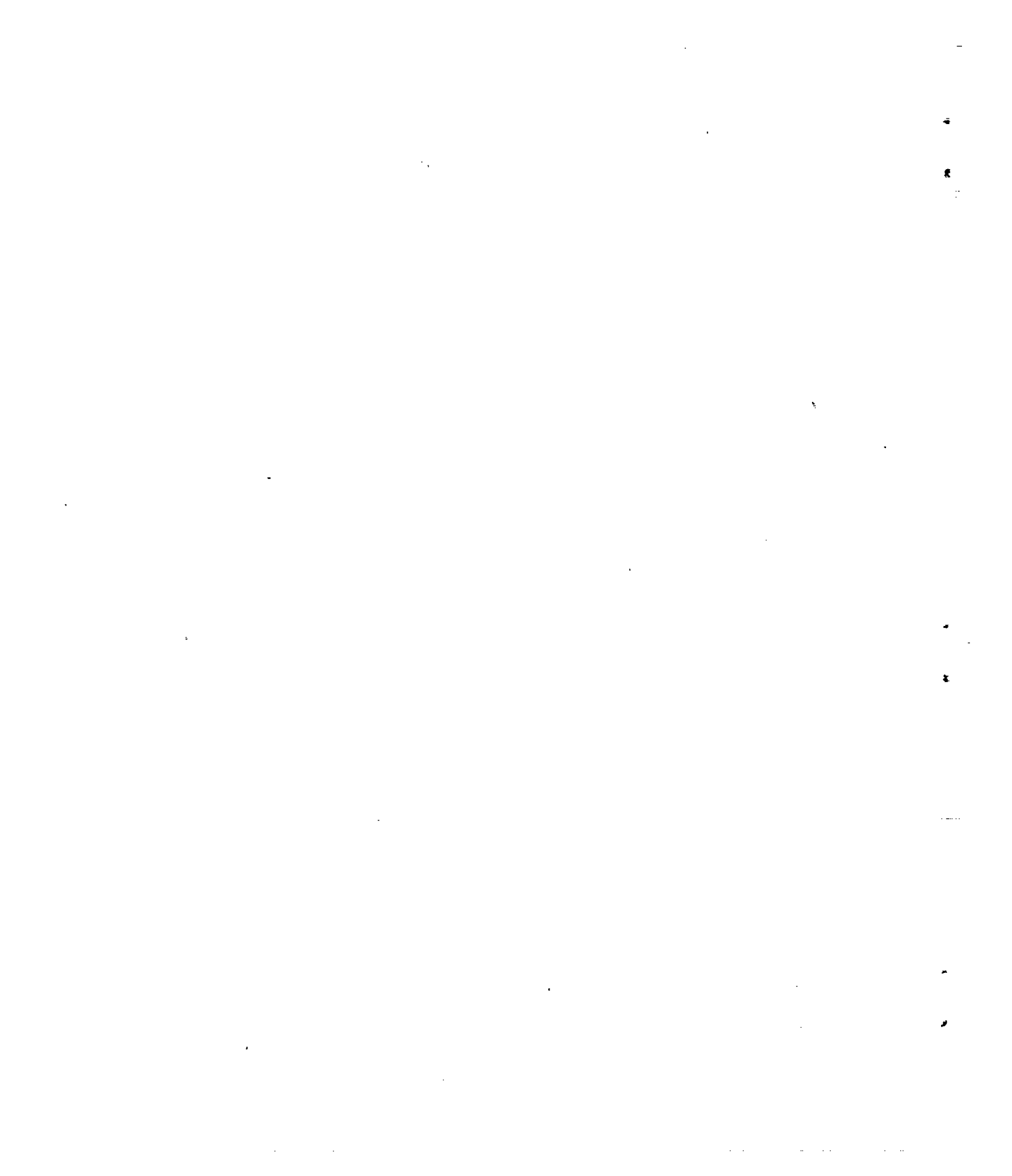
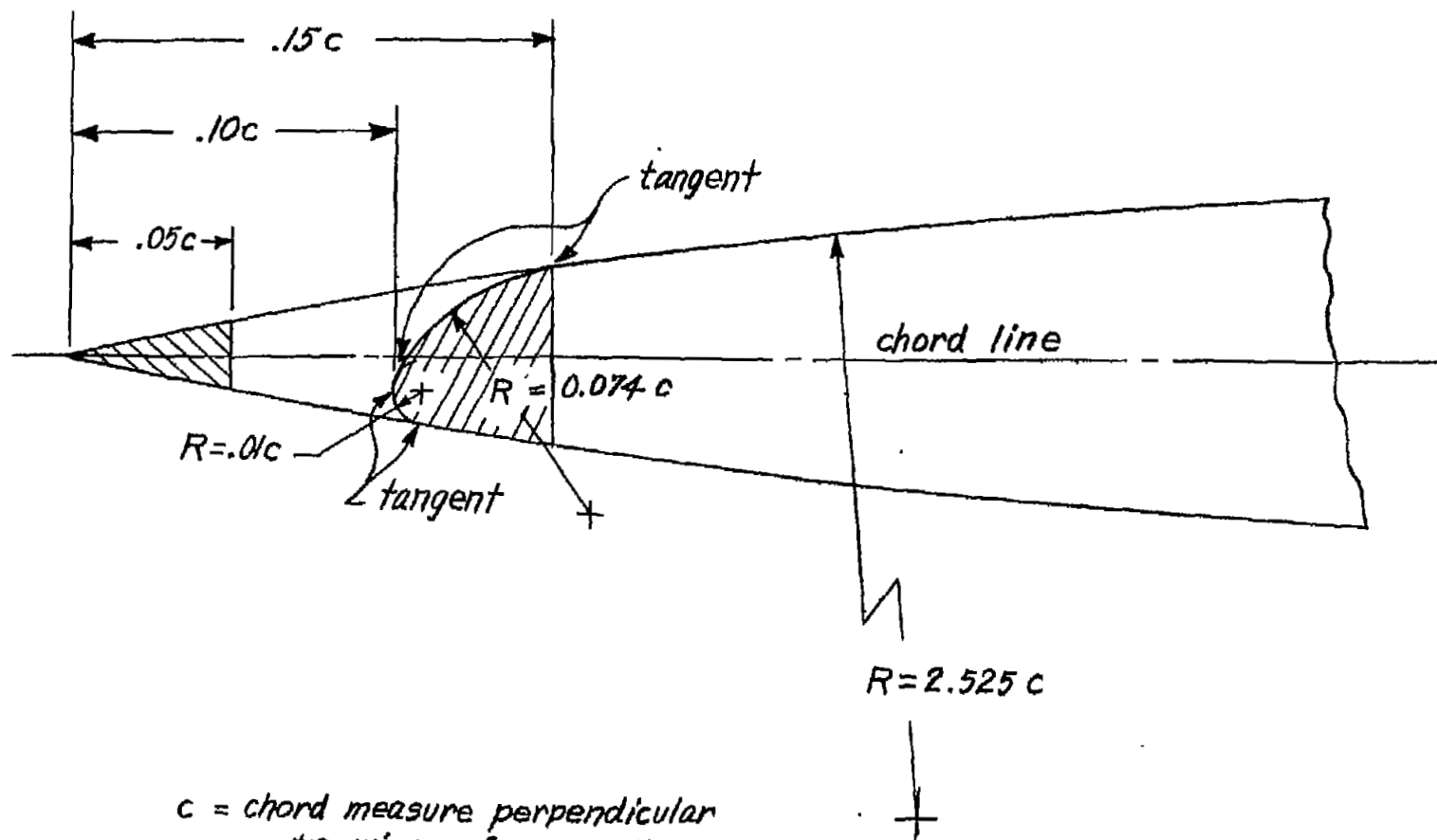


Figure 4.- Split flaps and nose flaps deflected on a model with a 42.8 - 4.00 - 0.50 wing.
 $\delta_{f_s} = 55^\circ$; $\delta_{f_r} = 30^\circ$.

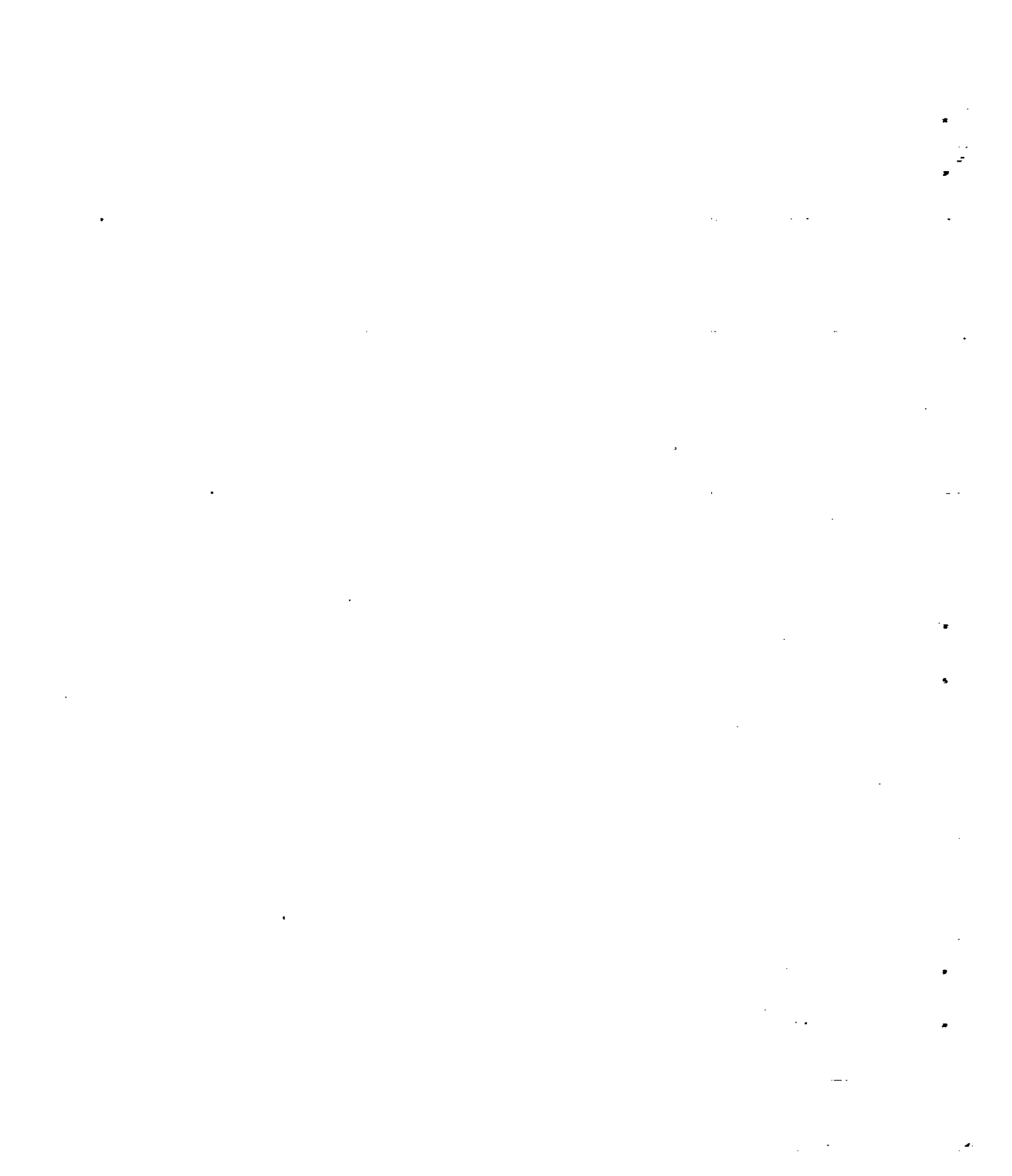




c = chord measure perpendicular
to wing reference line
(see three-view drawing)

NATIONAL ADVISORY
COMMITTEE FOR AERONAUTICS

Figure 5.— Geometric lines of the circular-arc wing nose slot on a model with a 42.8-4.00-0.50 wing.



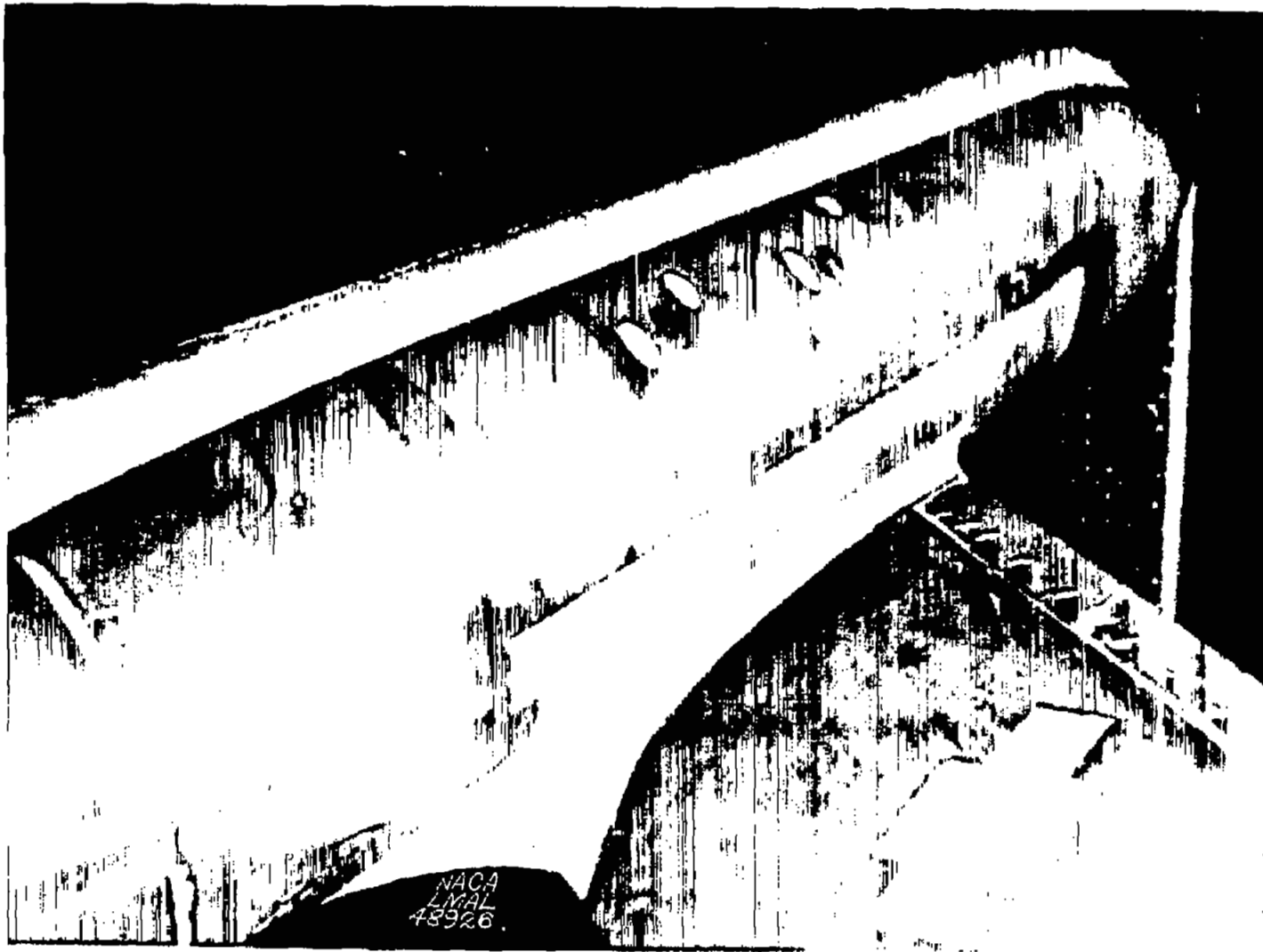
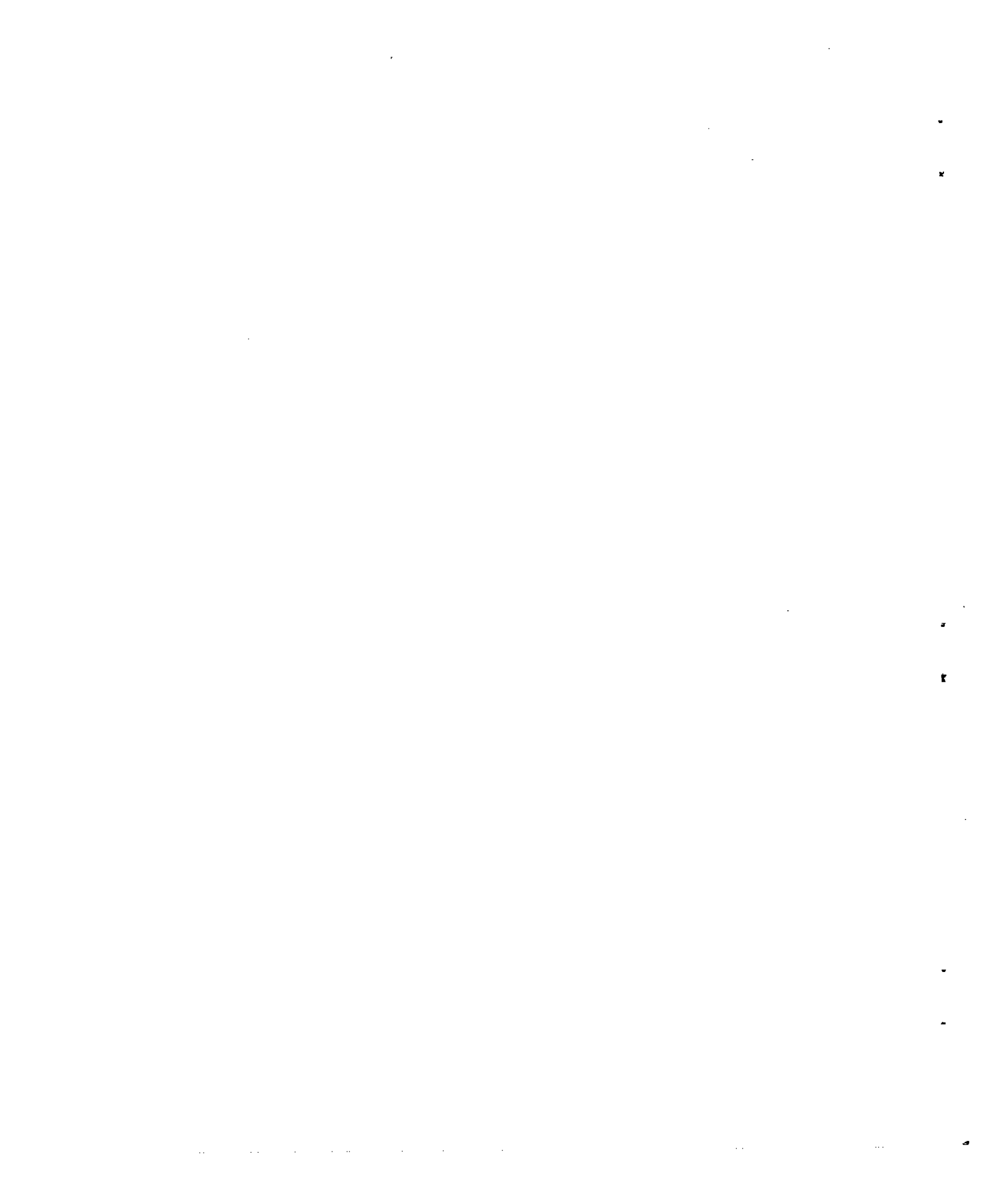


Figure 6.- A photograph of wing fillets tested on a model with a 42.8 - 4.00 - 0.50 wing.



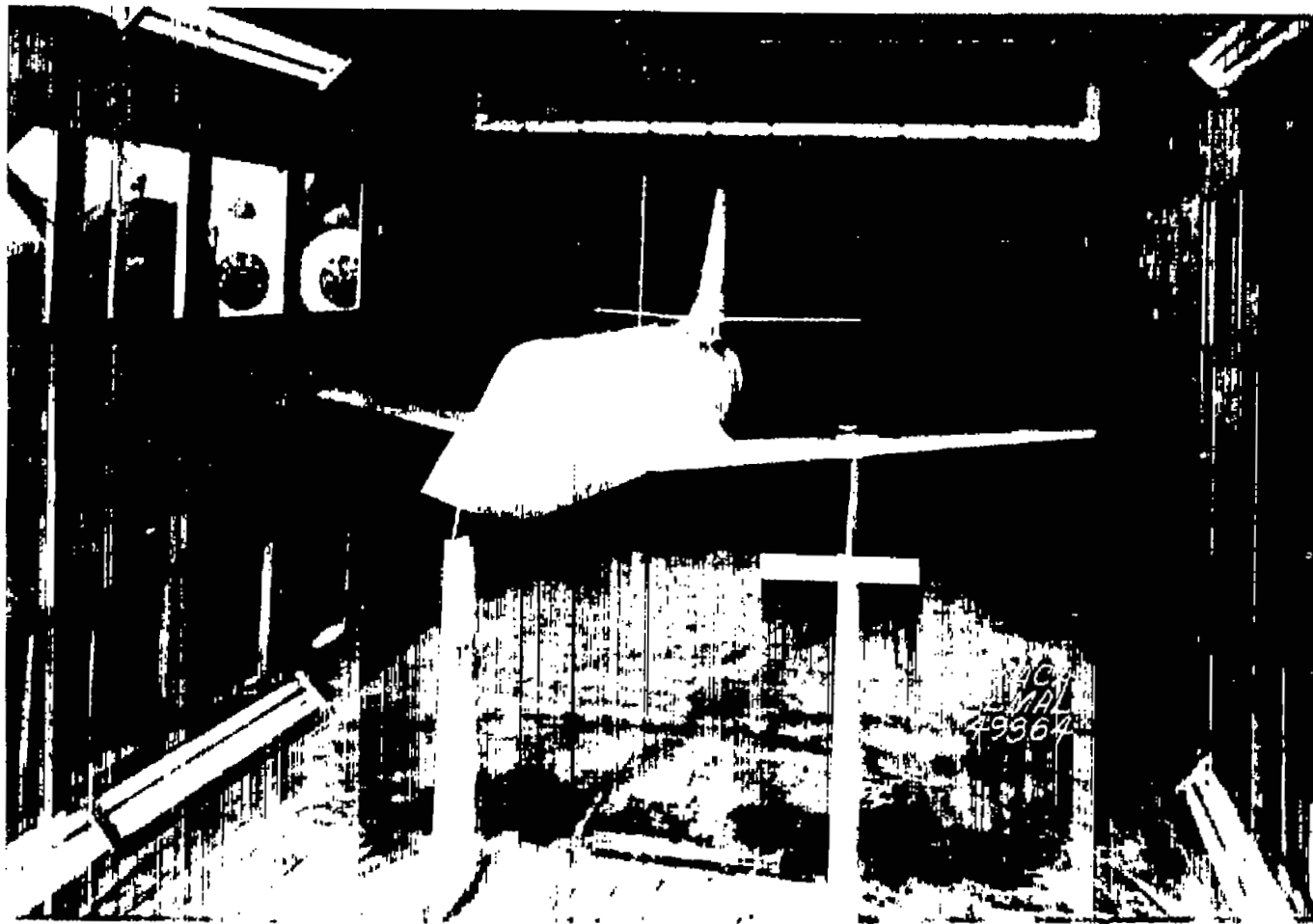
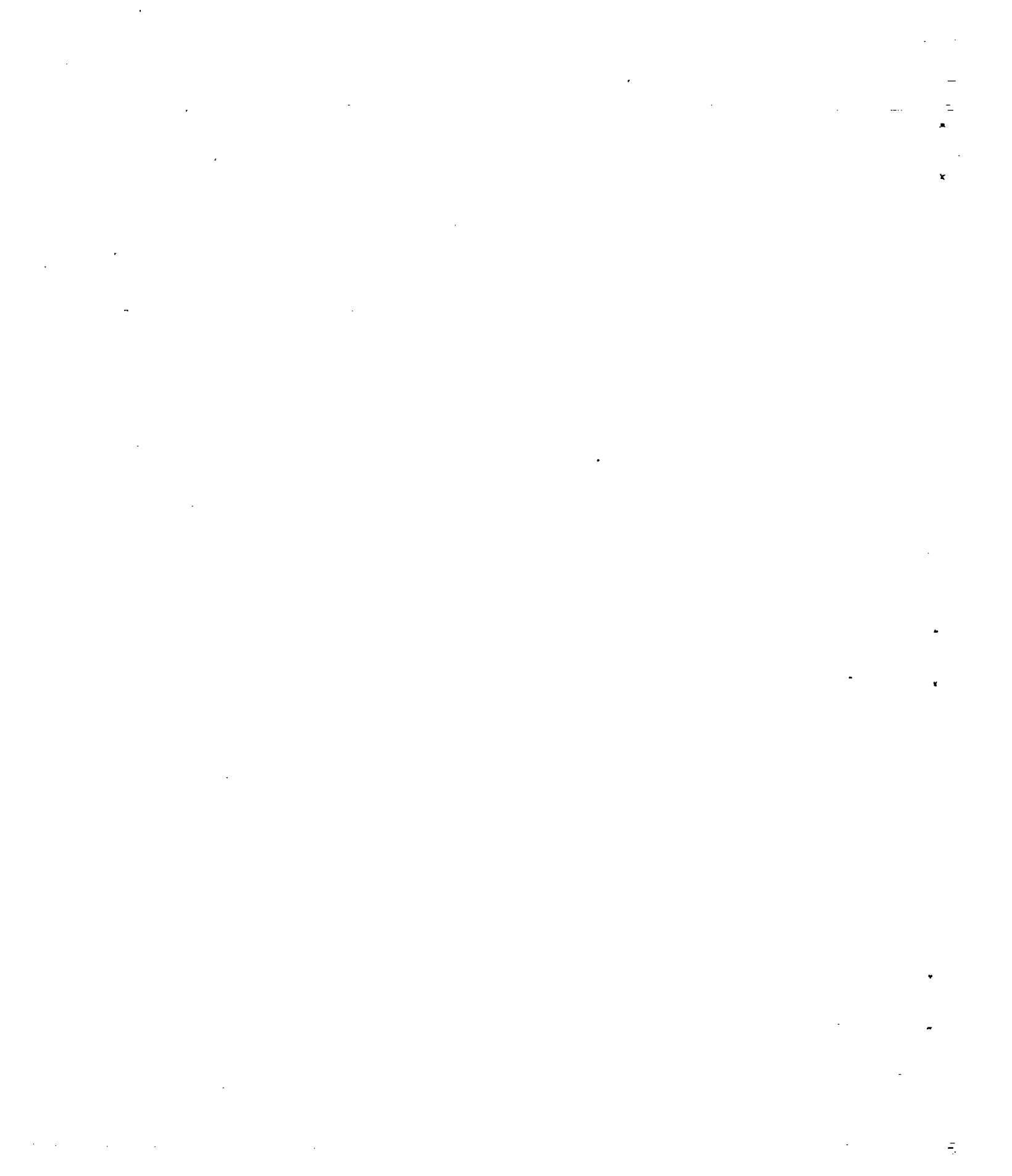


Figure 7.- Photograph of the small fuselage model with a 42.8-4.00-0.50 wing mounted in the Langley 300 MPH 7- by 10-foot tunnel. $\delta_{f_p} = 0^\circ$; $\delta_{f_n} = 0^\circ$.



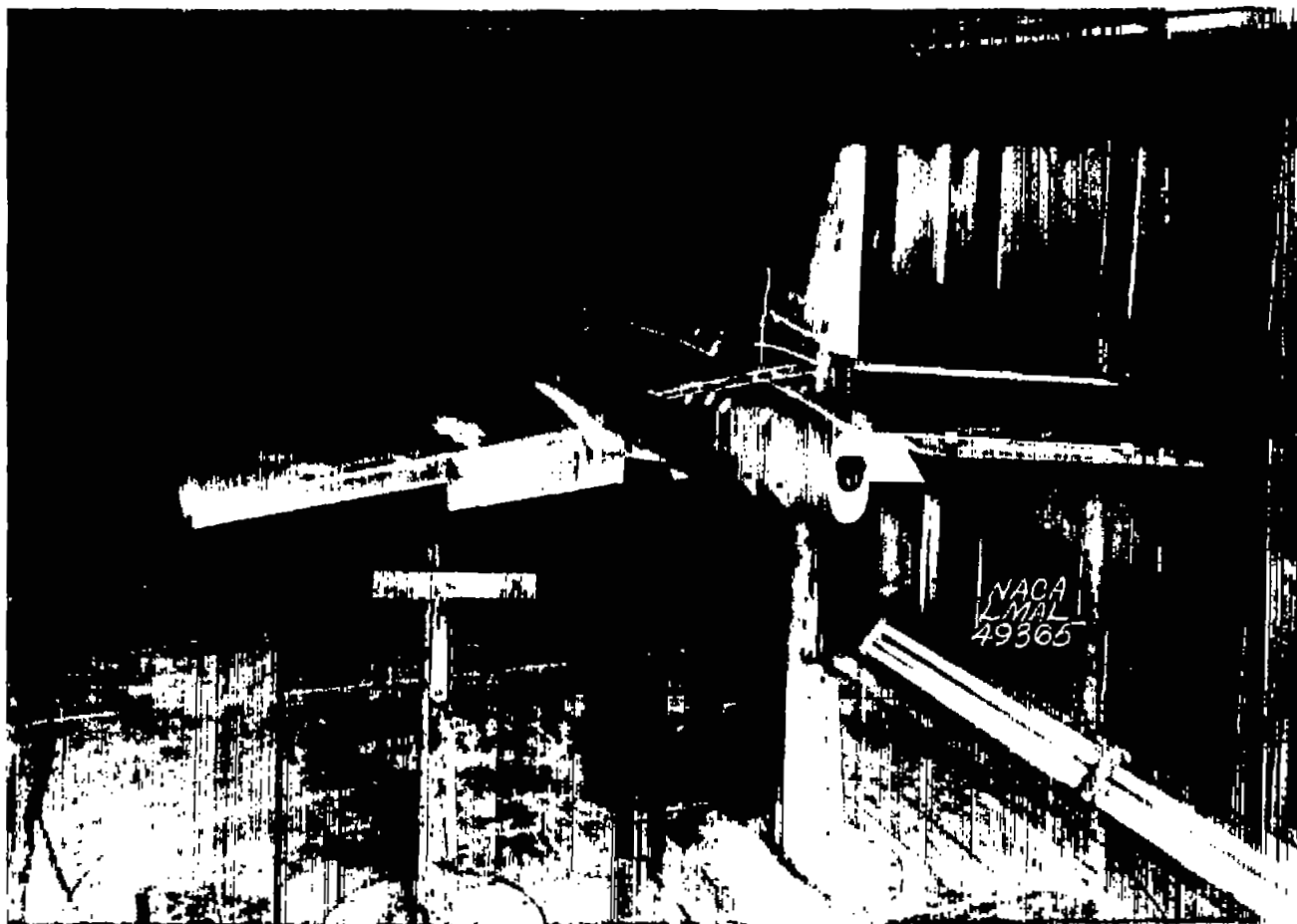
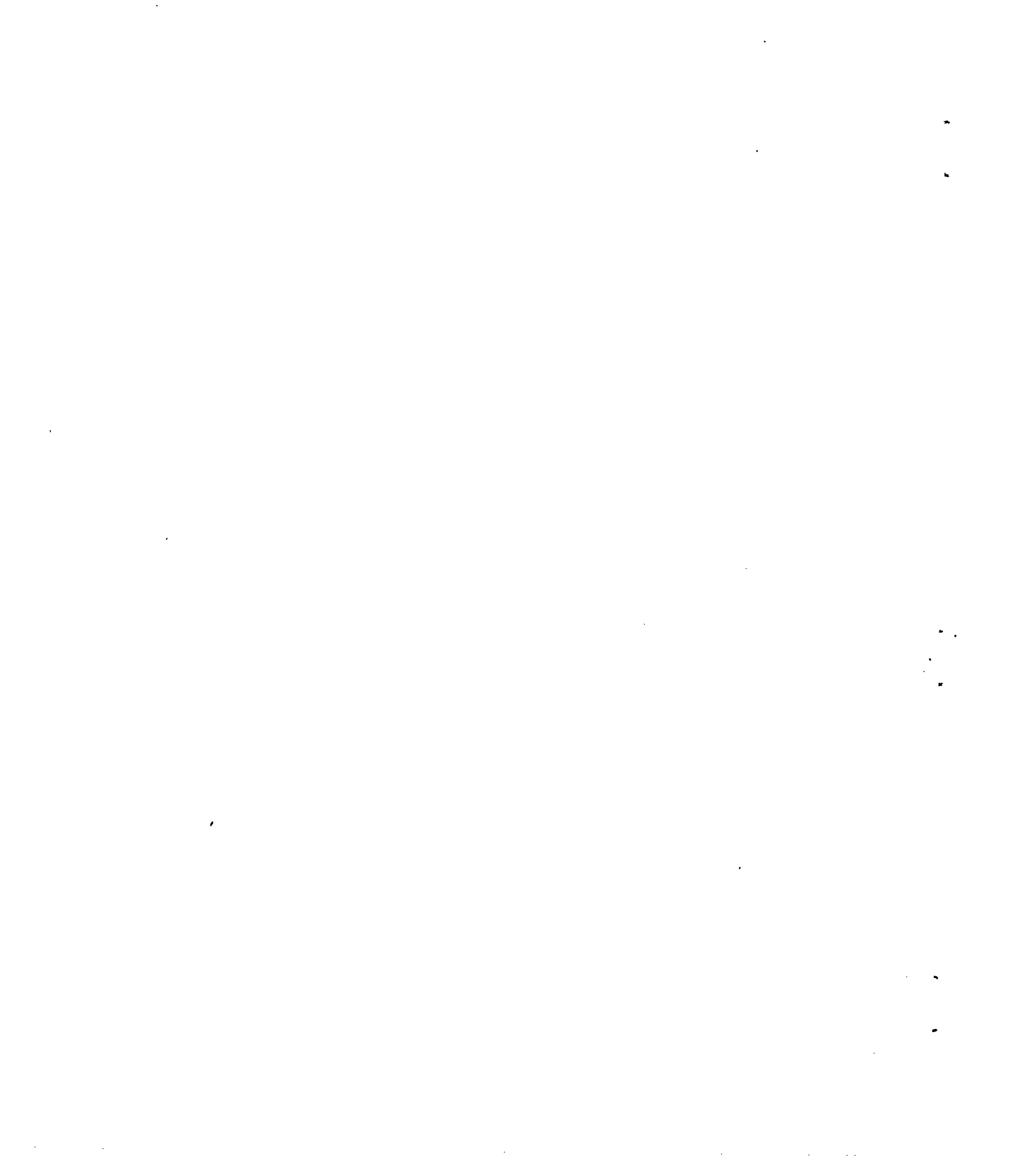


Figure 8.- Photograph of the small fuselage model with a 42.8-4.00-0.50 wing mounted in the Langley 300 MPH 7- by 10-foot tunnel. $\delta_{f_p} = 0^\circ$; $\delta_{f_n} = 0^\circ$.



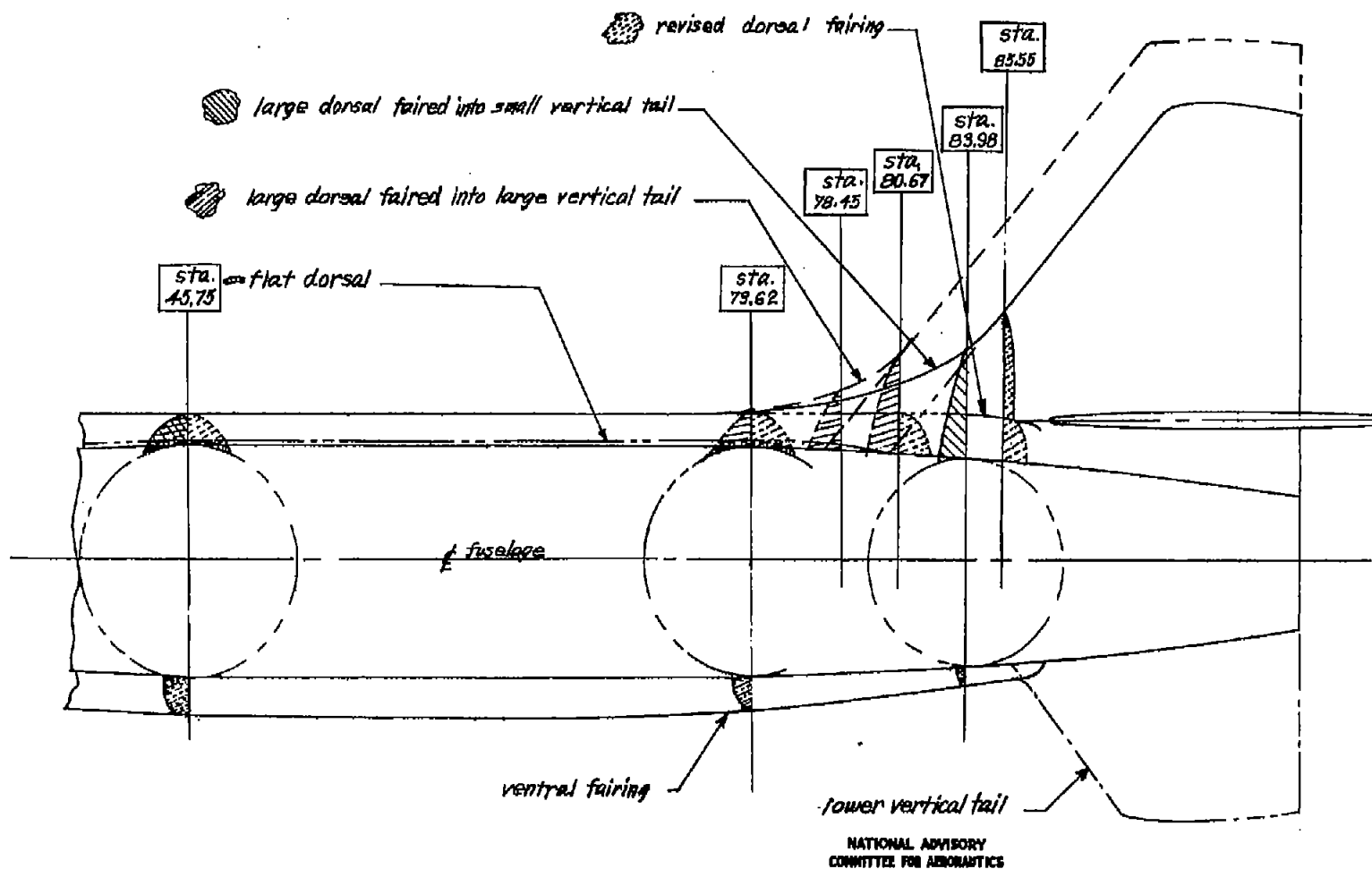
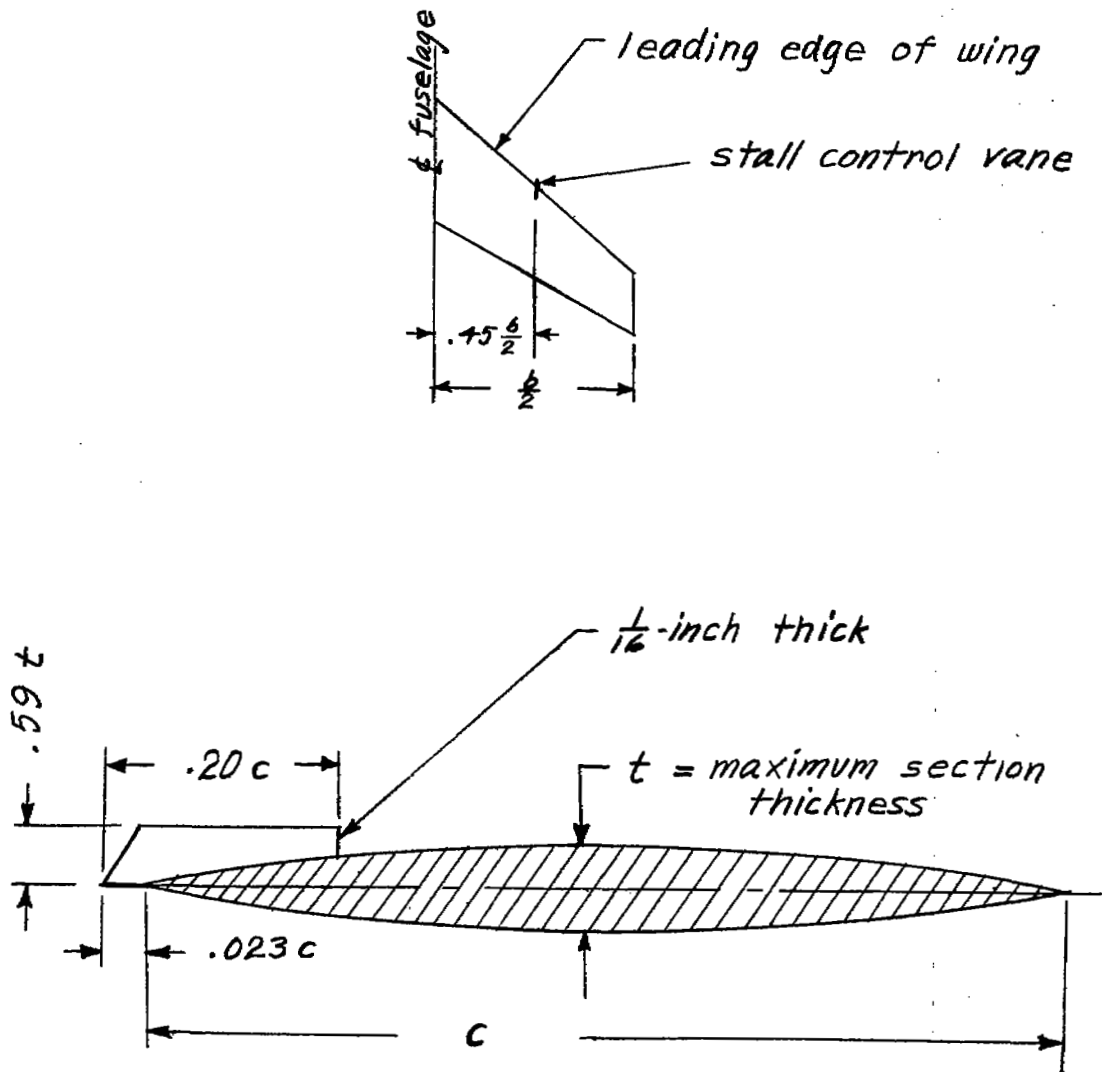


Figure 9.-- The geometric lines of the dorsals and ventrals of a model with a 42.8-4.00-0.50 wing, small fuselage.



NATIONAL ADVISORY
COMMITTEE FOR AERONAUTICS

Figure 10.-- Details of the stall control tested at the 0.45 semispan station on a model with a 42.8-4.00-0.50 wing.

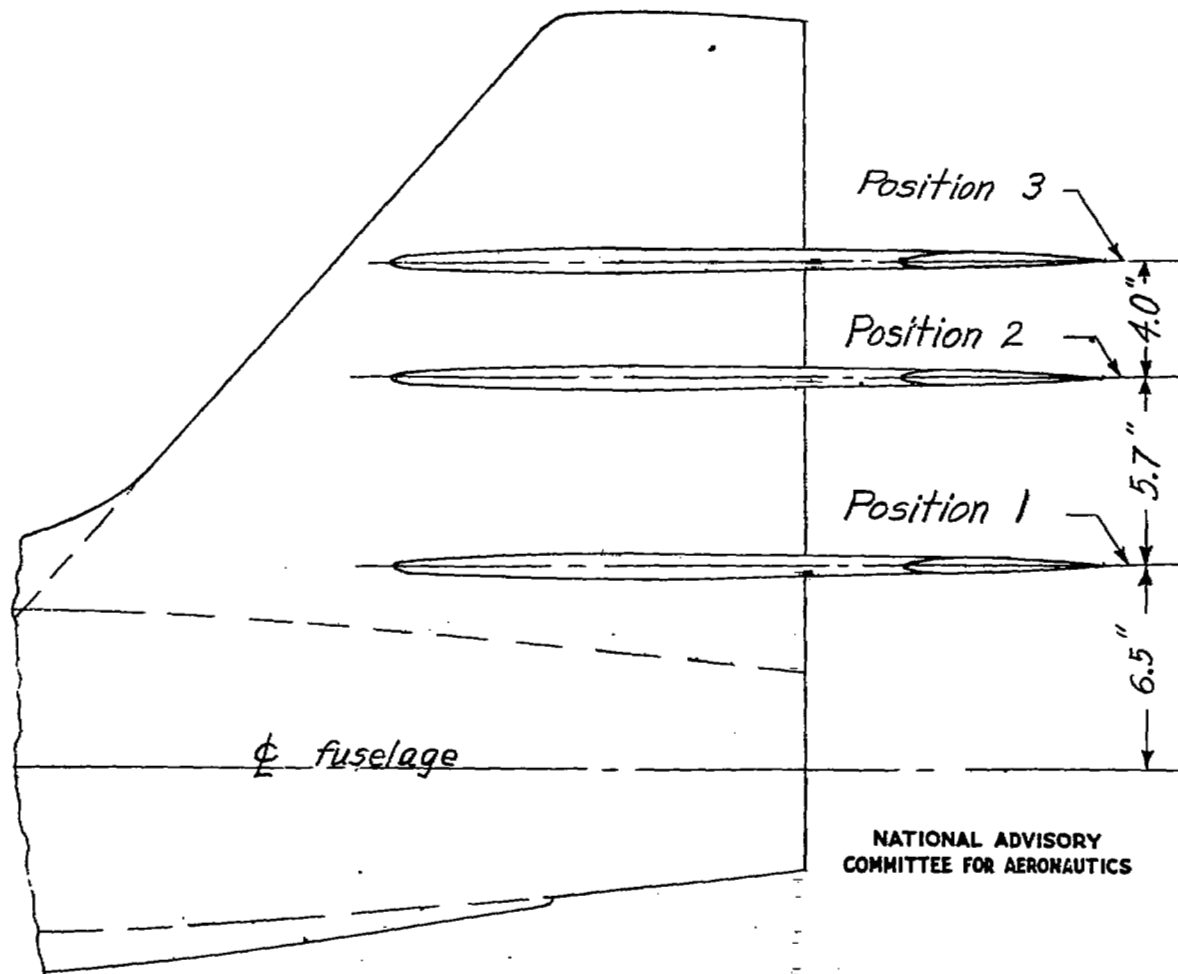


Figure 11.-- Horizontal-tail positions as tested on a model with a 42.8-4.00-0.50 wing.

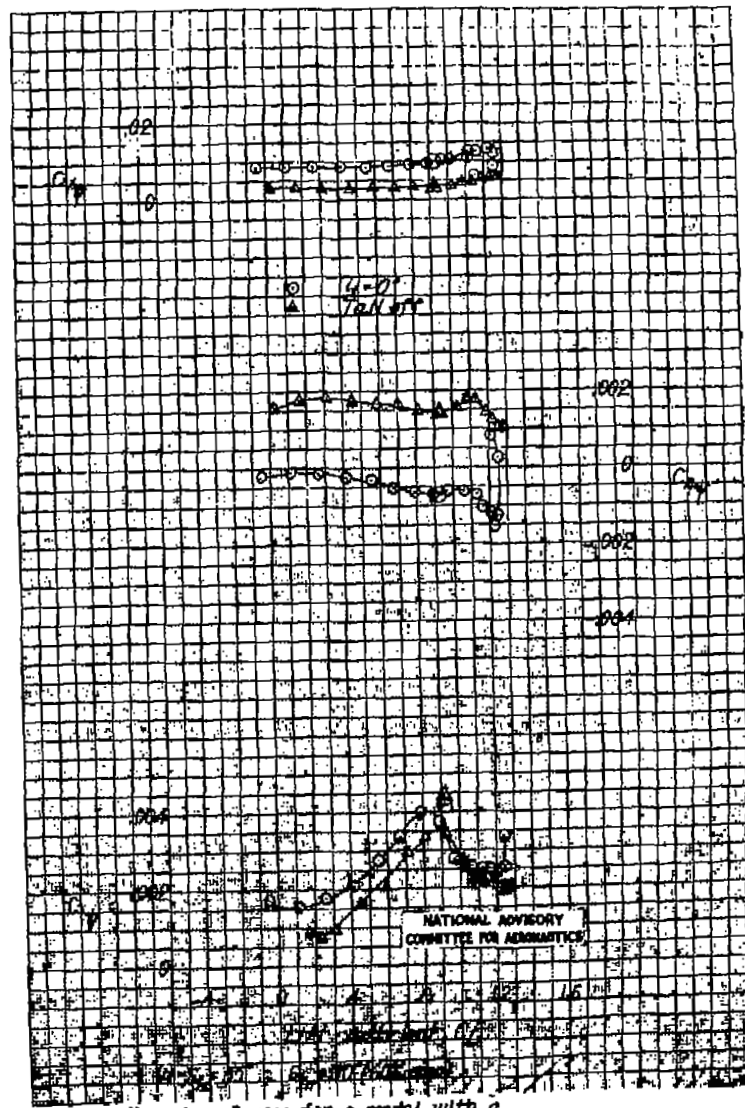
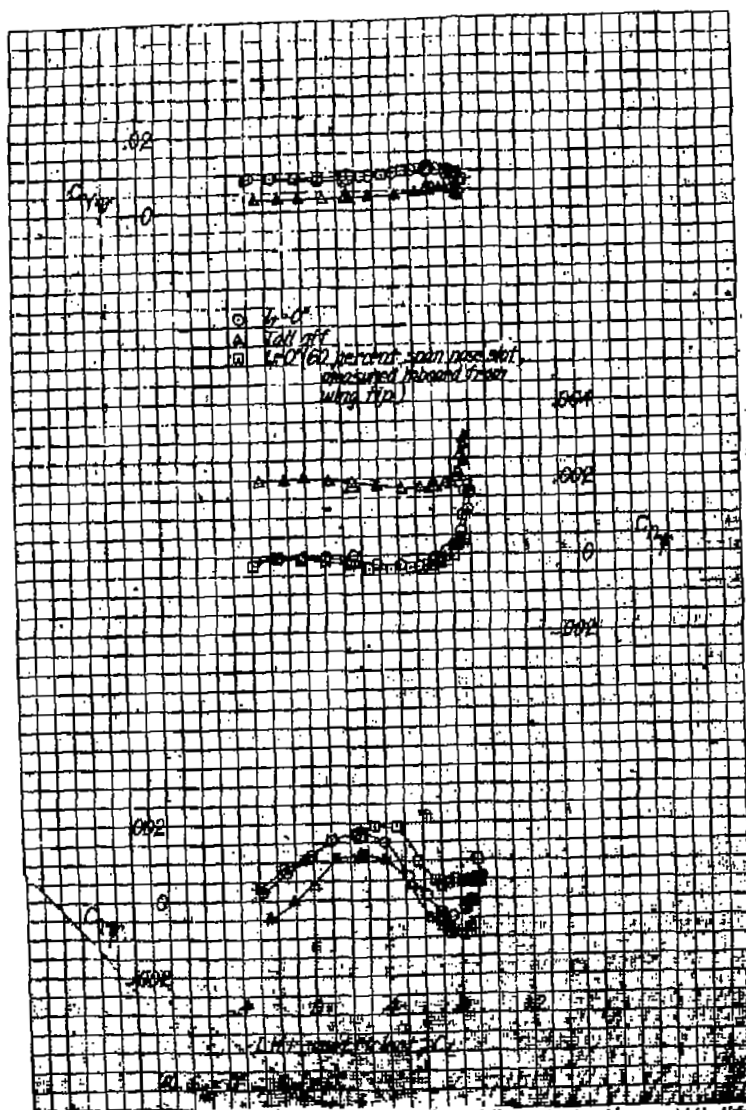
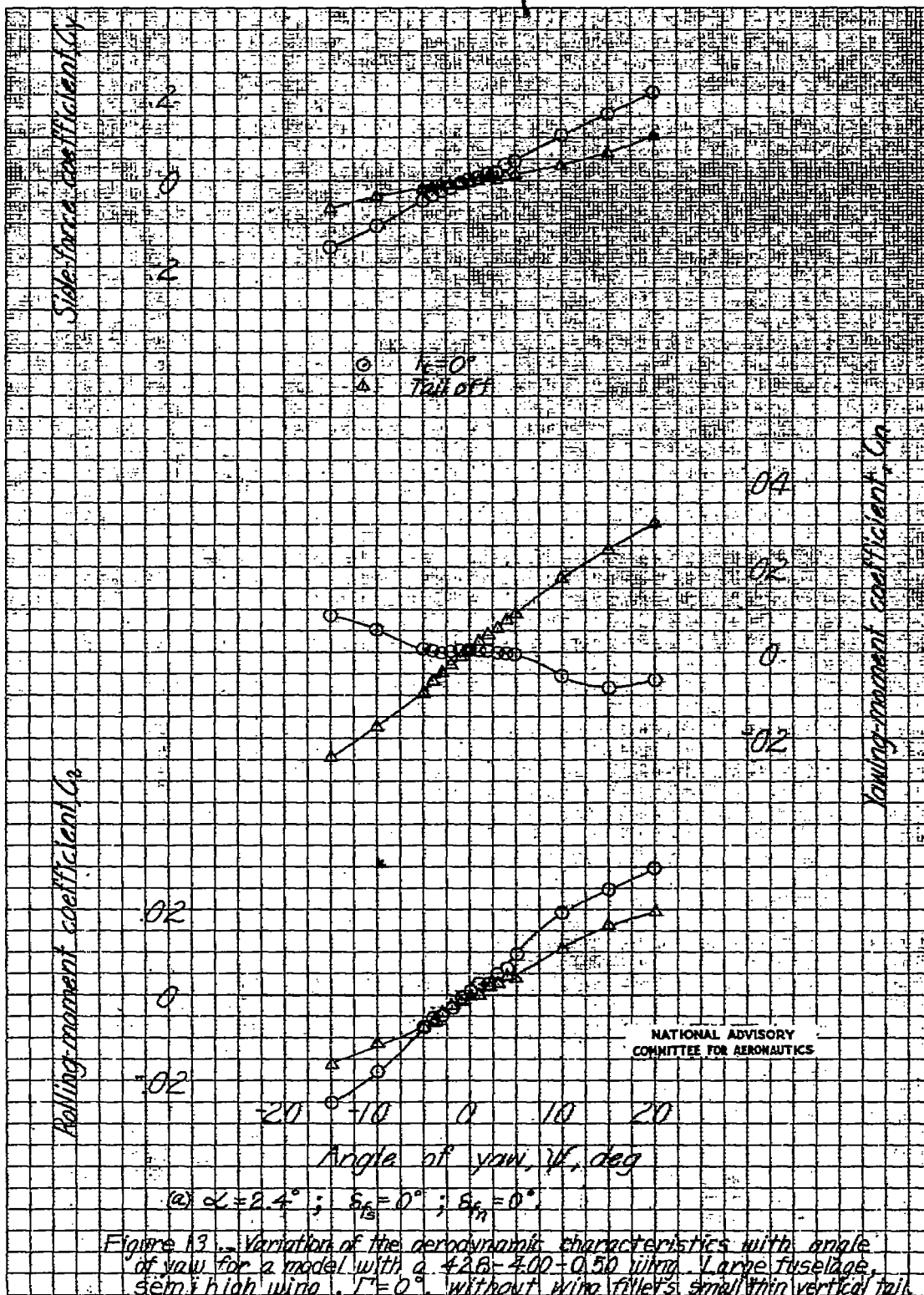
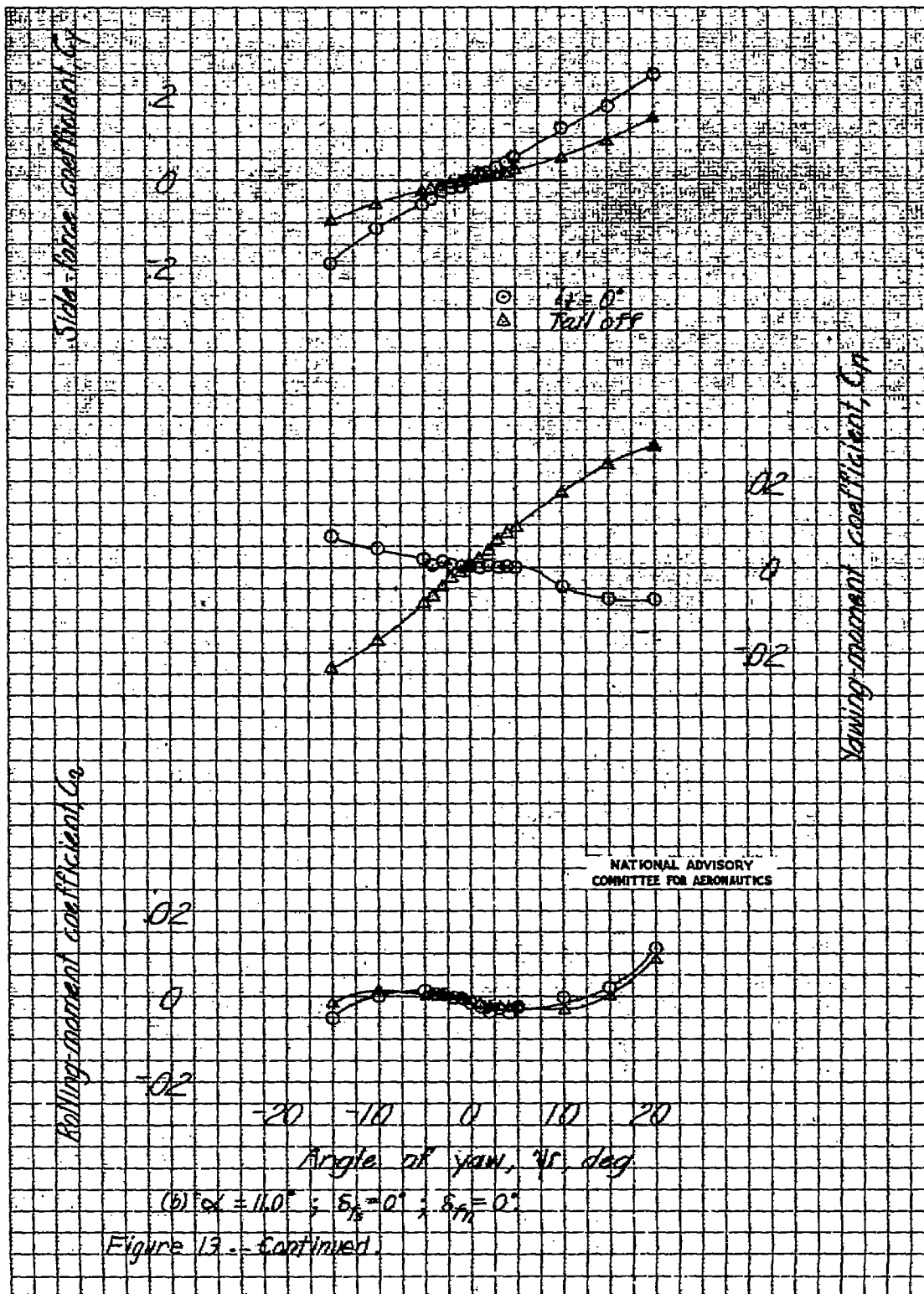
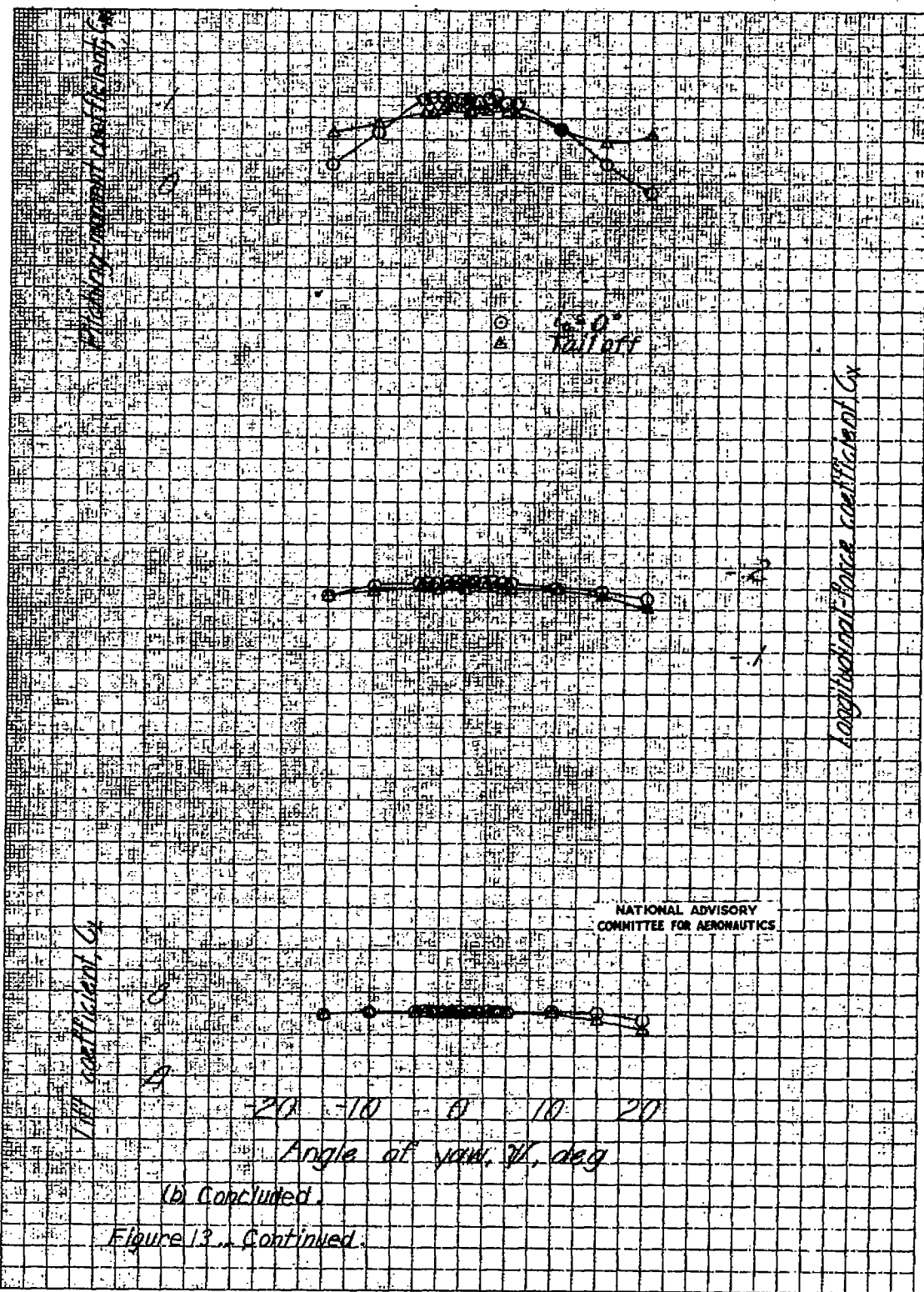


Figure 12. Variation of lateral stability derivatives with lift coefficient at small angles of yaw for a model with a 42.5-4.00-0.50 wing. Large fuselage, semihigh wing, $\gamma=0^\circ$, without wing fillets, small thin vertical tail.



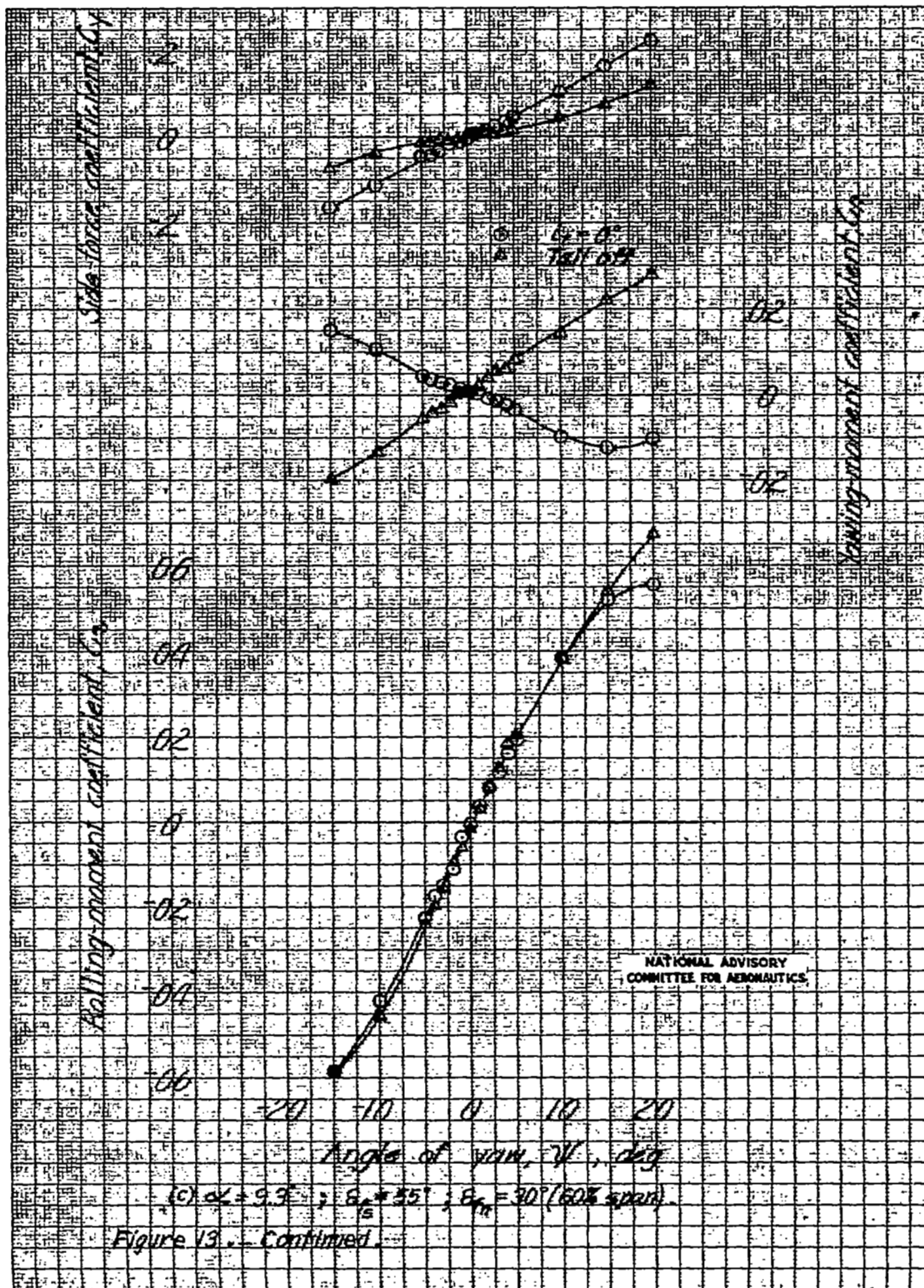


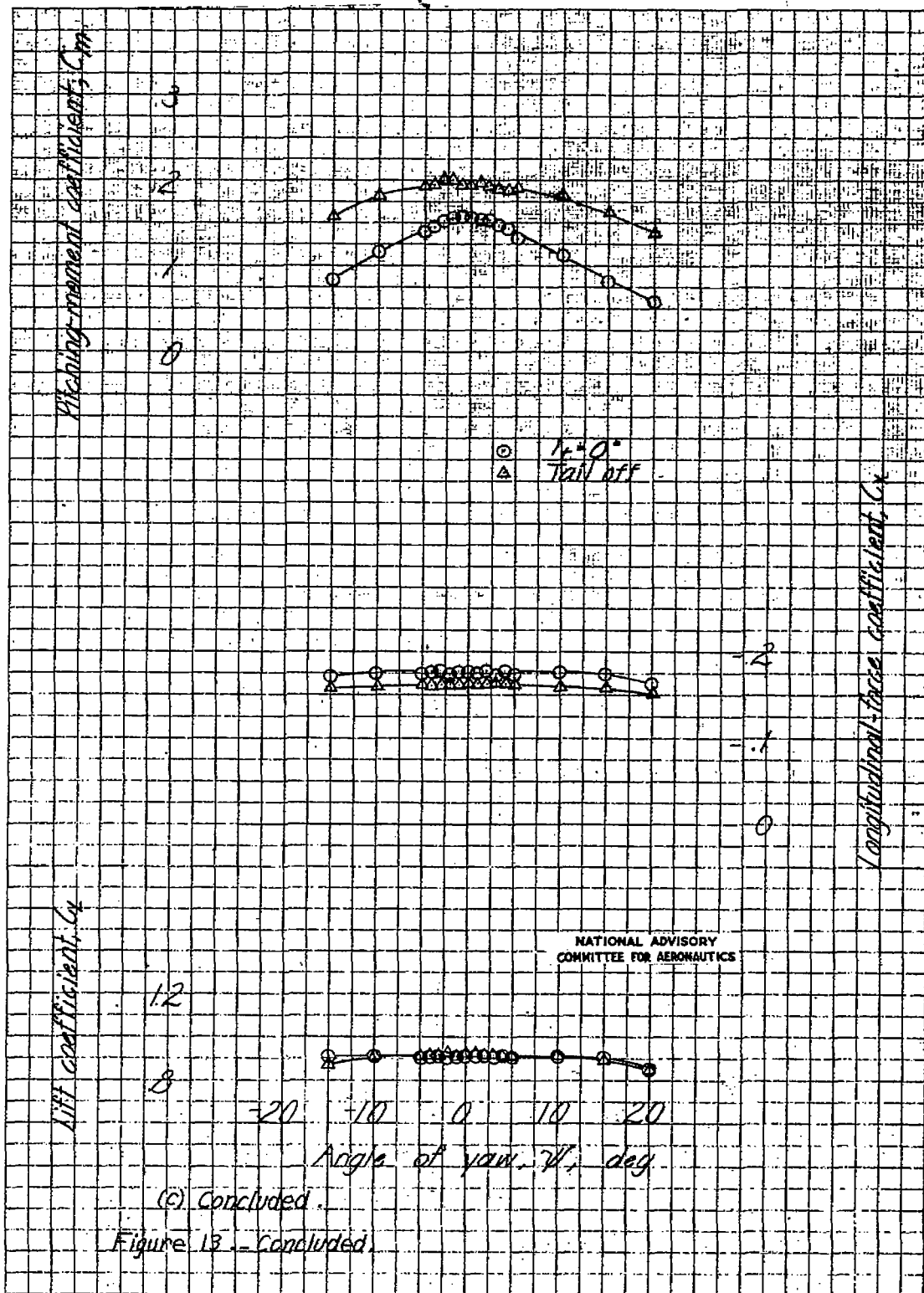


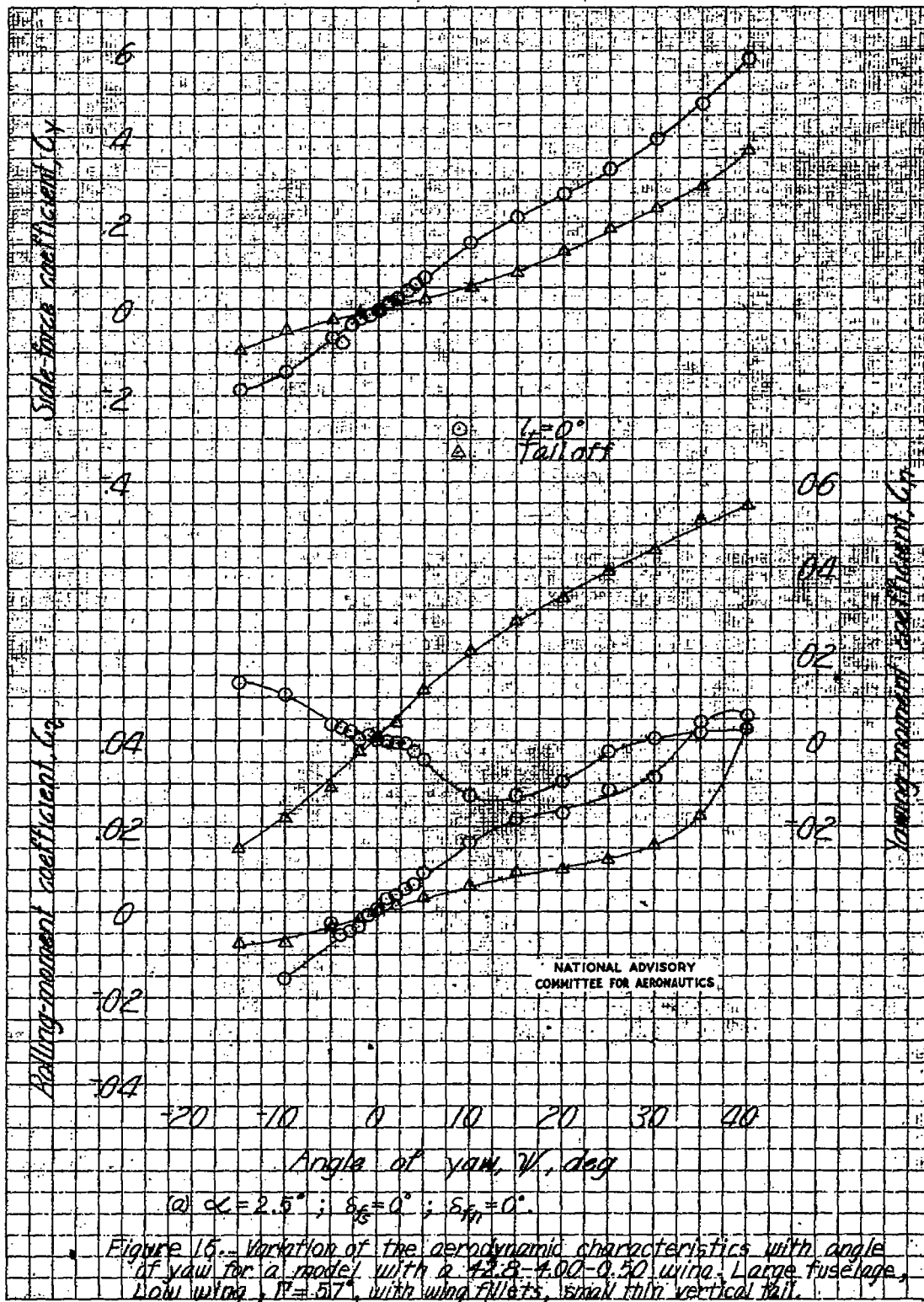


(b) Concluded.

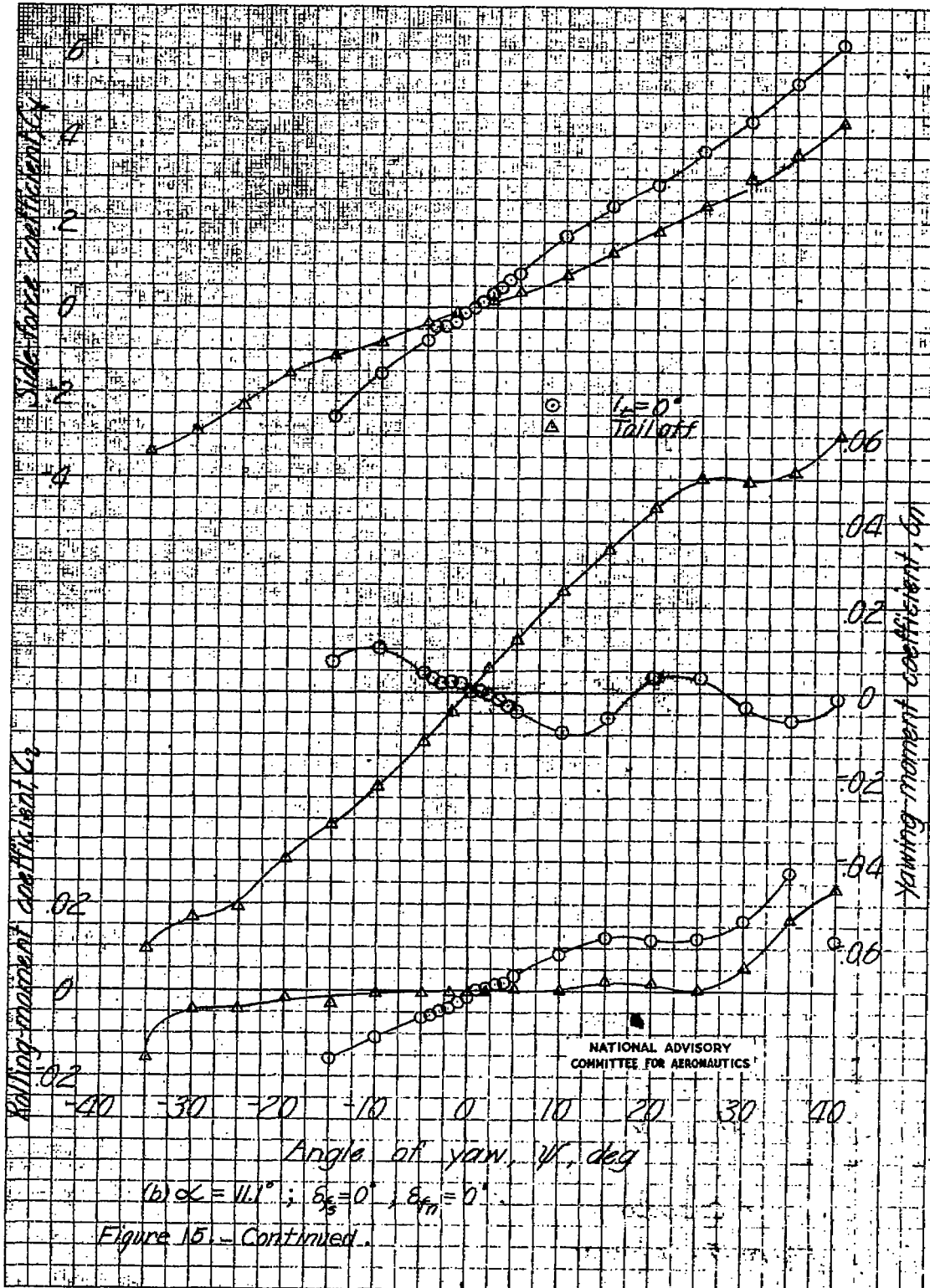
Figure 13, Continued.

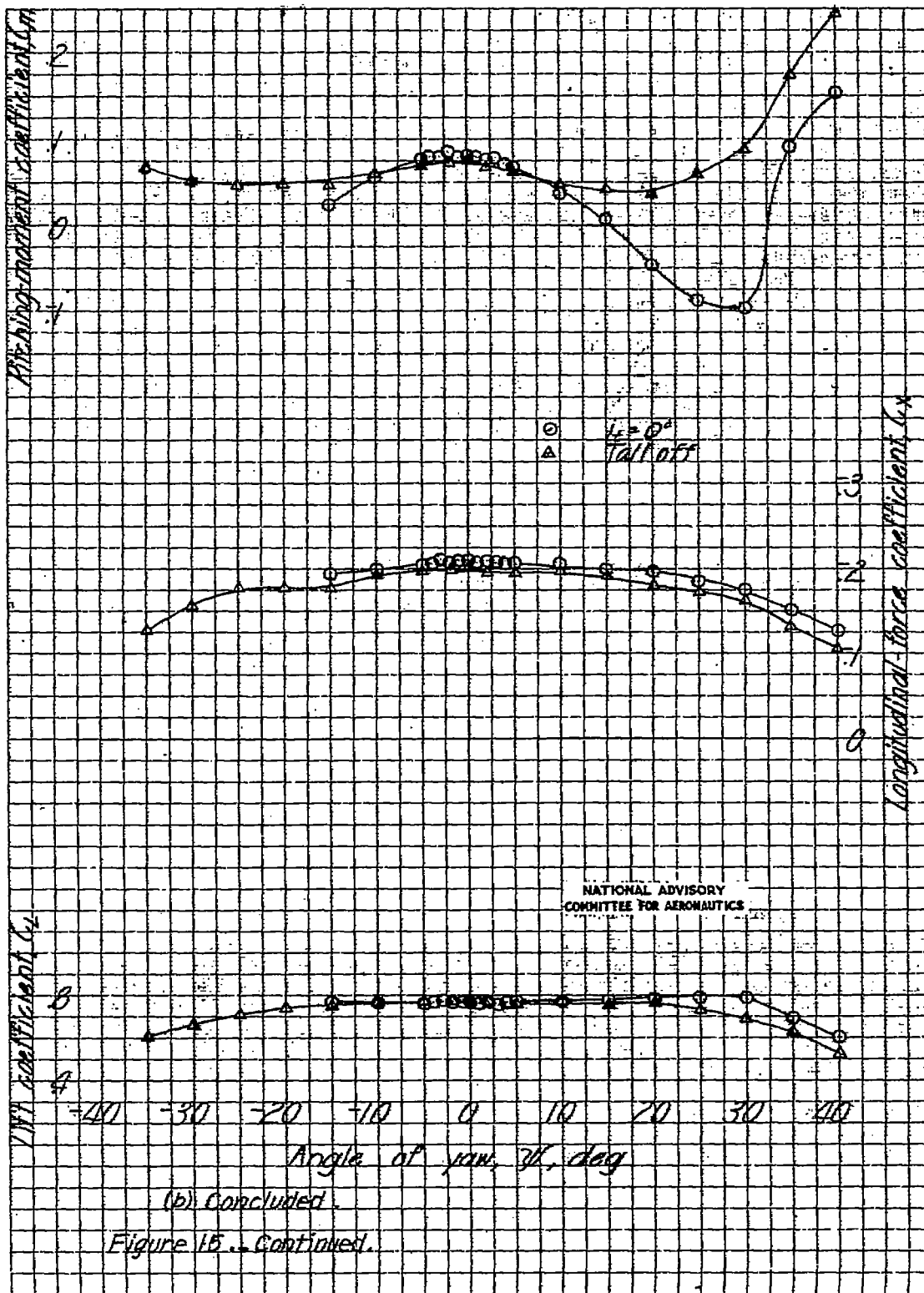


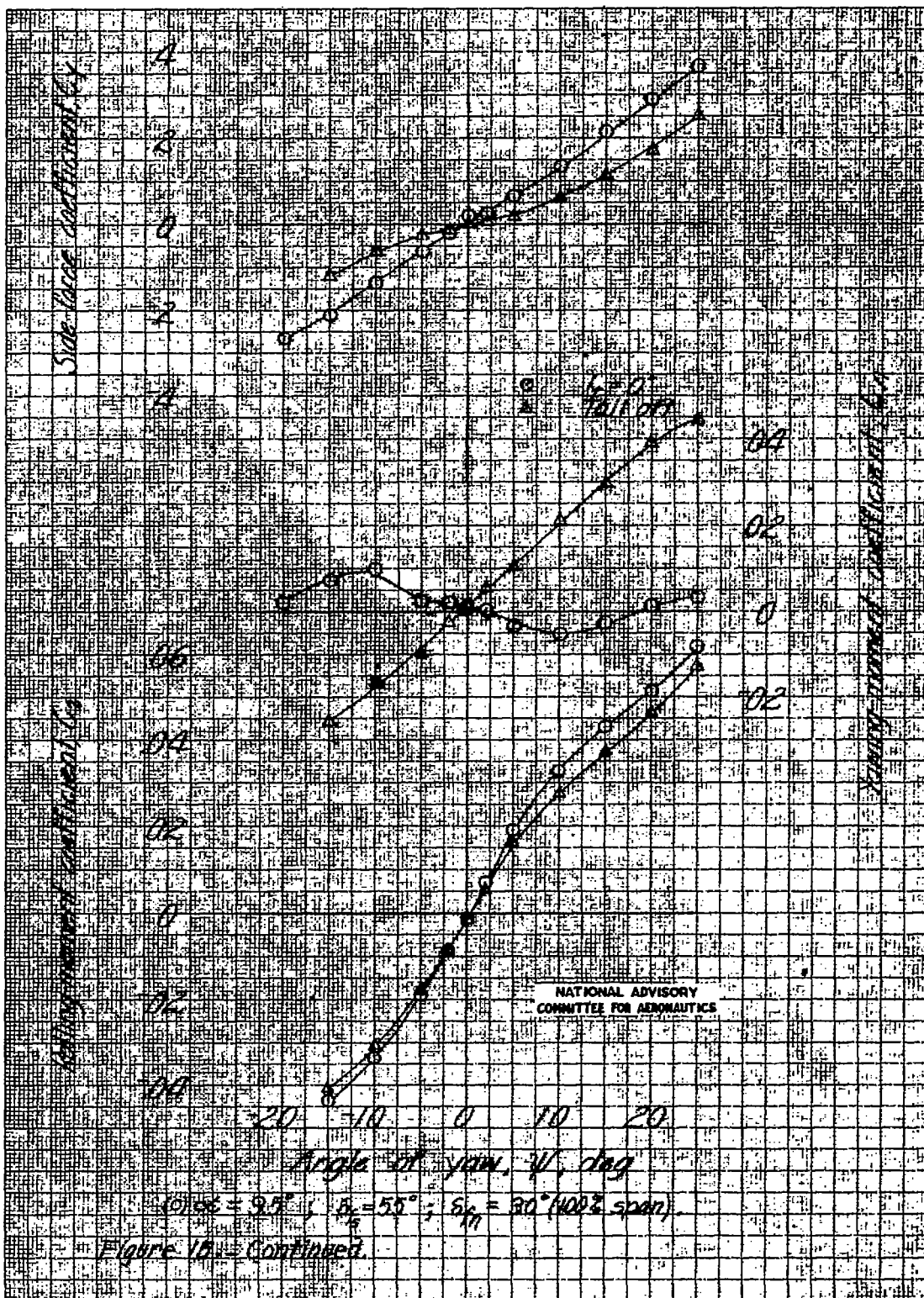


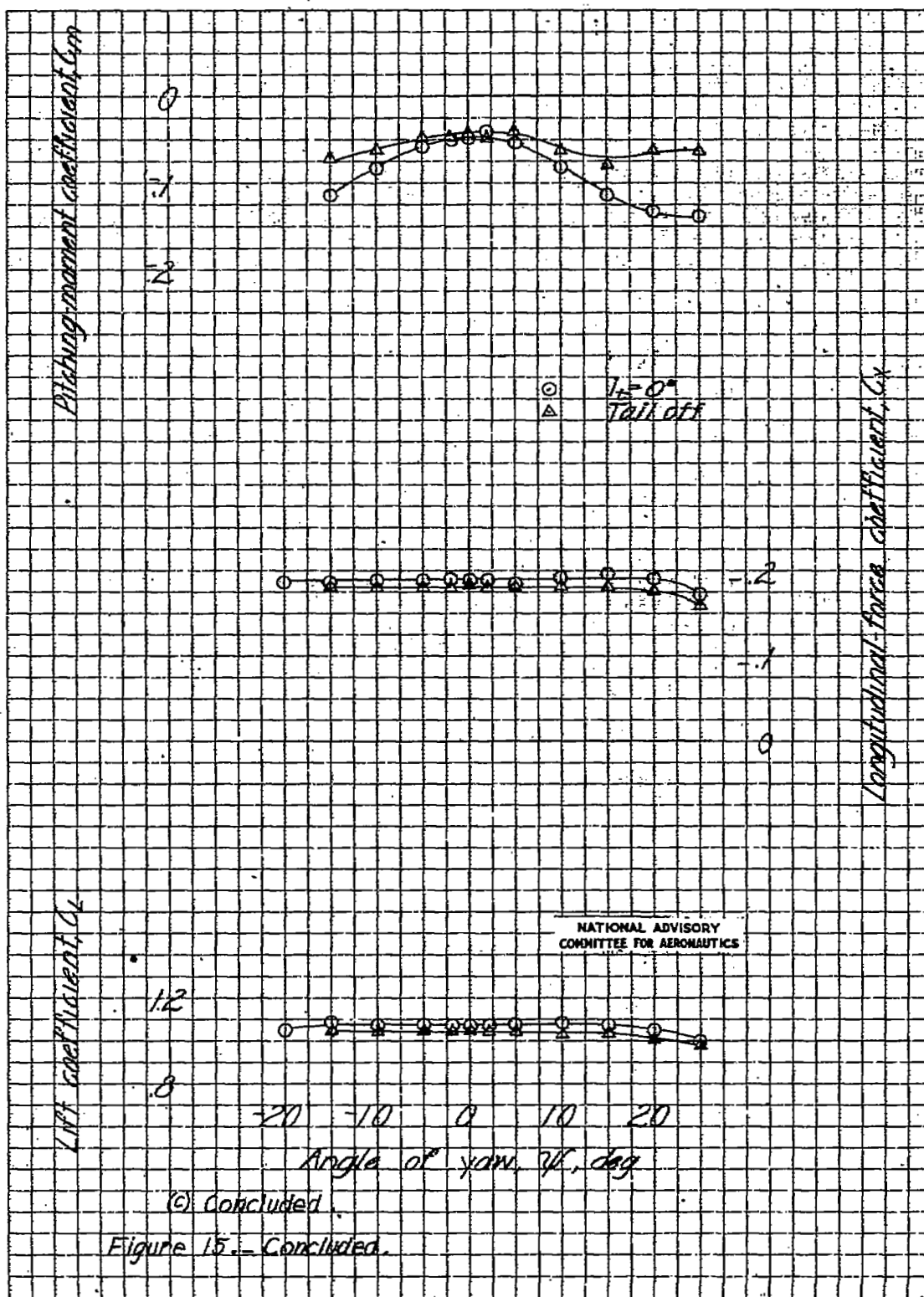












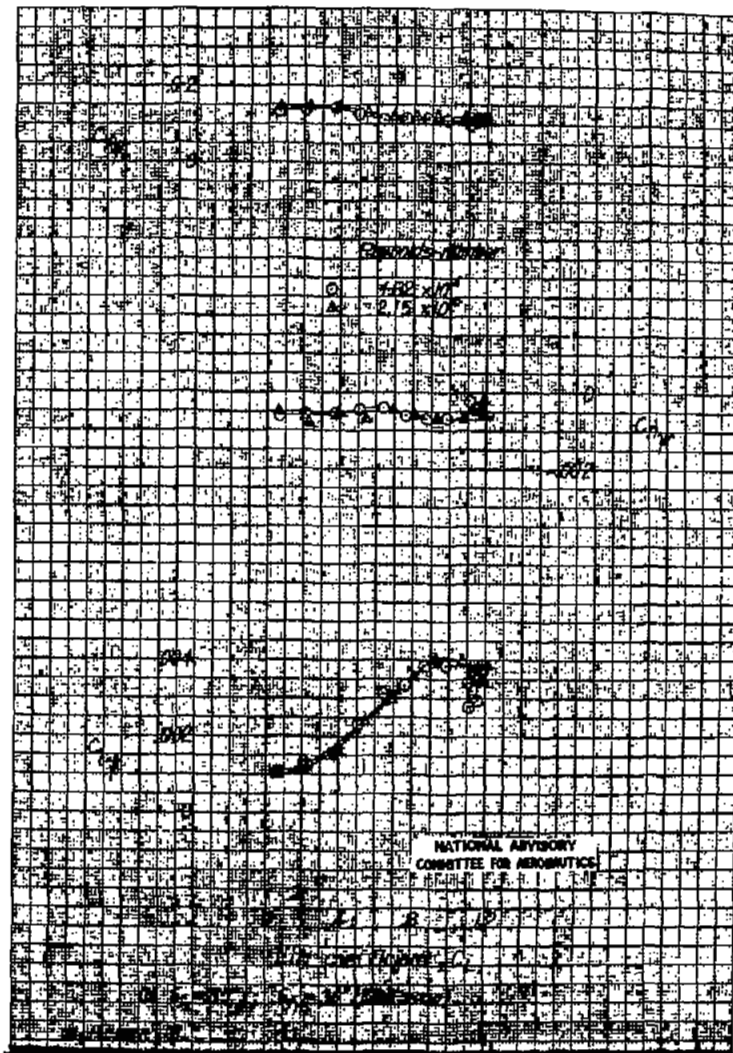
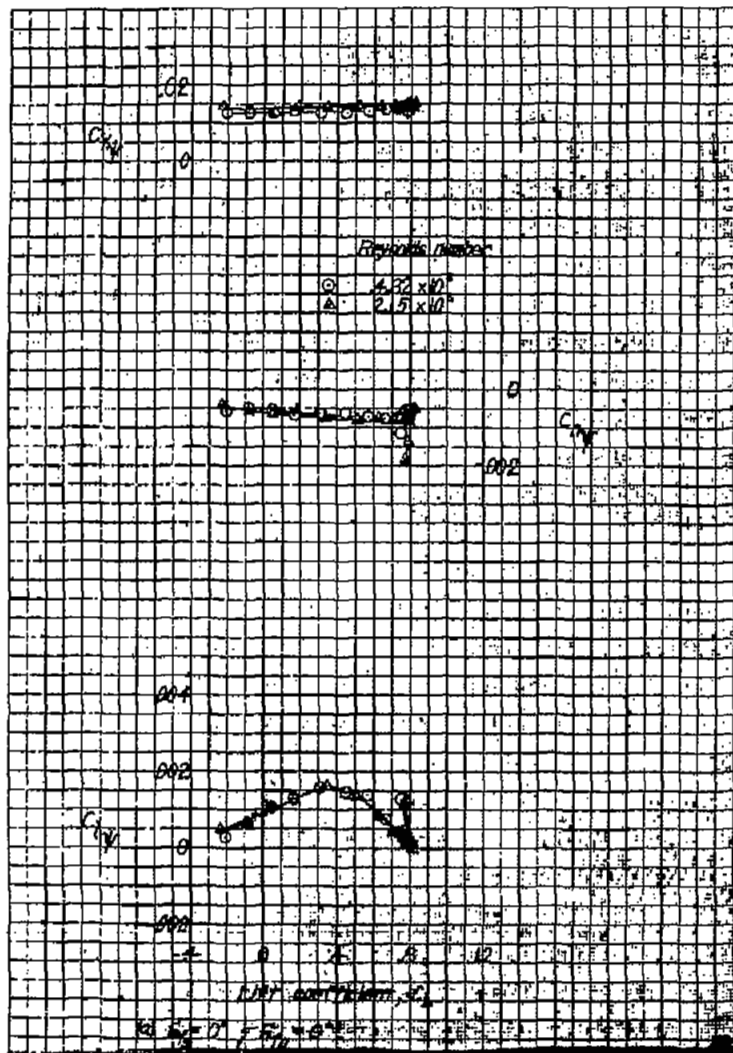


Figure 16.—Effect of Reynolds number of the lateral-stability derivatives with lift coefficient at small angles of yaw for a model with a 42.8-4.00-0.50 wing. Large fuselage, low wing, $\Gamma = 5.7^\circ$, with wing fillers.

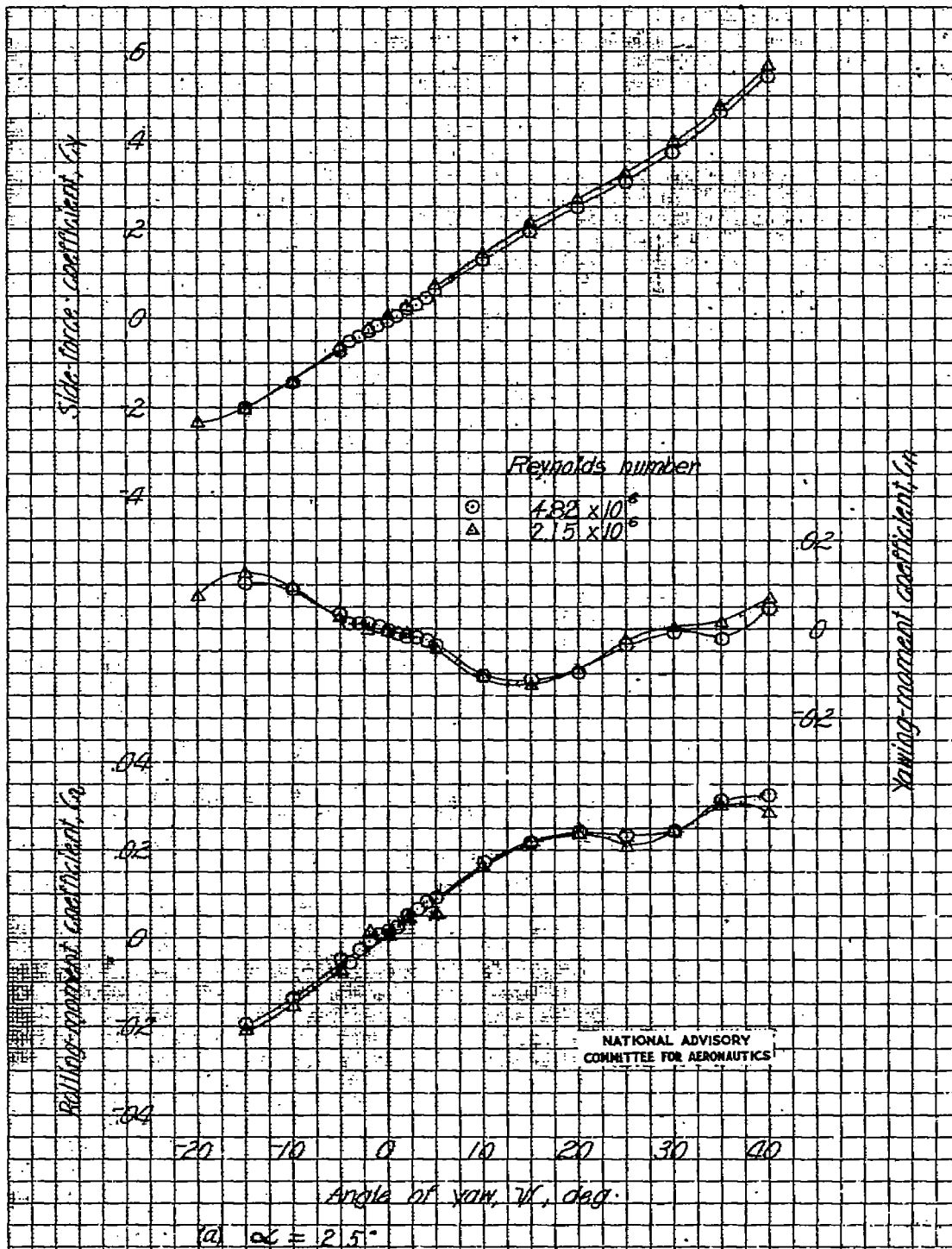
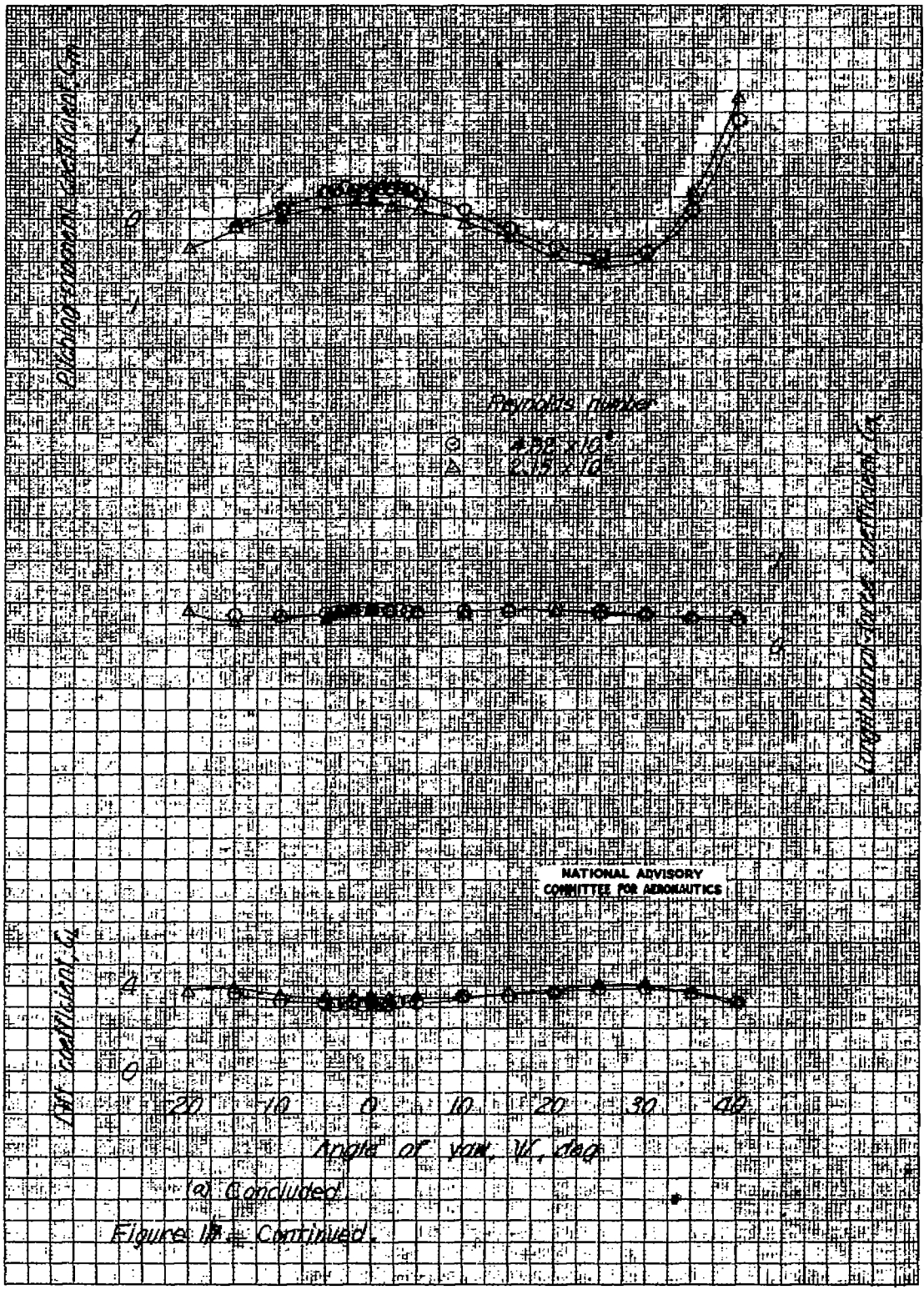
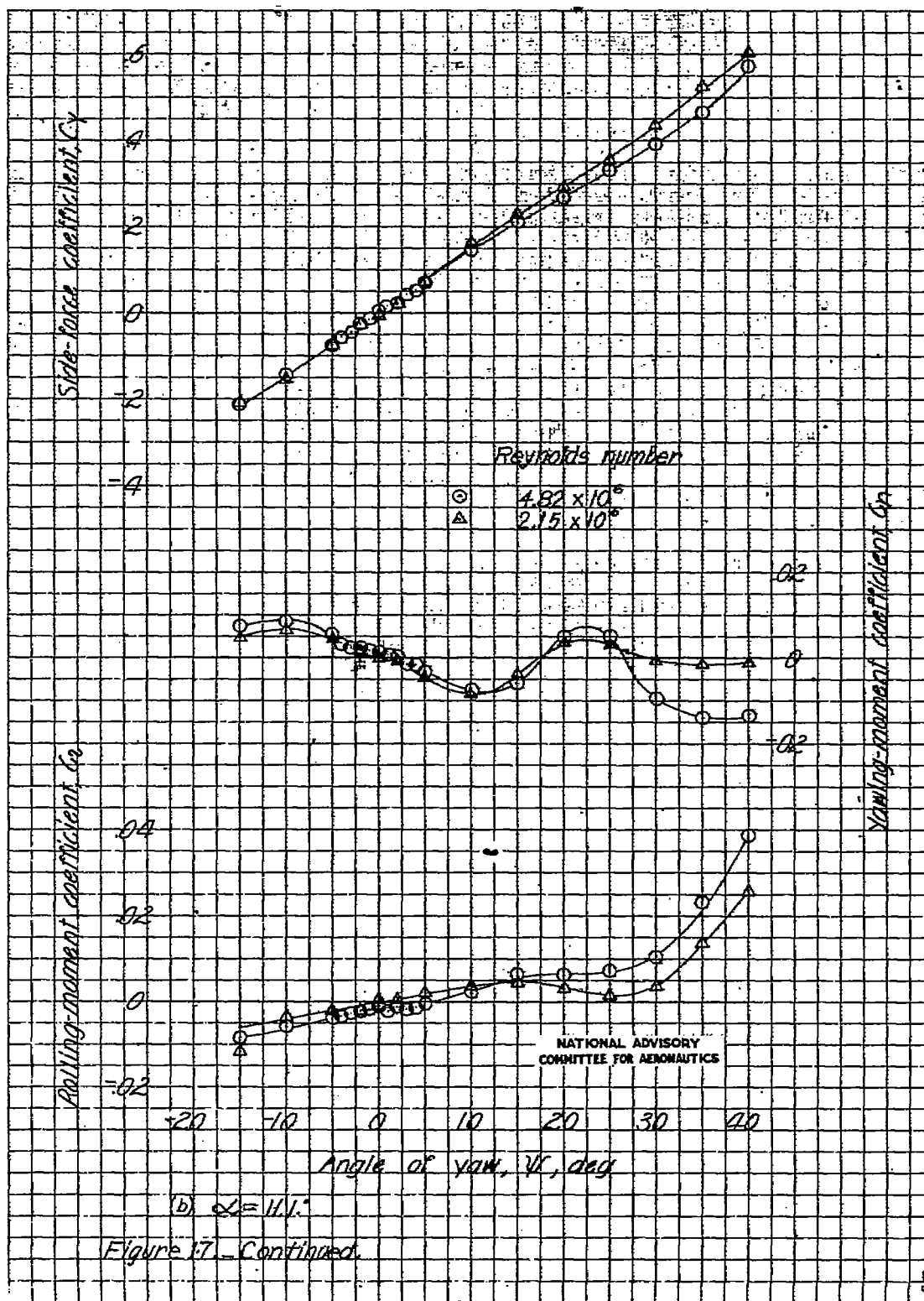
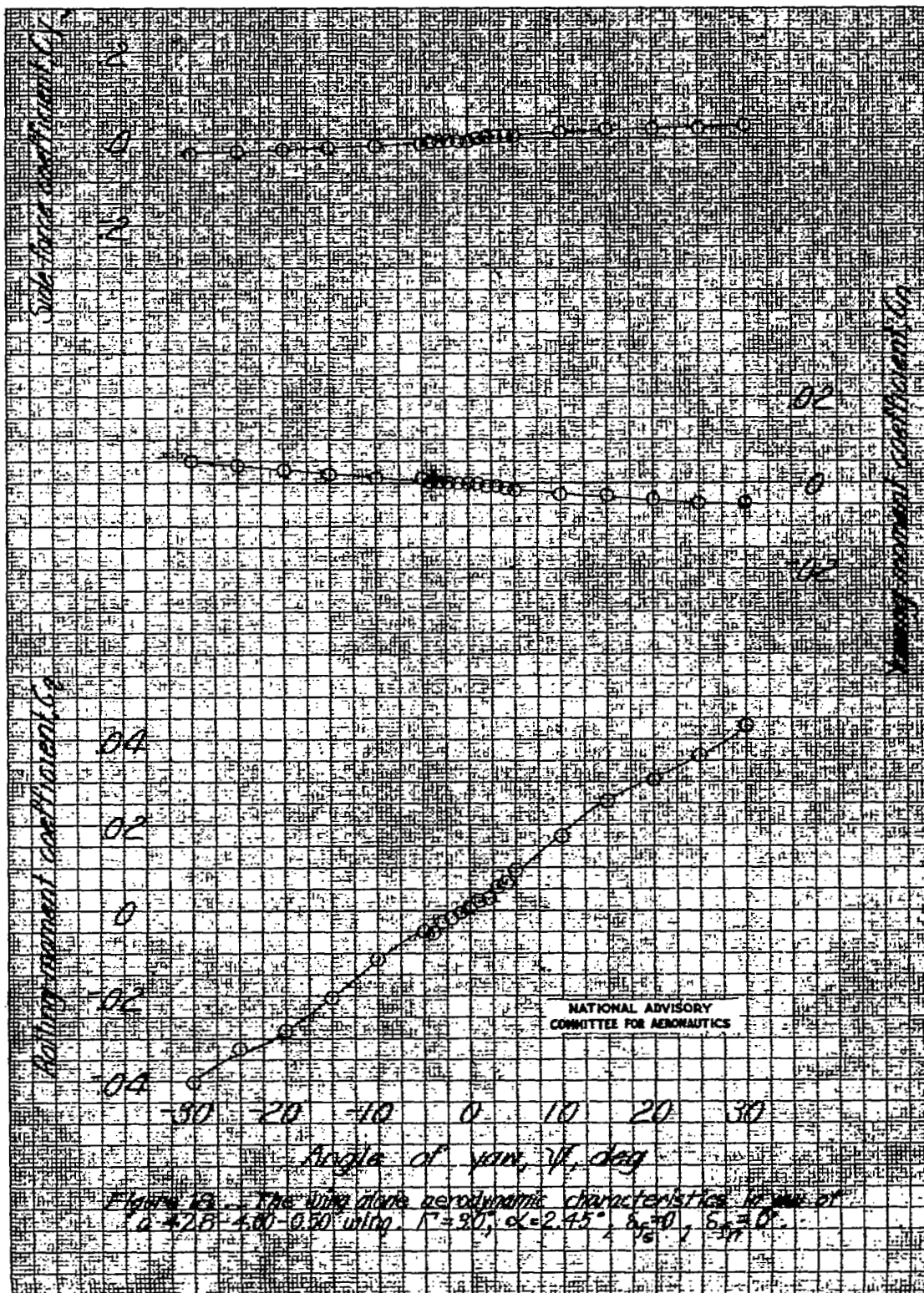


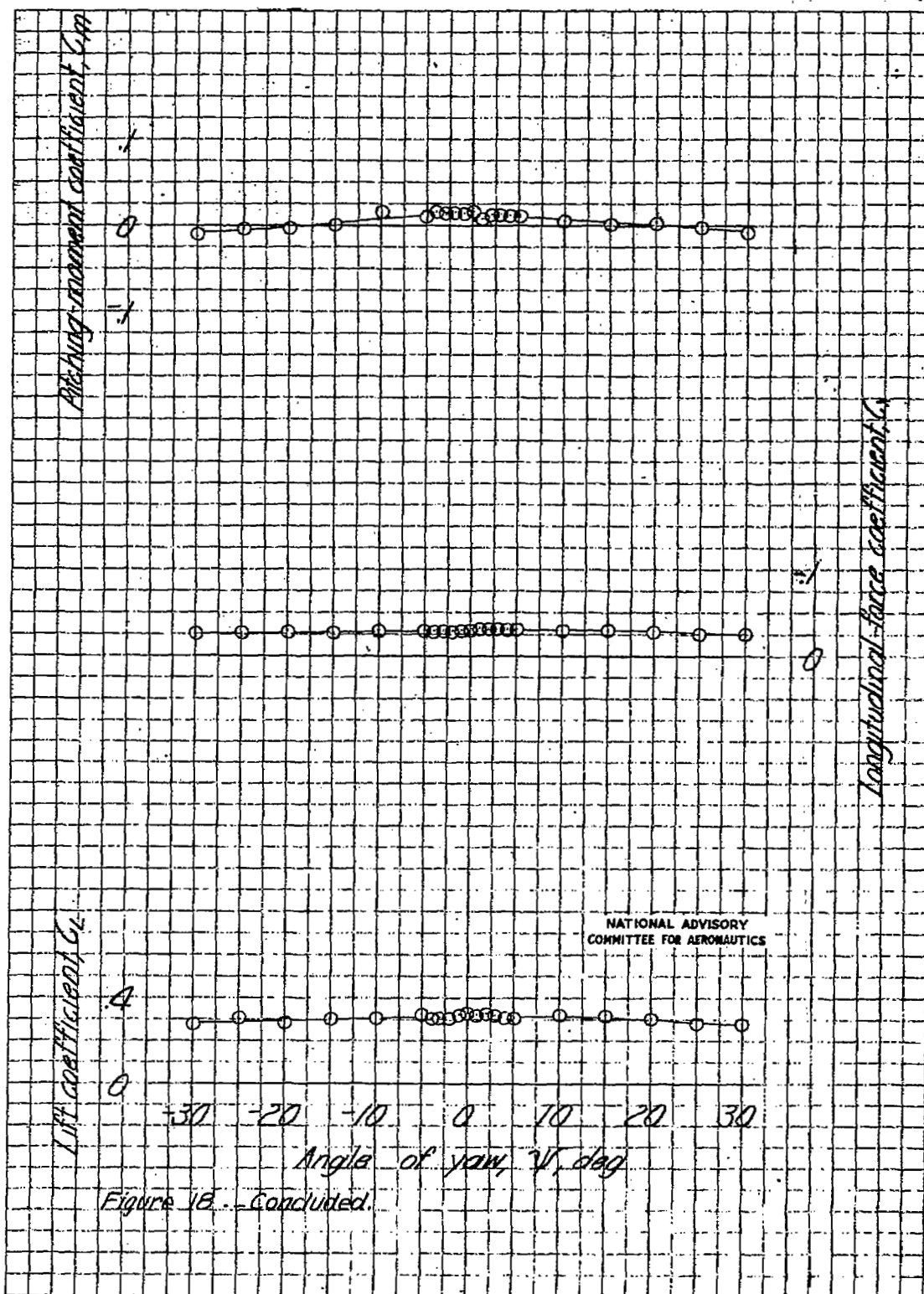
Figure 17. Effect of Reynolds Number on the aerodynamic characteristics in yaw of a model with a 428-400-0.50 wing. Large fuselage, low wing, $F = 5.7^\circ$, $\delta_{f_1} = 0^\circ$, $\delta_{f_2} = 0^\circ$, with wing fillets.











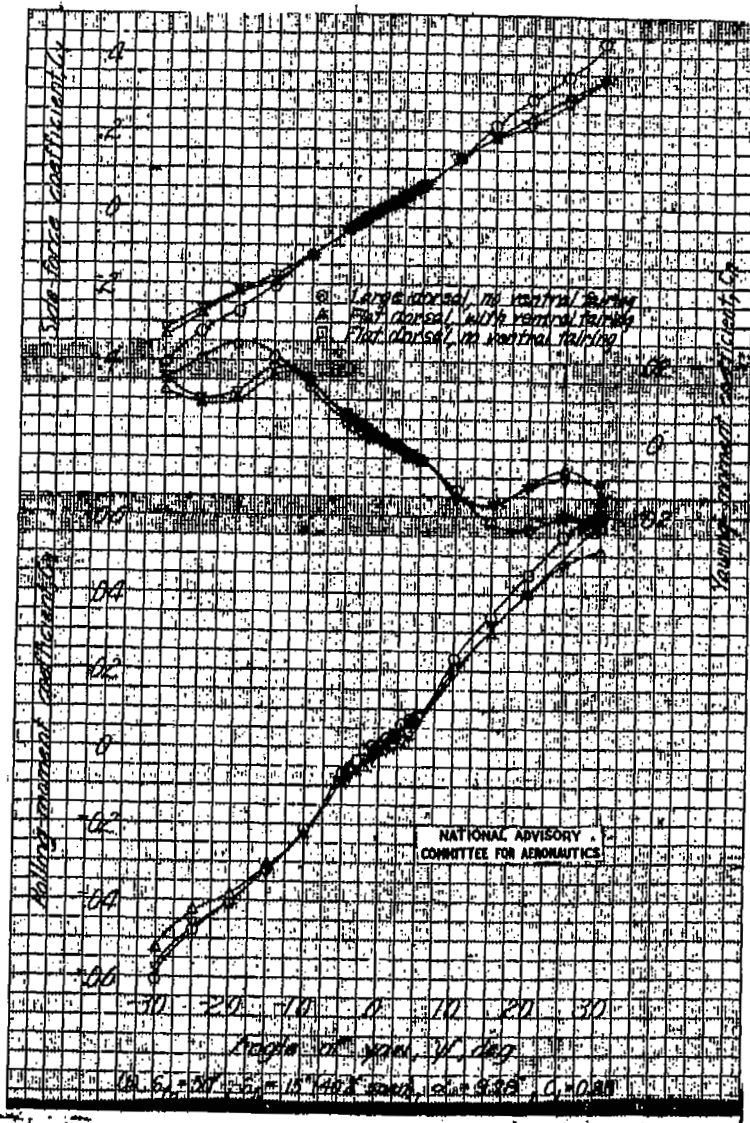
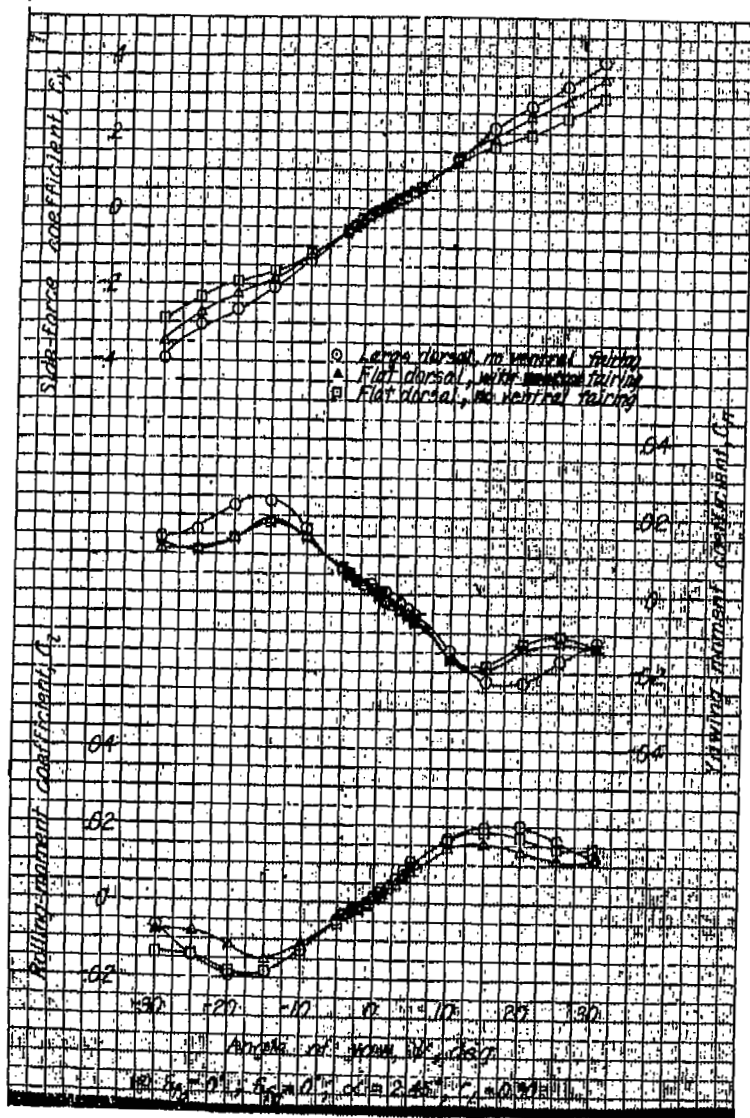
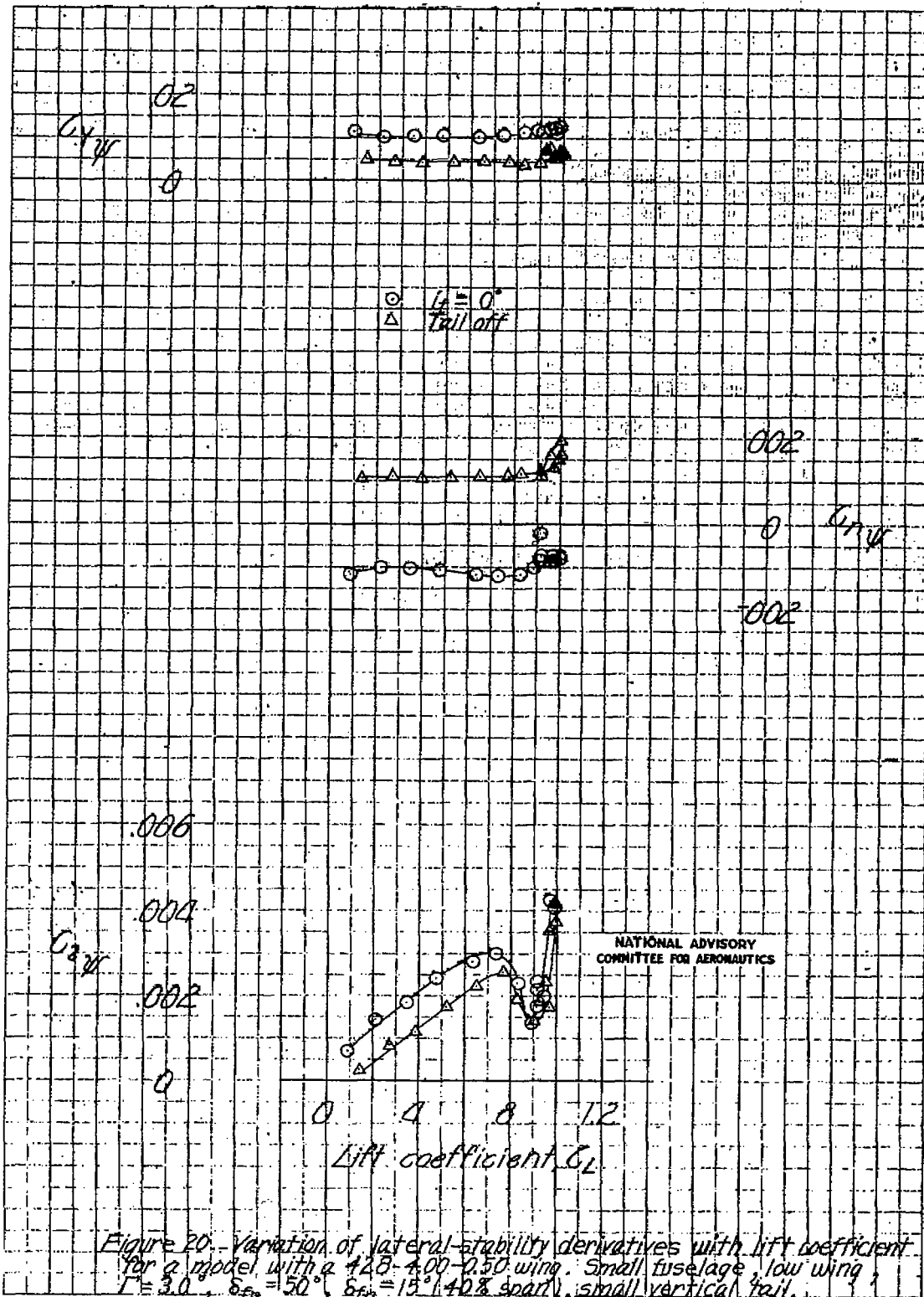
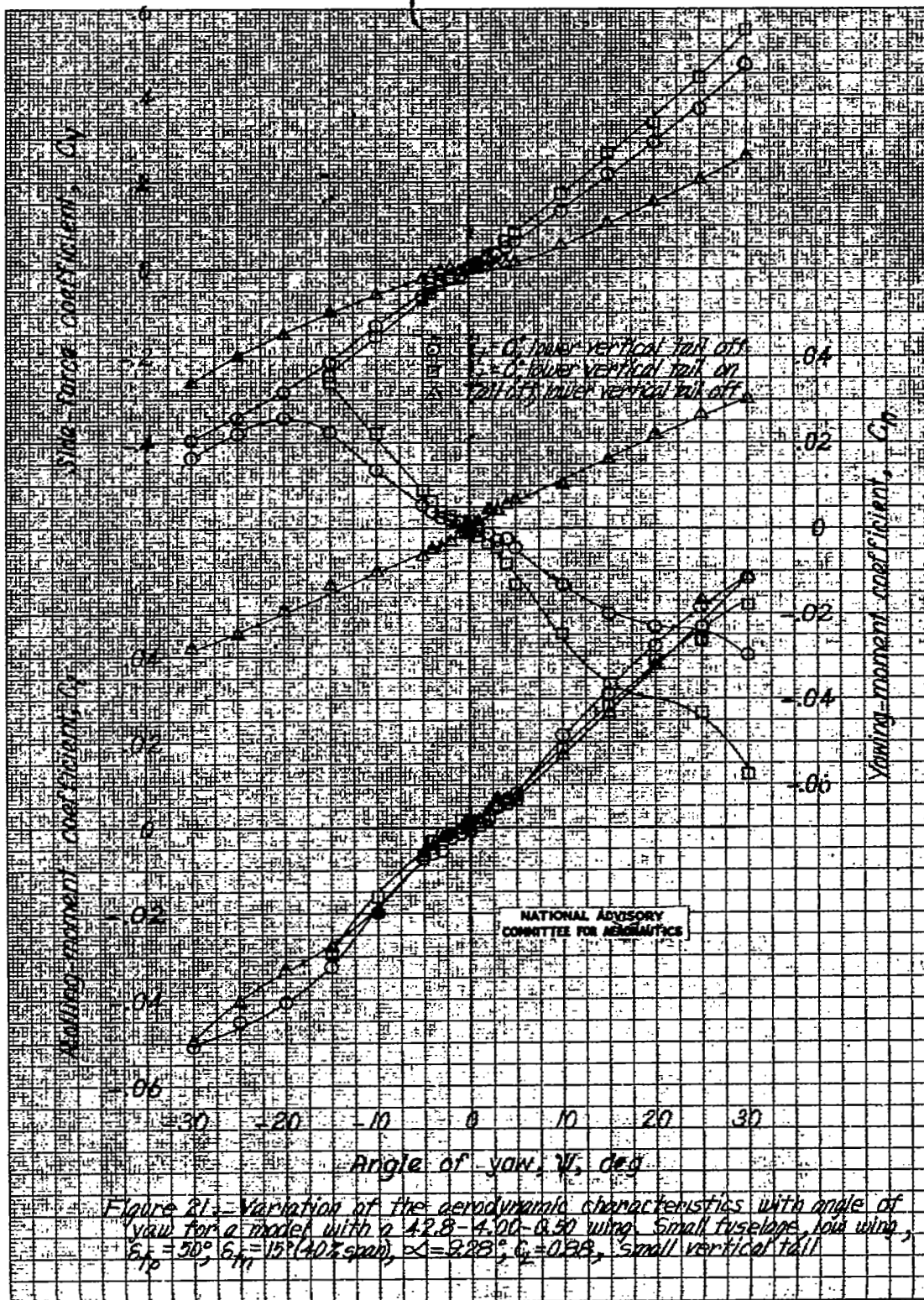


Figure 19.—Effect of dorsal and ventral fairings on the aerodynamic characteristics in yaw of a model with a 42.8-4.00-0.50 wing. Small fuselage, low wing, $\Gamma=30^\circ$, small vertical tail.





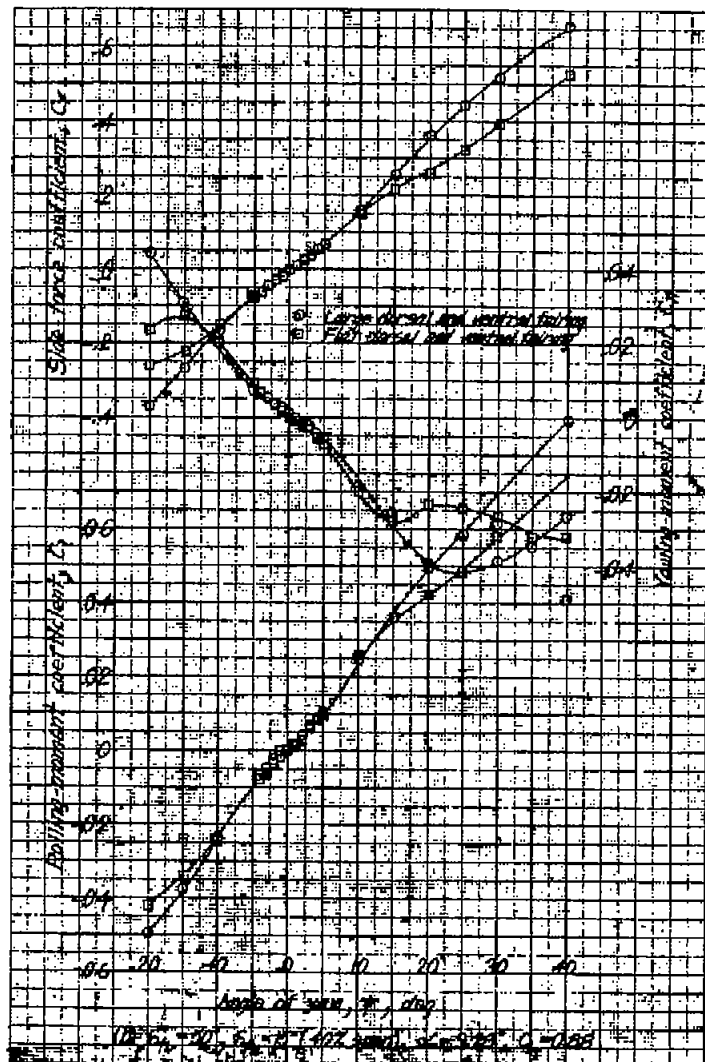
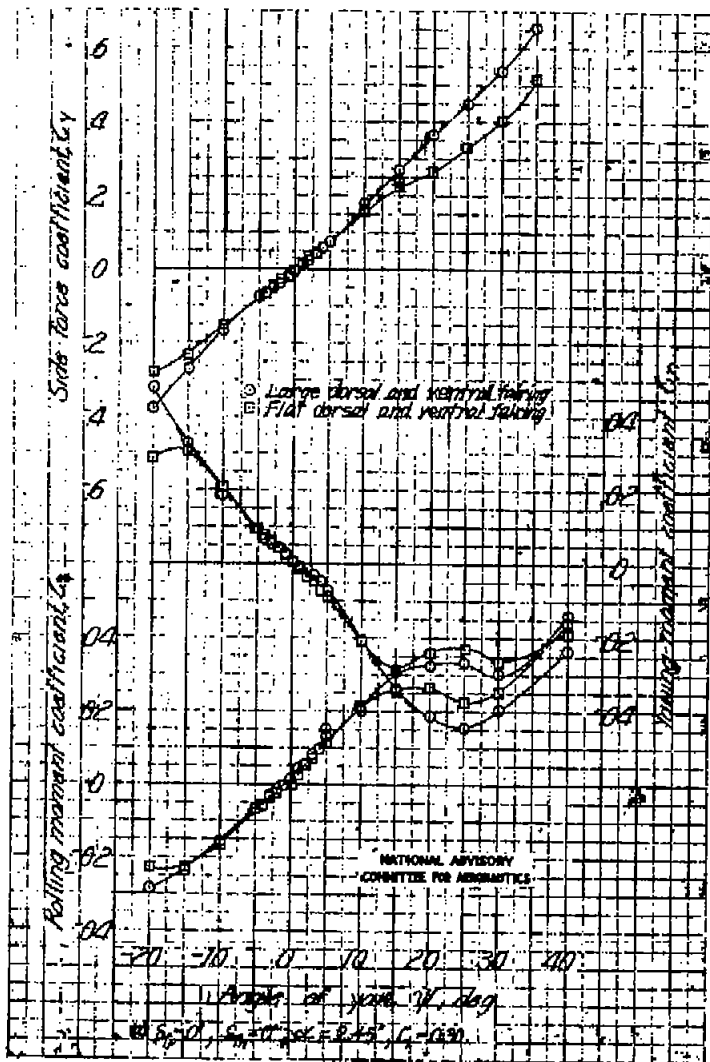
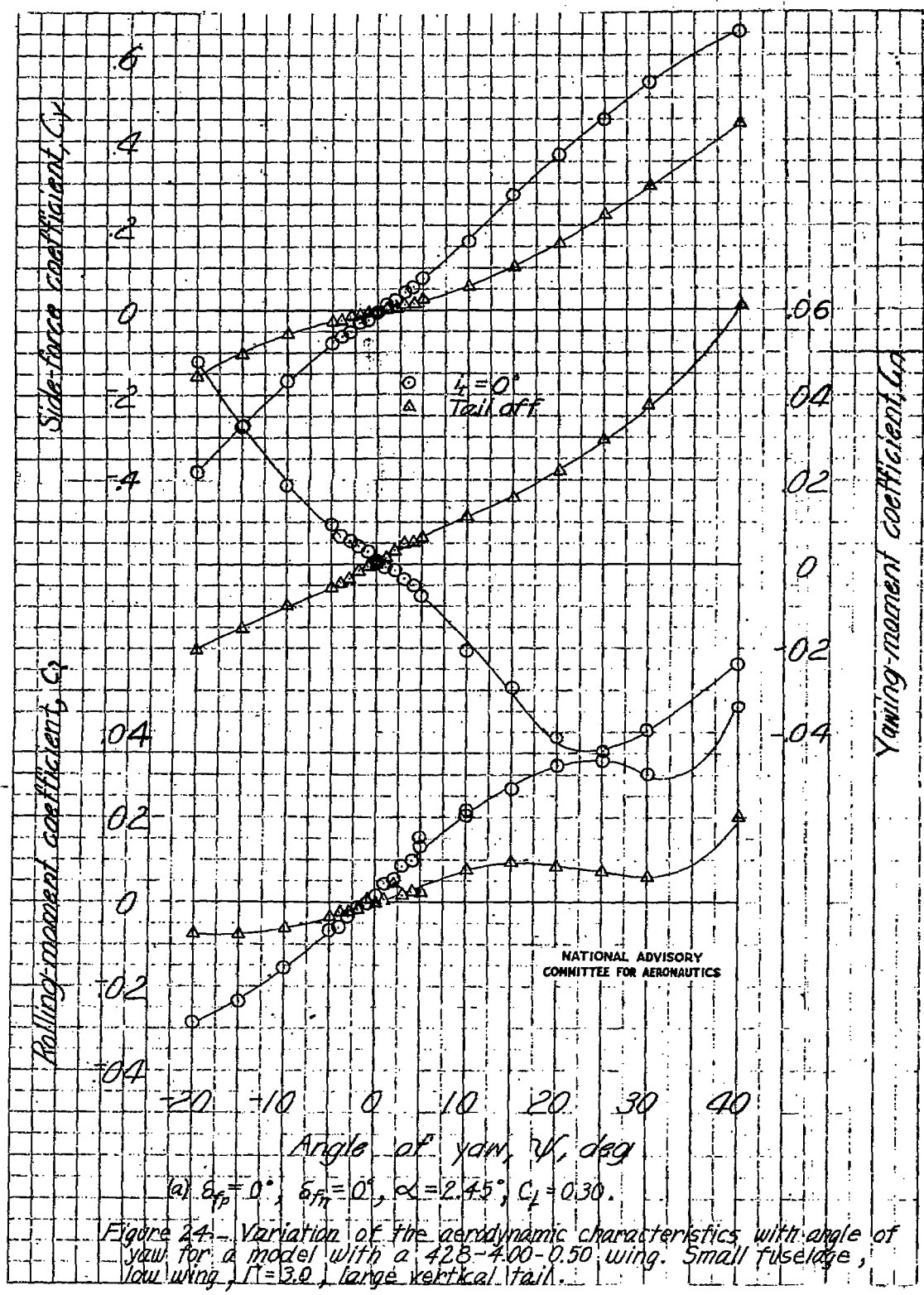
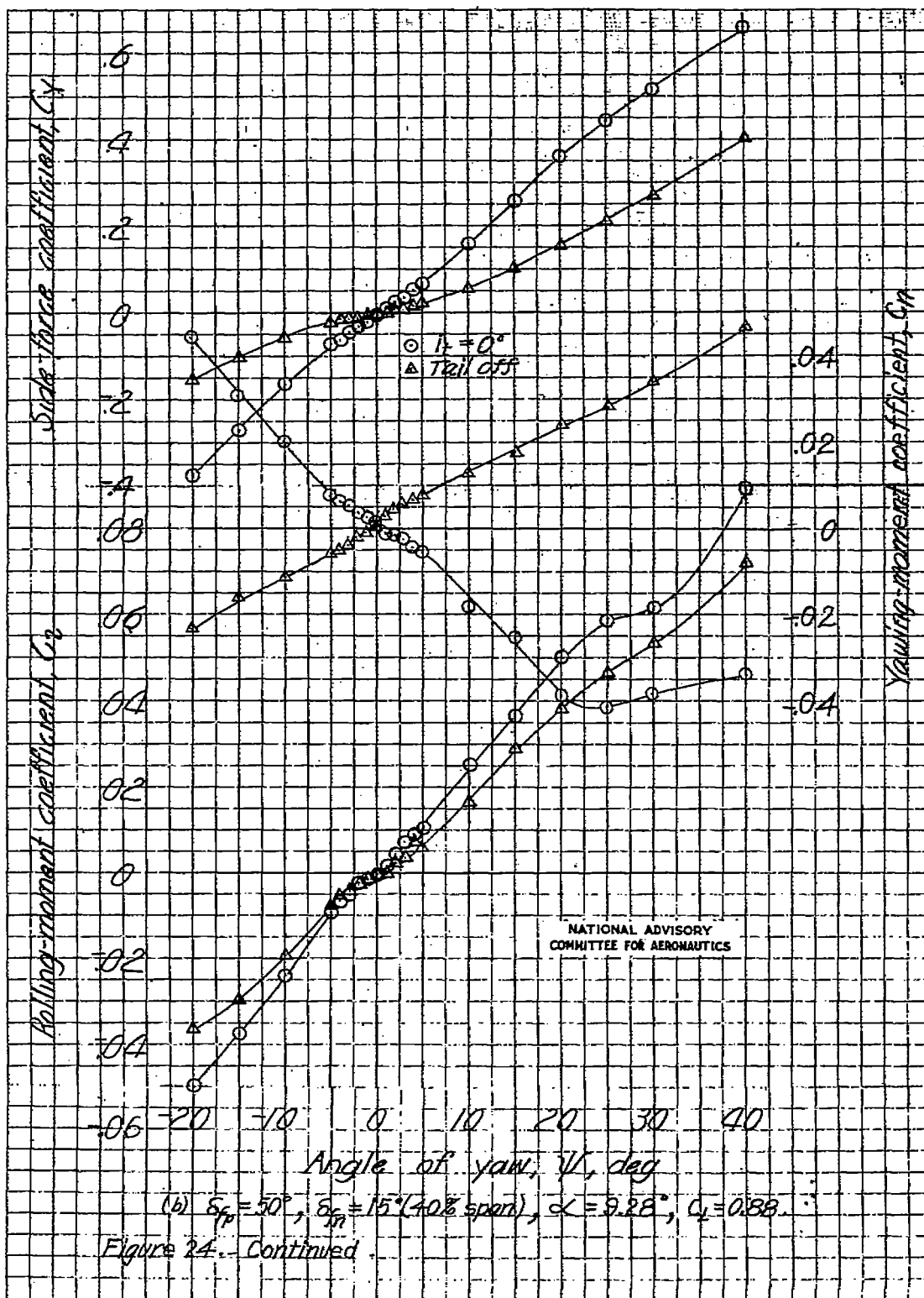
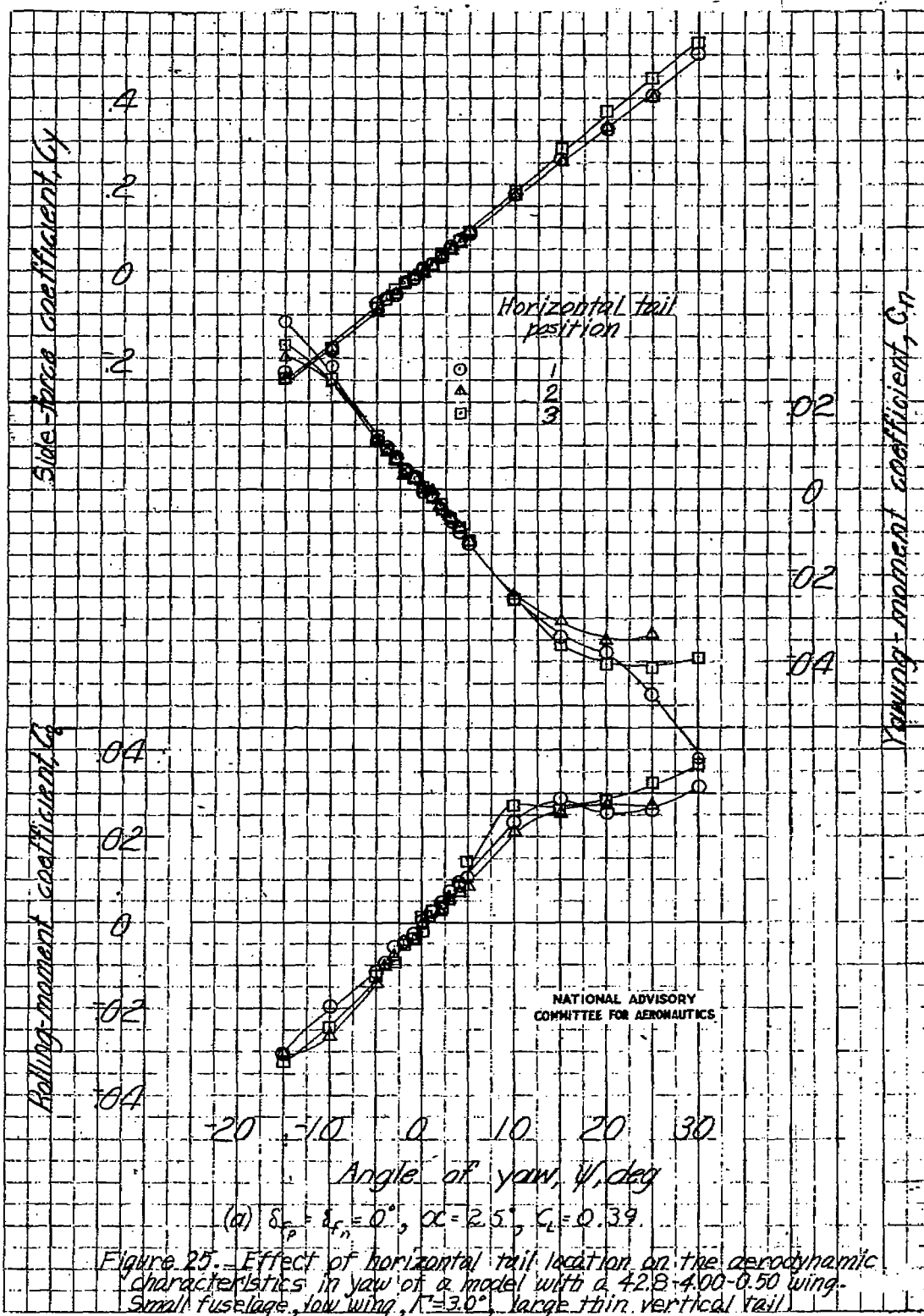
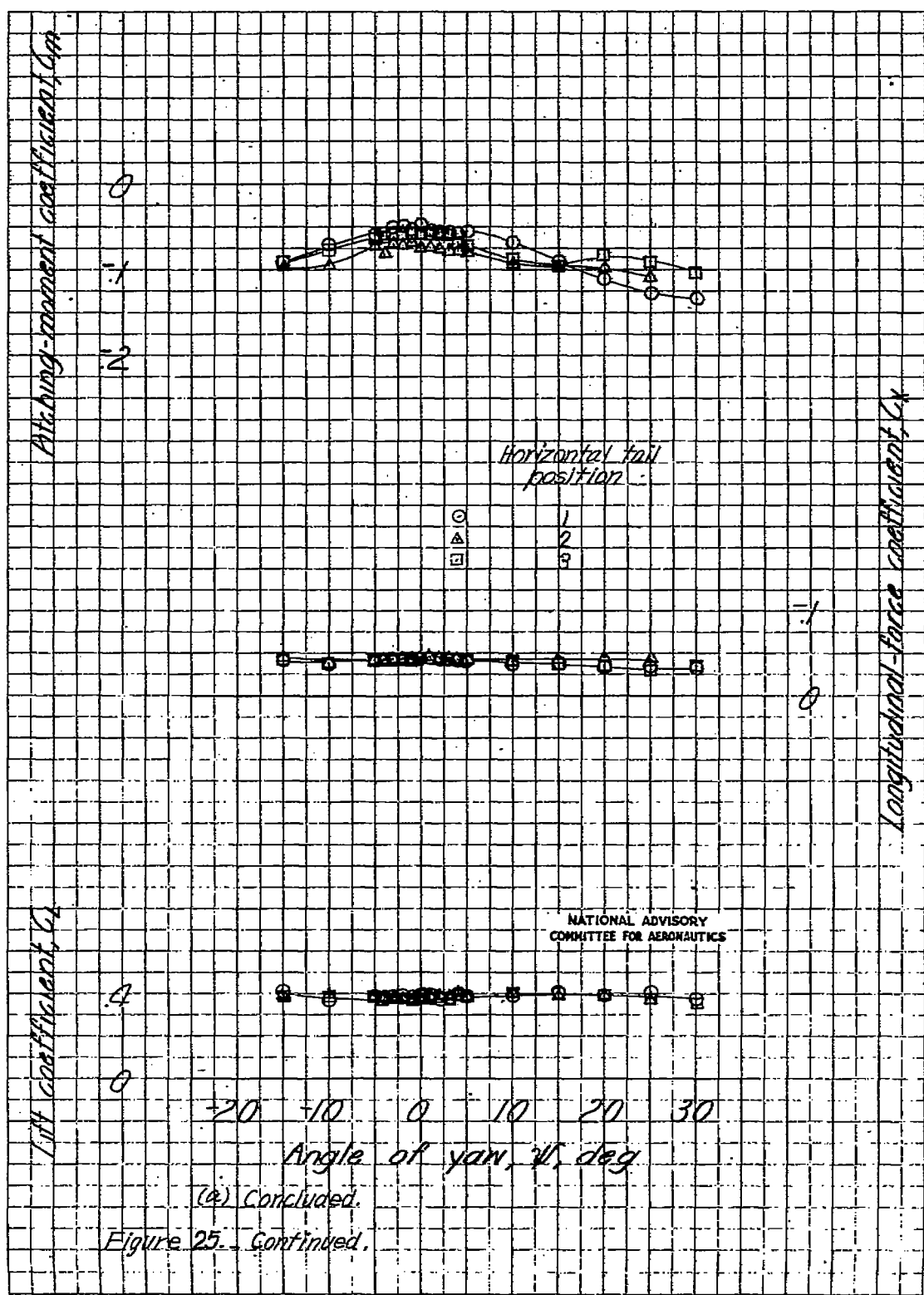


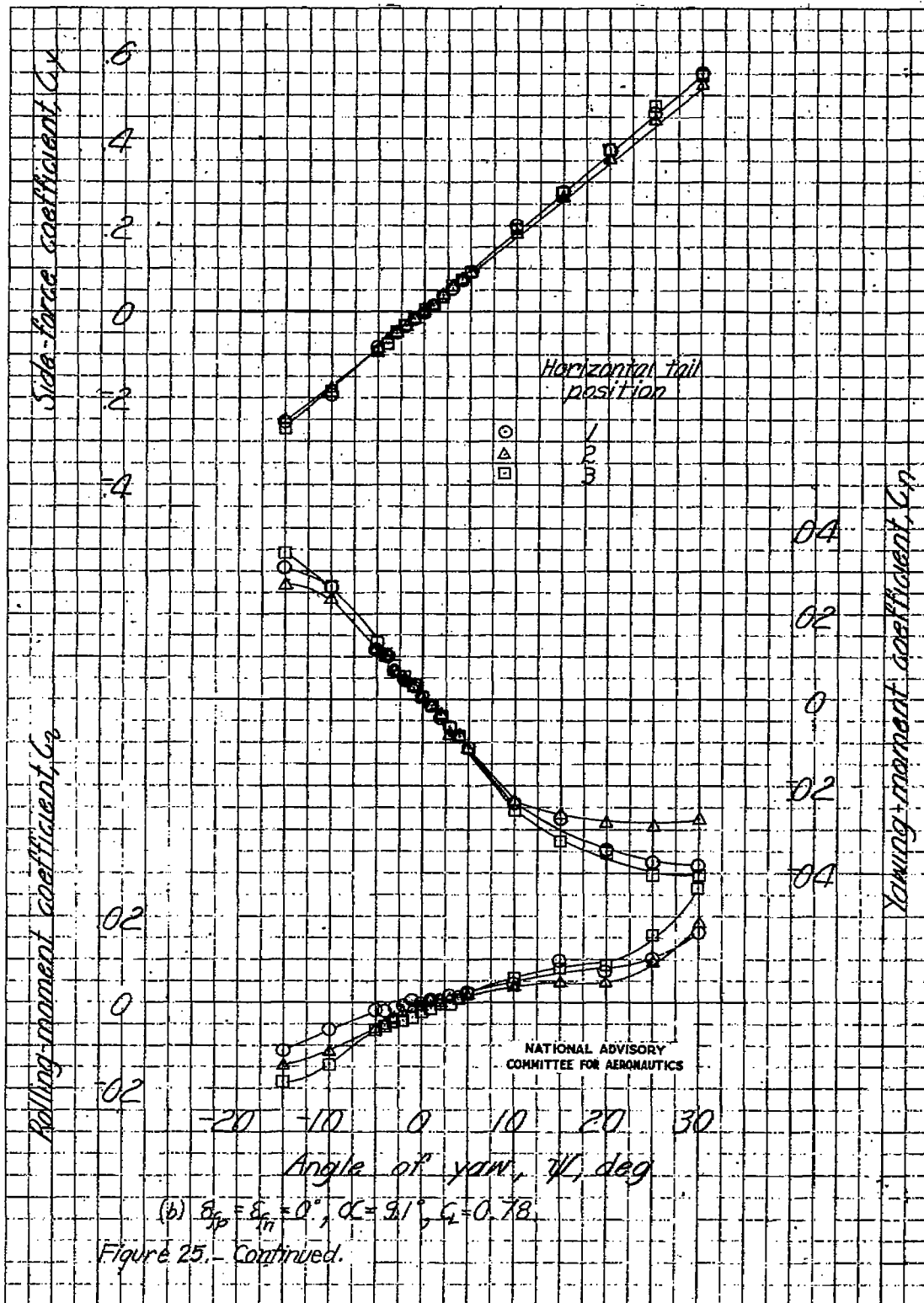
Figure 22.—Effect of dorsal fairings on the aerodynamic characteristics in yaw of a model with a 42B-4.00-0.50 wing. Small fuselage, low wing, $\Gamma = 3.0$, large vertical tail.

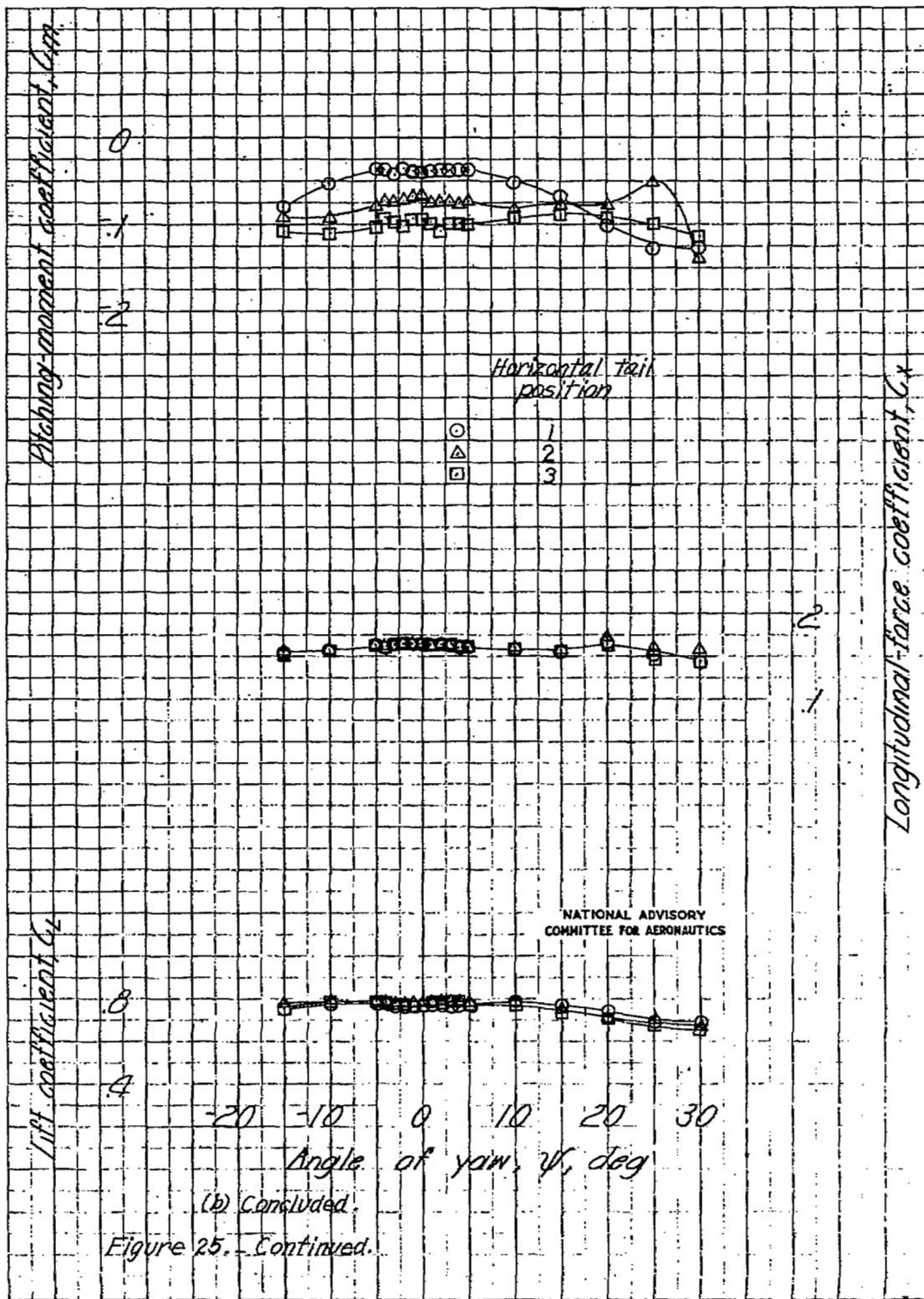


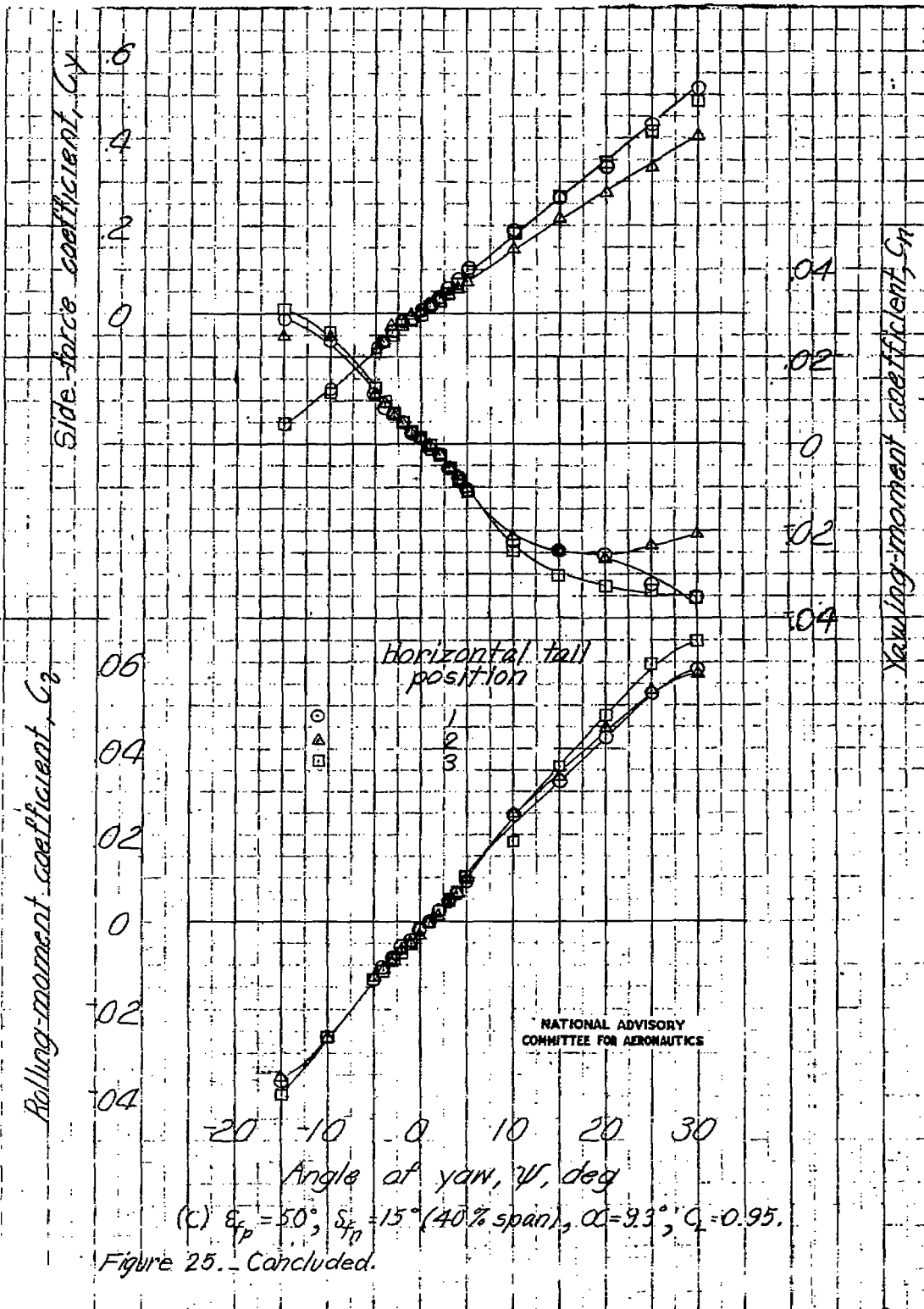


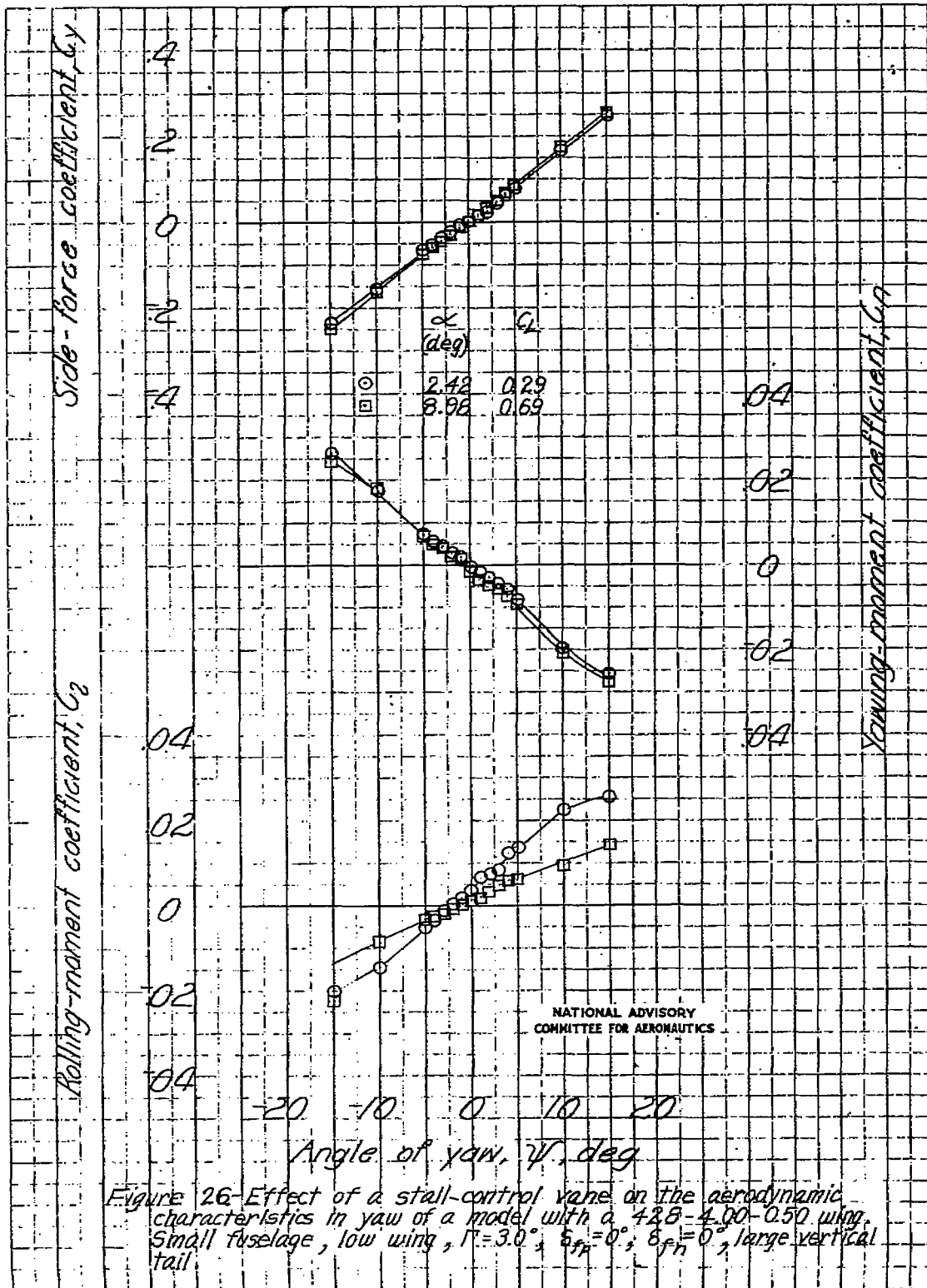


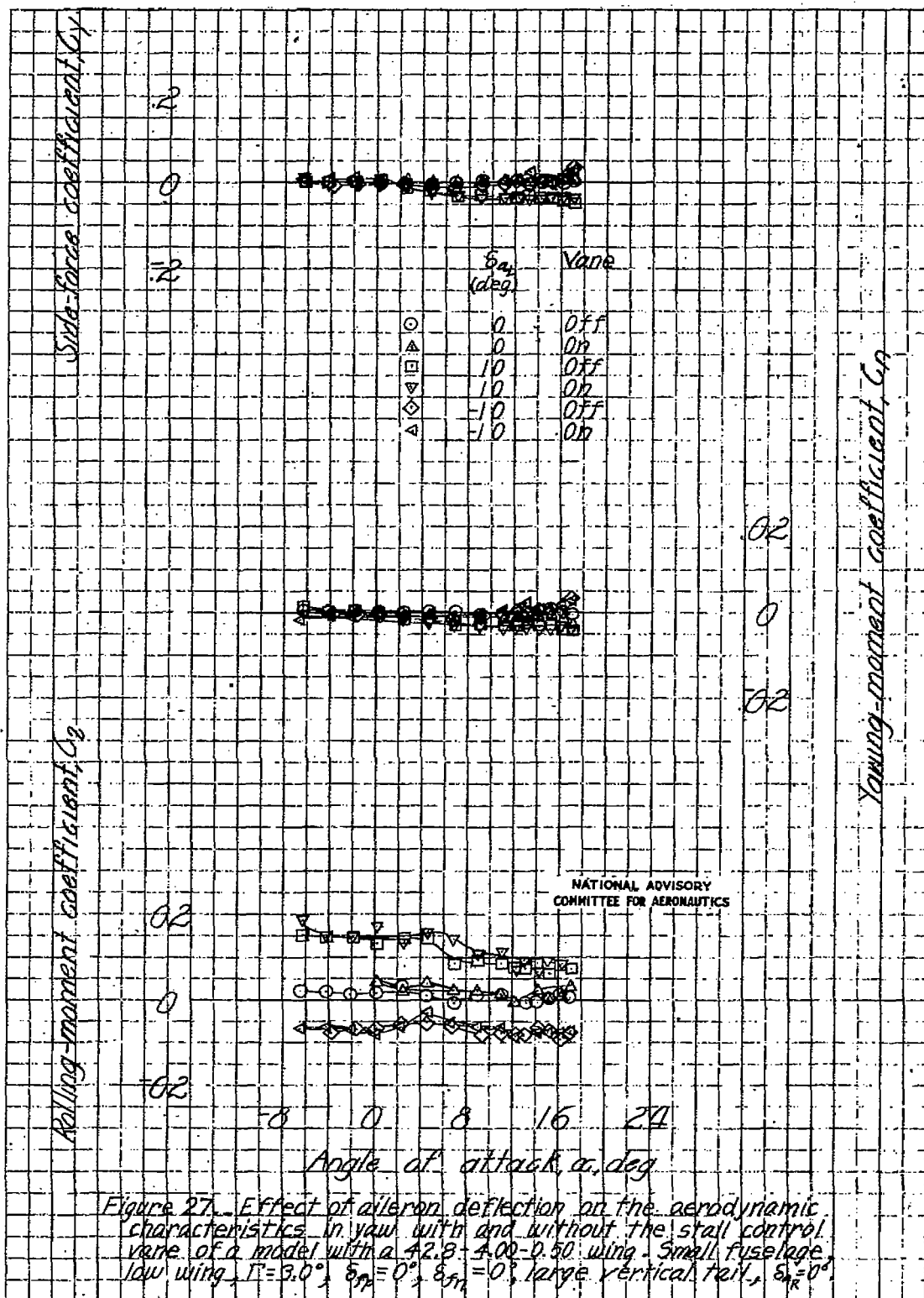


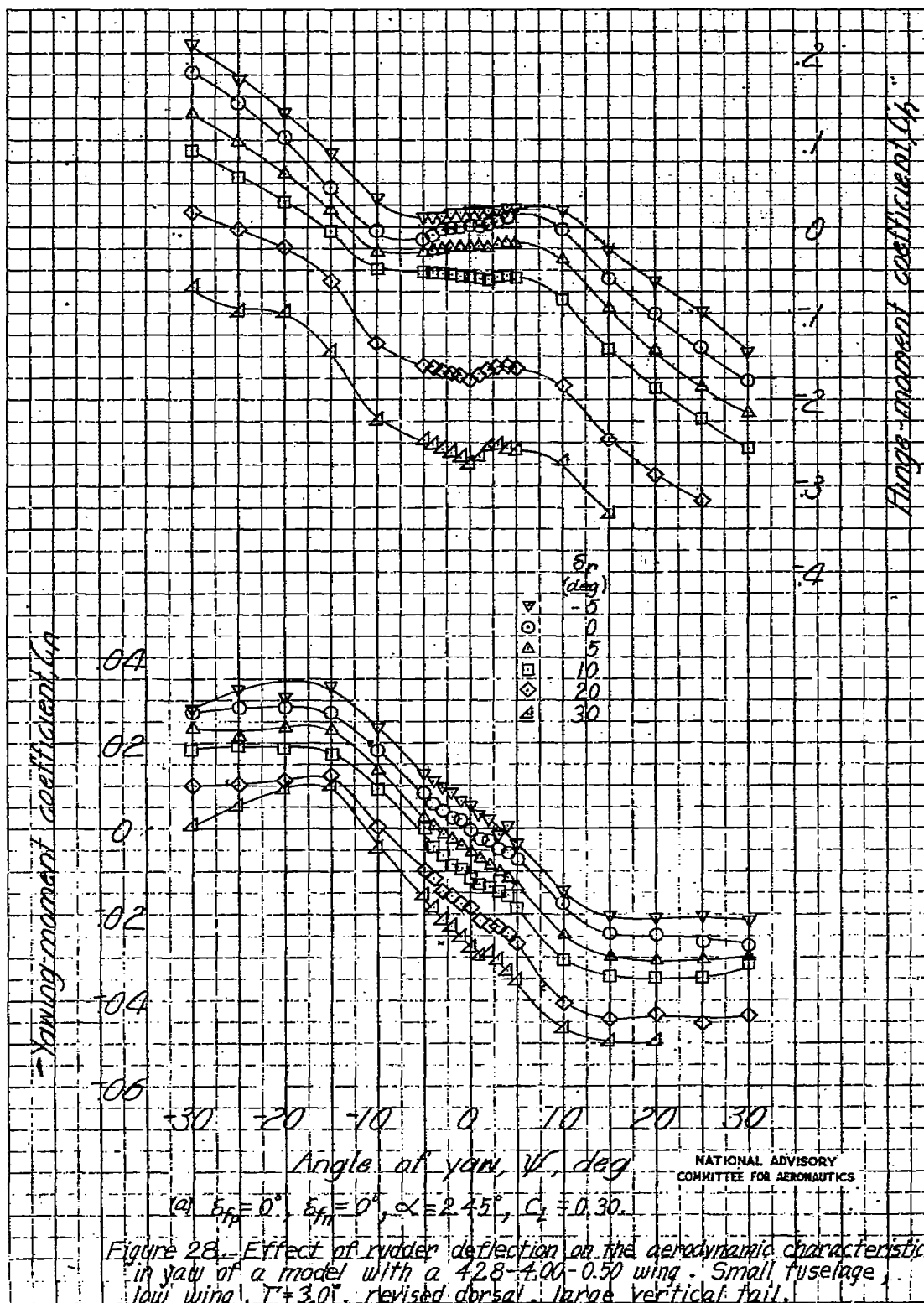


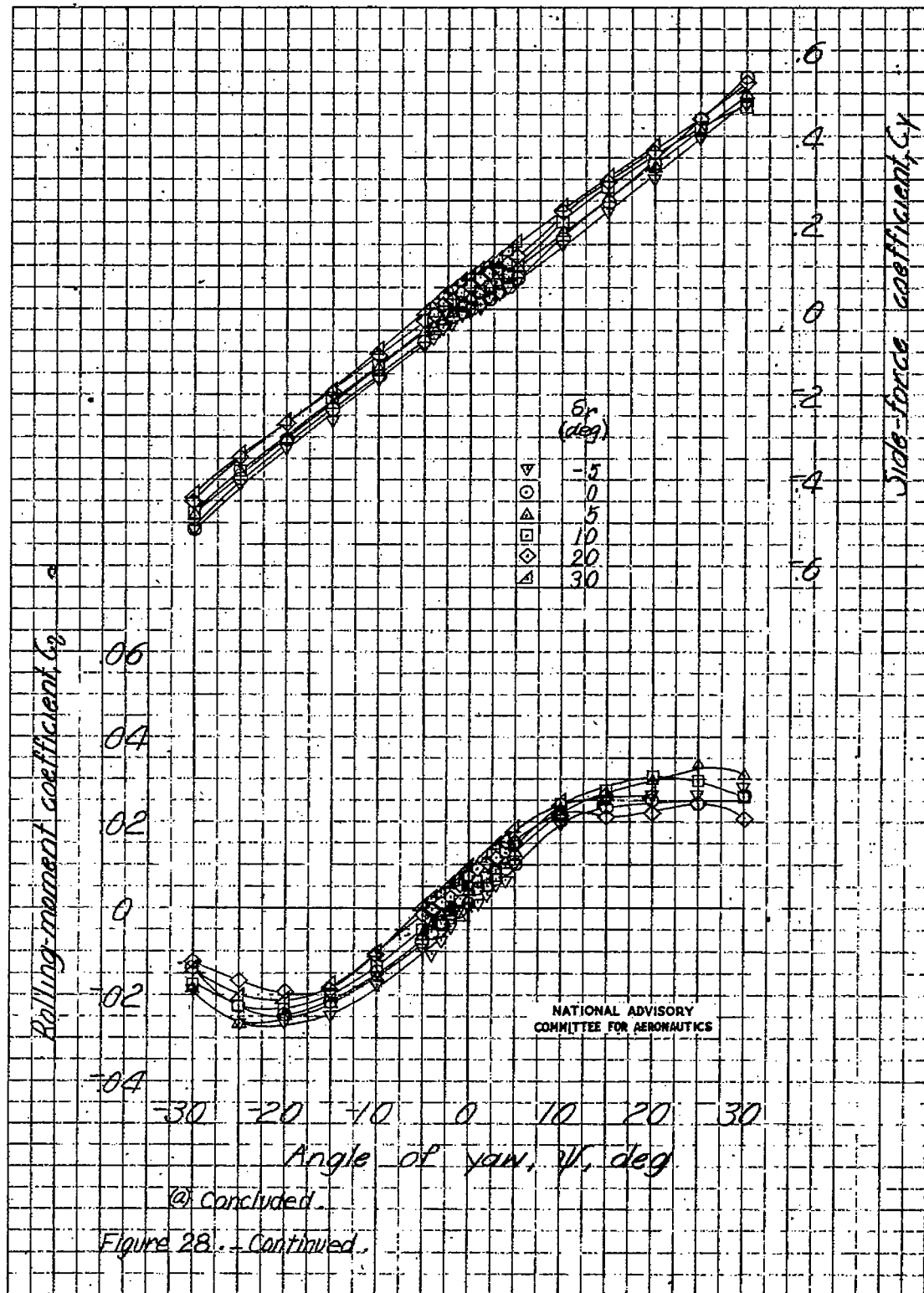


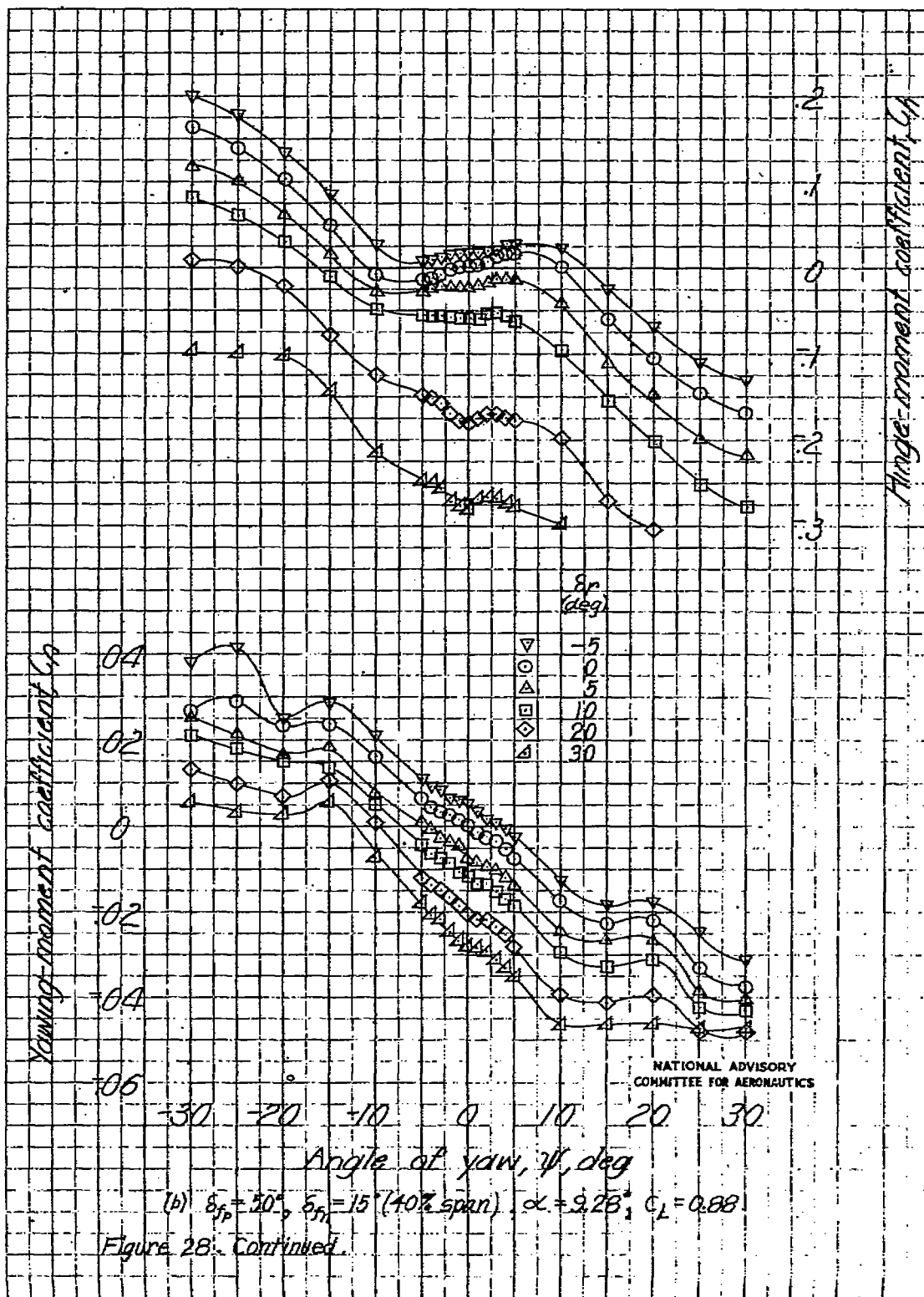


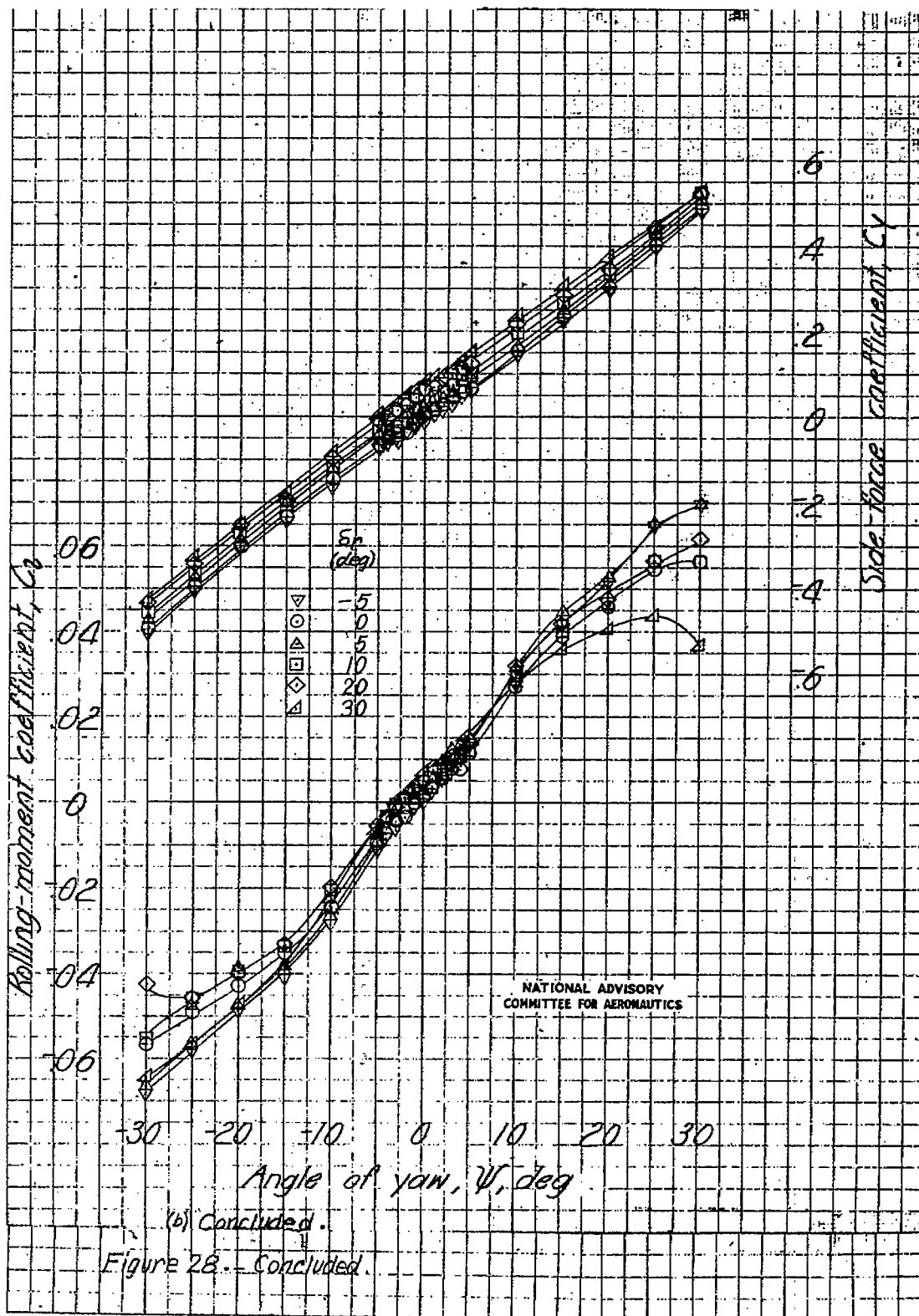












NASA Technical Library



3 1176 01436 7784